An Analysis of Variable Compression Ratio Engine

by

Andrew Maxfield Mitchell

A thesis submitted in partial fulfillment
of the requirements for the degree of
Master of Science in Engineering
(Mechanical Engineering)
in the University of Michigan-Dearborn
2017

Master's Thesis Committee:

Professor Keshev Varde, Chair
Associate Professor Eric Ratts
Professor Yi Zhang

Acknowledgements

I would like to sincerely thank Professor Keshav Varde of the University of Michigan for allowing me to conduct this interesting research. During my Master's research, I changed jobs twice, and experienced the birth of my first child. Professor Varde was very understanding, and his patience regarding this project was much appreciated. I would also like to thank Mr. John Hoard, Associate Research Scientist at the University of Michigan who served as my thesis advisor. His expertise in internal combustion engine operation was invaluable to my research.

Tremendous thanks also go to my good friend David Maietta. He not only provided me continual assistance in the fabrication of the demonstrator engine, but also was pivotal in the design of the Microsoft Excel simulation program.

Special thanks go to my parents, Greg Mitchell and Judy Shemwell, who were an invaluable support to me throughout my college career, both financially and emotionally. Their persevering encouragement to my technical passion made this all possible.

I would also like to thank my wife Nicole Mitchell for her enduring patients and support through this process. Finally, I would like to thank my wonderful son Felix Mitchell who recently turned two years old. Whenever I encountered a particularly challenging aspect of this project, thinking of Felix would always give me the extra bit of inspiration to press on.

Table of Contents

List of Tables

List of Figures

List of Appendices

List of Terms and Abbreviations

TDC	Top Dead Center	T	Temperature
BDC	Bottom Dead Center	P	Pressure
ATDC	After Top Dead Center	V	Volume
BTDC	Before Top Dead Center	F	Force
ABDC	After Bottom Dead Center	v	Linear Velocity
BBDC	Before Bottom Dead Center	a	Linear Acceleration
CR	Compression Ratio	m	Mass
VCR	Variable Compression Ratio	θ	Angular Position
PWR	Power	ω	Angular Velocity
TRQ	Torque	η	Efficiency
MPB	Mass Percentage Burned	C_v	Heat Capacity at Constant Volume
MBT	Mean Best Torque	C_p	Heat Capacity at Constant pressure
EGT	Exhaust Gas Temperature	R	Gas Constant
IMT	Intake Manifold Temperature	H	Heat Transfer Coefficient
EMP	Exhaust Manifold Pressure	W	Work
IMP	Intake Manifold Pressure	Q	Heat
CCP	Crank Case Pressure	U	Internal Energy
VE	Volumetric Efficiency	γ	Variator angle
NA	Naturally Aspirated	ρ	Density
FEA	Finite Element Analysis	k	Ratio of Specific Heats
EVO	Exhaust Valve Opening	σ	Stress
1D	One Dimensional	ε	Contact Ratio (Gear Teeth)
B	Bore	τ	Torque
S	Stroke	β	Connecting Rod Tilt Angle
l	Connecting Rod Length	μ	Rod to Gear-Mesh-Tangent Angle
h	Compression Height	r	Radius
D	Diameter	j	Combustion Chamber Height

Abstract

The variable compression ratio engine presents several advantages to efficiency and power density. At low power output, the engine can be made to operate as a high compression ratio naturally aspirated engine. When high power output is demanded, the engine can be made to operate as a low compression ratio heavily boosted engine. The tremendous power density potential also presents the engine designer with a large opportunity for displacement downsizing while still meeting power requirements for the application.

Chapter 1: Thesis Statement

The compression ratio of an internal combustion engine is an important control parameter for effective engine design. The compression ratio is defined as the total maximum volume within a piston cylinder assembly, with respect to its minimum volume when the piston is closest to the cylinder head. Typical values in modern spark ignition engines range from 8:1 on the low end, to 12:1 or on the high end. The engine designer can freely adjust the target compression ratio in an overhead valve engine by placement or omission of structural material in the combustion chamber area.

The engine designer must consider factors such as performance and efficiency goals, fuel type, fuel quality, ambient operating conditions, and level of boost pressure, if any, when setting a target compression ratio. The target compression ratio is therefore a compromise intended to satisfactorily meet multiple conflicting requirements.

An area of growing interest are systems which allow the engine compression ratio to be adjusted. This adjustment can occur while the engine is running, permitting the best possible compression ratio to be set, depending on the requirements of the user, the ambient conditions, and the fuel being used. There are many diverse system designs, which can facilitate the adjustment of compression ratio, but the end benefit to engine characteristics is largely the same; the efficiency can be maximized at low power levels, while not significantly reducing the maximum peak power capability of the engine.

The body of this work will focus on a specific mechanical system, which enables the adjustment of engine compression ratio. A comprehensive computer simulation will be studied to assess the characteristics of the variable compression ratio engine, and compared to more conventional designs. Additionally, the novel mechanical components involved in this mechanism will be subject to structural analysis. Finally, additional friction losses imposed by the unique system will be quantified.

The goal of this analysis is to show that such a variable compression ratio mechanism can present a large benefit to the performance and overall efficiency of an internal combustion engine, without presenting significant weaknesses.

Chapter 2: Establishing the VCR Engine Geometry

A 2012 patent search of 216 existing Variable Compression Ratio (VCR) engine designs revels four basic concepts.

1. Mechanisms that alter the space between the piston crown and wrist pin, usually using metered oil pressure cavities.
2. Mechanisms that adjust the position of a plunger in the cylinder head.
    - *Small remote control compression ignition engines employ a simple manually controlled version of this system.*
3. Multilink connecting rods attached to actuators, which effectively alter the piston to crank offset.
    - *The newly (2016) announced Infinity VC-T engine employs this system.*
4. Cylinder heads that are able to pivot or translate with respect to the engine block.
    - *The Saab SVC concept engine developed around 2000-2001 employs this system.*

The VCR mechanism studied throughout this text is different from the art described above. This text will study a VCR engine that has the overall cylinder positioning of a conventional radial piston engine. Radial piston engines were very popular in aircraft from the early 1900's until the 1940's when turbine engines became more suitable for military and commercial aviation. Radial engines remained common for small private aircraft for many more years, but these small planes more often use horizontally opposed (also known as "flat", or "boxer") engines in recent decades. A few companies continue to produce radial engines, but these are typically in very low quantities for very specialty applications. Since the early 1900's a few automobiles and motorcycles have been powered by radial engines, but these applications have always been very uncommon.

Although the radial configuration has almost completely fallen out of favor in the aviation sector, and never became popular at all for automotive applications, it does lend itself uniquely and effectively to the variable compression mechanism described here. This variable compression mechanism employs an arrangement of connecting rods onto a master rod retainer. The engine examined herein employs a 5-cylinder arrangement, but other odd-numbered cylinder

arrangements greater than 1 are possible. The number of cylinders *should* be odd-numbered to maintain a regularly spaced firing order for a four-stroke cycle.

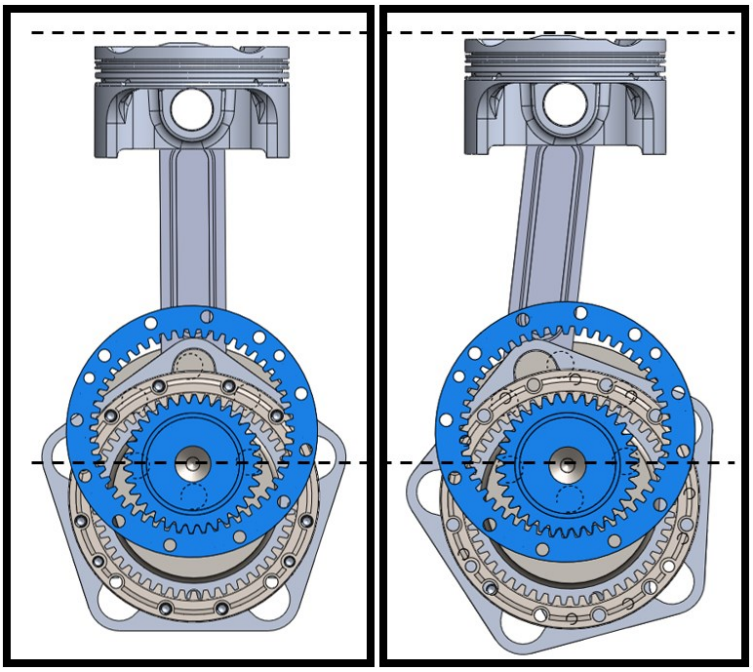

Figure 1: Basic Mechanical Layout

The engine is shown at Bottom Dead Center (BDC) in both images. The image on the left has had the variator set to maximum compression ratio, and on the right, the variator has been set to low compression ratio.

In the image above, the means by which the engine compression ratio changes is shown. Many parts are omitted for clarity. Only one of the five connecting rods and pistons are shown. The blue ring gear in the foreground is coaxial with the crankshaft axis of rotation. This gear only changes in angle slightly as the engine operates (it does not revolve continuously). The smaller blue pinion gear is coaxial with a crankshaft journal that is exactly mid-way between the main journal axis and the rod journal axis. This pinion gear meshes with both the blue ring gear in the foreground, and the grey ring gear in the background. As the crankshaft spins, this pinion gear "rolls" around the inside of the blue ring gear in a similar movement to the tracing of a hypotrochoid. Despite this abundance of rotation and movement of the pinion gear, the fact that the two ring gears have the same number of teeth facilitates a convenient result; So long as the blue ring gear remains fixed, the grey ring gear in the background will not *rotate*, it will only *orbit* about the crankshaft axis of rotation. This facilitates the reciprocation of all pistons attached to the master rod retainer (1 of 5 being shown in the diagram above). If the blue ring gear is pivoted

by 15° counterclockwise, for example, the pinion gear will transfer that change angular orientation to the gray gear in the background. This transfer is able to occur *while* the crankshaft is spinning. In the diagram to the right above, the blue ring gear has been commanded to rotate 15° counterclockwise, and the resultant change to the components in the background is obvious. Note that in both the right and left side in the figure, the engine is at Bottom Dead Center (BDC). However, the vertical position of the piston has changed somewhat due to the master rod retainer being angled to the side. Similarly, when the piston reaches Top Dead Center (TDC) it will be much closer to the cylinder head in the left-hand configuration than when in the right-hand configuration.

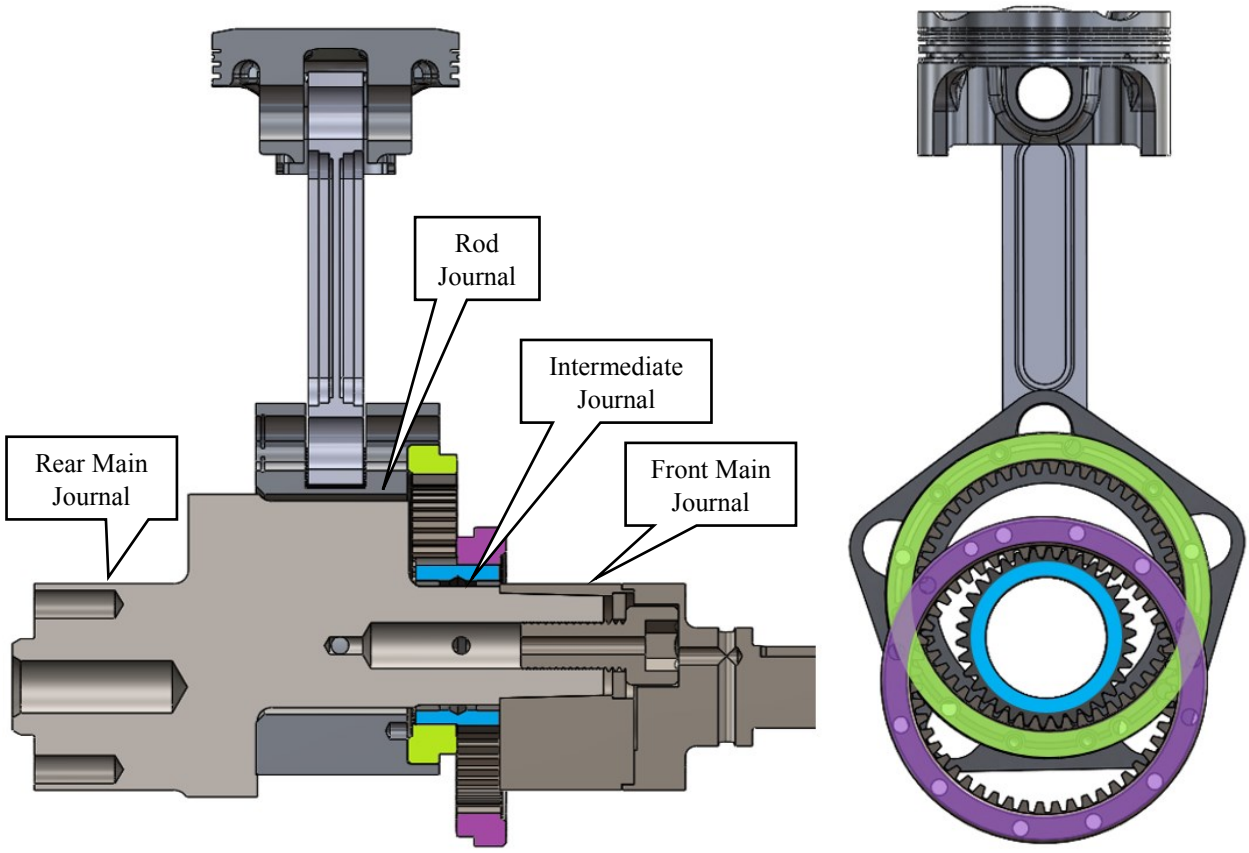

Figure 2: Side and front view of gear mesh

Here the engine is displayed in both a sectioned view from the side with the crankshaft visible, and a full view from the front, with the crank hidden. Again, only one of five pistons and connecting rods are shown for clarity. The gears are color-coded for clarity. The purple ring gear stays stationary, aside from being actively rotated by a few degrees when the engine compression

ratio is commanded to change. This angular re-positioning occurs relatively slowly with respect to the angular speed of the crankshaft. The smaller blue gear orbits on the intermediate journal, and keeps the two ring gears synchronized. The green ring gear is attached to the pentagon-shaped component which controls the motion of the five connecting rods. The green gear typically *orbits* about the centerline of the crankshaft main journals, but is indirectly re-angled via the purple and blue gear motion. Note that the crankshaft is made of two main pieces bolted together. This allows the blue gear to be slid onto the intermediate journal prior to the front crank section being bolted into the main rear crank section. A special alignment fixture must be used to ensure the front and rear crank journals are nearly perfectly co-axial while the two sections of crankshaft are bolted to each other. Harley Davidson multi-piece crankshafts are assembled in a similar way. An alternative approach would be to use a single piece crankshaft, and to split the blue gear meridianally, and then reconstructing with fasteners after in position on the journal. This method is likely to compromise the strength of the gear teeth adjacent to the parting line, so was not used in this design.

This mechanism could be applied to more conventional inline or V-engine configurations, but the number of individual ring and pinion gears would increase, and the means to keep them all synchronized would become complicated. By employing a radial layout, all of the cylinders are kept in a single plane, so a single variator mechanism is able to adjust the compression ratio on multiple cylinders simultaneously. The radial engine layout also offers a less obvious benefit to the ring and pinion gear system; the amount of force transmitted by the gear teeth remains comparatively low. While a radial 3-cylinder does not offer much of an advantage here, an engine with five cylinders will reduce the force needing to go through the teeth because the compression energy needed by a cylinder can largely be directly transferred over by the prior cylinder undergoing its power stroke. In the case of a 5-cylinder radial engine, the firing order would be 1, 3, 5, 2, 4, 1, and so on. This means that while cylinder 1 is undergoing its power stroke, cylinder number 3 is undergoing its compression stroke.

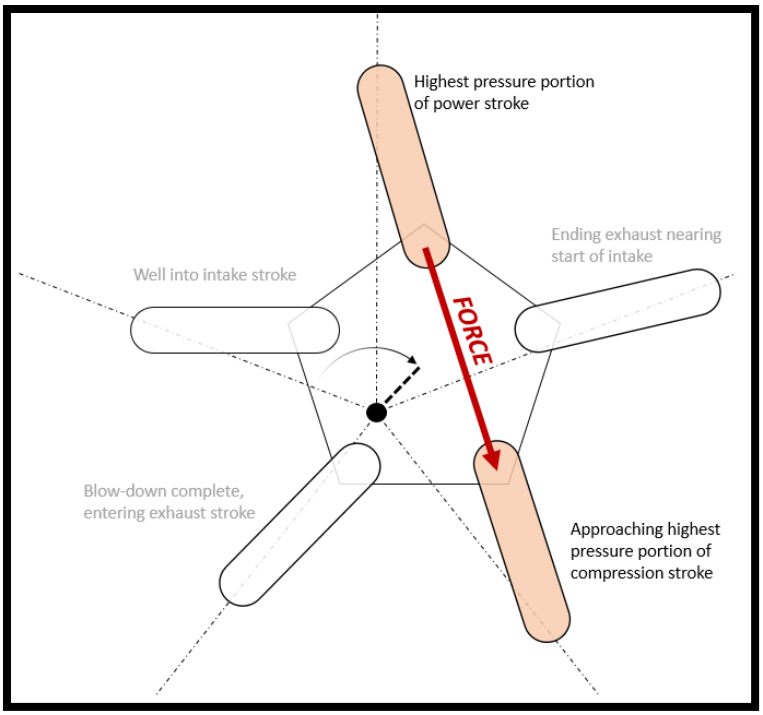

Figure 3: Force transfer system for a 5-cylinder configuration

In the diagram above, the black dot is the crankshaft rotational axis. The pentagon is the master rod retainer, which is currently shown about 45° after TDC for cylinder 1. The five dash-dotted lines radiating out from the center are the centerlines for the five cylinders. The five connecting rods are shown, and the state of each corresponding cylinder is described. The two rods currently experiencing significantly increased compressive forces (due to high cylinder pressures) are highlighted in red. The red force arrow visually demonstrates how the high gas force in cylinder number 1 is able to directly supply energy to cylinder number 3, which is finishing its compression stroke. If designed carefully, this effect can be used to greatly mitigate the amount of force needed to be transferred by the variator and synchronizer gear teeth. In a conventional piston engine the energy supplied to a cylinder undergoing its compression stroke comes from a combination of other cylinders experiencing their power strokes and energy retained in the flywheel. This is typically acceptable because this large transfer of force only need transmit through a relatively stiff and robust crankshaft flywheel assembly. In the case of the synchronizer gear based VCR engine, this becomes more challenging since any forces *indirectly* transferred from one cylinder to another must be met with a resistive force at the comparatively delicate gear teeth. For this reason, effort should be taken to reduce the amount of *indirect* force transfer between cylinders and instead

promote a *direct* force transfer between cylinders as can be accomplished with the layout described above. Higher cylinder counts can further reduce the gear tooth loading but higher cylinder counts typically lead to increased complexity and cost. In this case, a 5-cylinder arrangement appears to be a reasonable compromise between reduced gear tooth loading, and overall engine complexity.

Chapter 3: Geometric Engine Simulation

The internal kinematics of this engine are more complex than a typical piston engine, so in order to mathematically define the motion of the piston, unique equations must be developed. First, a few terms must be defined with reference to the simplified engine diagram below.

The important parameter that must be determine is Sy, the vertical position of the center of the wrist pin, and most of the other variables referenced in the diagram to the right are only calculated so that Sy can be determined. Once Sy is determined for a given crank angle and variator angle, then the instantaneous cylinder volume may be calculated, which will lead to the determination of pressure and temperature profiles within the cylinder.

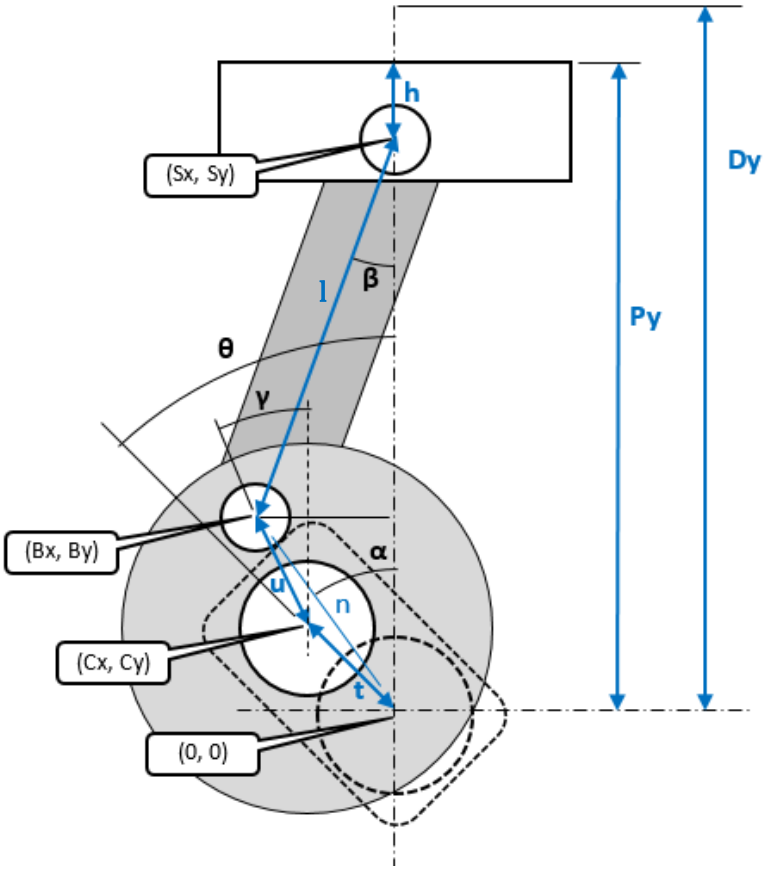

Figure 4: Conrod system sketch

The mechanical system may appear complicated, but fundamental trigonometric equations can be used to determine all values in terms of the design constants **(t, u, l)** and the independent variables **(θ, γ)**. Once the X and Y coordinates for point B are determined, the Y coordinate for point S can be found using the Pythagorean Theorem.

$$B_x = t \sin\theta + u * \sin\gamma$$

$$B_y = t \cos\theta + u * \cos\gamma$$

$$S_y = B_y + \sqrt{l^2 - B_x^2}$$

Combining the above equations results in the general equation

$$S_y = t\cos\theta + u\cos\gamma + \sqrt{l^2 - (t\sin\theta + u\sin\gamma)^2} \qquad \textit{(Eq. 1)}$$

This position equation may be used to determine the location of the center of the piston wrist pin, and therefore the position of the piston itself. The movement of the piston will be used to calculate many properties of the working fluid within the piston-cylinder assembly. To accomplish this, the first and second derivatives of the position equation will be found. The first derivative of the piston position is the piston velocity, and the second derivative is piston acceleration.

The first two terms have simple derivatives:

$$\frac{d}{d\theta} t\cos\theta = t\left(\frac{d}{d\theta}\cos\theta\right) = t(-\sin\theta) = -t\sin\theta$$

$$\frac{d}{d\theta} u\cos\gamma = u\left(\frac{d}{d\theta}\cos\gamma\right) = t(0) = 0$$

The derivative of the square root term may be found using the chain rule:

$\frac{d}{d\theta}\sqrt{l^2 - (t\sin\theta + u\sin\gamma)^2} = \frac{d\sqrt{a}}{da}\frac{da}{d\theta}$, $where\ a = l^2 - (t\sin\theta + u\sin\gamma)^2\ and\ \frac{d}{da}\left(\sqrt{a}\right) = \frac{1}{2\sqrt{a}}$:

$$\frac{\frac{d}{d\theta}(l^2 - (t\sin\theta + u\sin\gamma)^2)}{2\sqrt{l^2 - (t\sin\theta + u\sin\gamma)^2}} = \frac{\frac{d}{d\theta}(l^2) - \frac{d}{dx}((t\sin\theta + u\sin\gamma)^2)}{2\sqrt{l^2 - (t\sin\theta + u\sin\gamma)^2}} = \frac{-\frac{d}{d\theta}((t\sin\theta + u\sin\gamma)^2)}{2\sqrt{l^2 - (t\sin\theta + u\sin\gamma)^2}}$$

Using chain rule a second time:

$\frac{d}{d\theta}((t\sin\theta + u\sin\gamma)^2) = \frac{da^2}{da}\frac{da}{d\theta}$, $where\ a = t\sin\theta + u\sin\gamma\ and\ \frac{d}{da}(a^2) = 2a$:

$$-\frac{\left(\frac{d}{d\theta}(t\sin\theta + u\sin\gamma)\right)(t\sin\theta + u\sin\gamma)}{\sqrt{l^2 - (t\sin\theta + u\sin\gamma)^2}} = -\frac{(t\sin\theta + u\sin\gamma)(t\cos\theta + 0)}{\sqrt{l^2 - (t\sin\theta + u\sin\gamma)^2}}$$

The three terms are now recombined to yield the equation for piston velocity:

$$v_{piston} = -t\sin\theta - \frac{(t\cos\theta)(t\sin\theta + u\sin\gamma)}{\sqrt{l^2 - (t\sin\theta + u\sin\gamma)^2}} \qquad \textit{(Eq. 2)}$$

The calculation for the second derivative is too lengthy to be examined in the body of this text, but will be covered in the appendix. The second derivative is calculated, yielding an expression for piston acceleration.

$$a_{piston} = -\frac{t^2 \cos^2\theta}{\sqrt{l^2 - (t\sin\theta + u\sin\gamma)^2}} - \frac{t^2\cos^2\theta(t\sin\theta + u\sin\gamma)^2}{(l^2 - (t\sin\theta + u\sin\gamma)^2)^{3/2}} + \frac{(t\sin\theta)(t\sin\theta + u\sin\gamma)}{\sqrt{l^2 - (t\sin\theta + u\sin\gamma)^2}} - t\cos\theta$$

(Eq. 3)

The equation for piston acceleration will be required to calculate the force on the piston due to inertia and acceleration in a later section.

Two plots are generated at extreme variator settings, 0° and 20°. Note that the units of piston velocity and acceleration are mm/rad and mm/rad² respectively. The "rad", or radians, referred to here are that of crank angle position. These units were selected so that engine rpm is irrelevant to the display of these graphs.

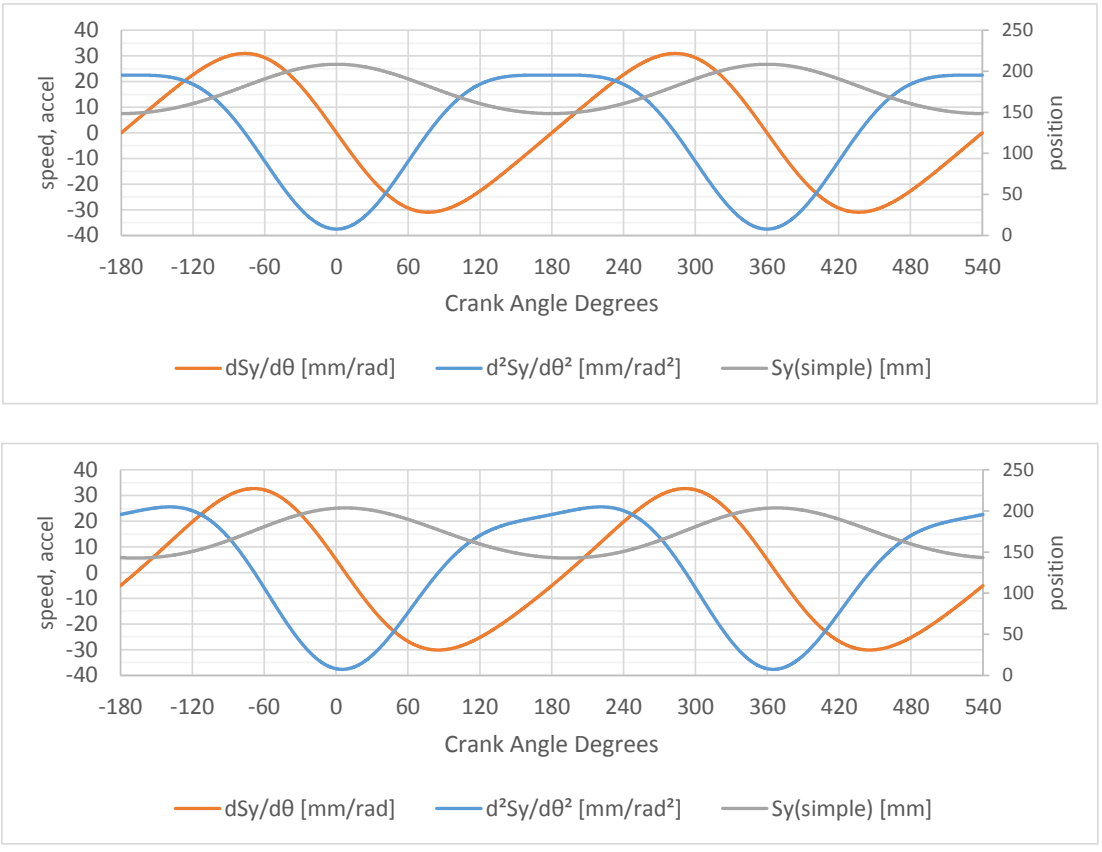

Figure 5: Piston position, velocity, and acceleration

Shown at 0° variator setting (top) and 20° (bottom). Throw = 30mm, rod length = 120mm, conrod big-end pin circle radius = 58.5mm.

From inspection of the two graphs above, several differences become apparent. The top dead center positions of the piston have shifted down from 208 to 203 mm as the variator angle increases. This is the primary function of the variator, and serves to alter the engine compression ratio. The actual swept volume changes slightly, but the difference in top dead center position is what has the largest effect on compression ratio. In addition to the shift in piston position, the shape of the function changes as well, which is more apparent when inspecting the velocity and acceleration plots. These are all unintended side effects of the variator system, which are caused by the nonzero affective crank offset at nonzero variator angles. Because of this, a few features of note become apparent, especially at large variator angles. The most relevant for the mechanical analysis is that the maximum positive piston acceleration increases from about 22 mm/rad² at zero variator angle up to about 25 mm/rad² at -20° variator angle. This maximum in acceleration occurs roughly 220°, *or 40° After Bottom Dead Center (ABDC)*. Higher rod to stoke ratios will push the maximum closer to BDC, and lower ratios increase the gap in timing between maximum acceleration and BDC.

As shown in the graphs below, when the rod length is decreased to 80mm (~1.33:1 rod/stroke ratio), the maximum acceleration climbs to 32 mm/rad², and occurs at 240°, *or 60° ABDC*. Conversely, when the rod length is increased to 180mm (3:1 rod/stroke ratio), the maximum acceleration only reaches about 26 mm/rad², and occurs at only about 200°, *or 20° ABDC*.

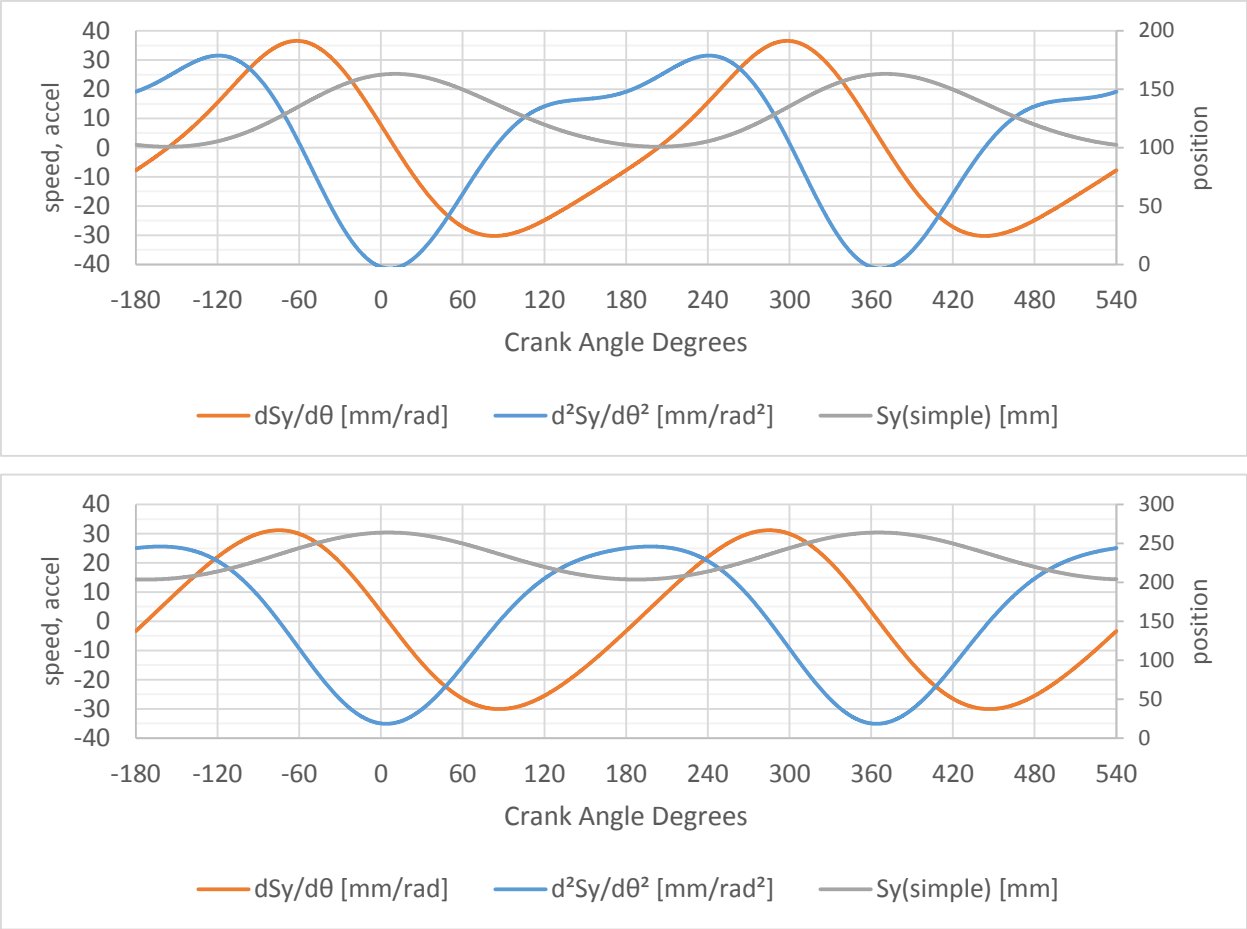

Figure 6: System with 80mm rods (top) and 180mm rods (bottom)
Throw = 30mm, conrod big-end pin circle radius = 58.5mm, variator angle = -20°

Lower piston accelerations are generally considered favorable to higher accelerations, which would suggest the longest rod possible should be used. However, the longer connecting rods will directly lead to an increase in overall engine size. For these reasons, the shortest rods possible that still yield a tolerable maximum acceleration should be used. In most of the following discussion, rods of 120mm length (2:1 rod to stroke ratio) will be considered.

At this point the position, velocity, and acceleration of the piston is fully defined in the Finite Element Analysis (FEA) program.

Chapter 4: Cylinder Volume

Before any analysis of pressure or temperature can occur, the instantaneous cylinder volume must be calculated based on the geometric equations generated in the prior section. A peak compression ratio of 12.15:1 was selected based on being somewhat higher than typical state of the art naturally aspirated gasoline engine available in 2017. Keeping in line with the previously discussed design constants of 120mm conrod center-to-center distance, a 30mm crank throw, and a 58.5mm conrod big-end pin circle radius will be used in this section unless otherwise noted. The piston compression height h is set to 28.9mm, and the bore is set at 94mm based on measurements taken on a production high performance cast piston from an engine with close to a 30mm crank throw.

Note that the piston bore of 94mm is uncharacteristically high for an automobile engine with only a 30mm crank throw (60 mm stroke). However, the piston being used for comparison is from a motorcycle, which typically have much higher bore to stroke ratios than automobile engines. Unless otherwise noted, the 94mm bore from the motorcycle components will be taken as the design constant.

With a 94mm bore and a 60mm stroke, the swept cylinder volume is 416.4 cm^3. To achieve a peak compression ratio of 12:15, then the TDC clearance volume should be 37.35 cm^3 [(37.35+416.4)/37.35 = 12.15]. When the variator is set to angles other than zero, the TDC clearance volume will obviously increase above 37.35, causing the geometric compression ratio to drop much lower than 12.15:1.

Based on this target for the minimum TDC volume (maximum compression ratio target), and using the equations for piston position found in the previous section, it is possible to find the instantaneous cylinder volume for any crank angle at any variator angle. This changing volume is plotted in the main FEA program, and many other cylinder conditions, such as pressure and temperature, are found based on the changing volume as input.

Chapter 5: Motoring Cylinder Temperature and Pressure

In the first part of the thermodynamic analysis, the cylinder walls, cylinder head, and piston will be considered an adiabatic boundary. A heat addition process to the working volume will be modeled, representing the combustion of a hydrocarbon fuel. In the initial analysis, no heat will be allowed to exit the boundary. Once the adiabatic simulation results are examined, a more realistic heat transfer model will be incorporated into the simulation, which will permit some heat to exit the boundary.

First, a "motoring" pressure and temperature profile will be determined, which does not include the heat addition process. Both the temperature and pressure will be calculated at each crank angle division in the FEA. The equations describing the results will be based on *changes* from the previous crank angle. The FEA is set up to begin at the start of the compression stroke, and at this specific starting crank angle position, the temperatures and pressures will be assumed or calculated based on input boundary conditions. This means that if the FEA is set to assess the engine at a specific Intake Manifold Pressure (IMP) and Intake Manifold Temperature (IMT). The IMP boundary setting will depend on the engine load case being examined. The IMP will be set at 320°K to approximate the effects of using a water to air intercooler. The pressure inside the cylinder at the start of compression will be a bit lower than intake manifold pressure due to Volumetric Efficiency (VE) less than unity. As noted, additional equations will be applied so that these starting boundary conditions can be more intelligently estimated.

From *Heywood*, the temperature change due to an adiabatic change in volume can be found using the following equation:

$$T_2 = T_1 * \frac{V_1}{V_2}^{(k_1 - 1)} \qquad \textit{(Eq. 4)}$$

Where V is cylinder volume and k is the ratio of specific heats, which is unit-less. The units used for cylinder volume are irrelevant since the units in the numerator and denominator cancel. The

ratio of specific heats changes primarily with gas temperature, and for dry air, this relationship closely follows the polynomial equation

$$k = 4.055 * 10^{-17}T^5 - 2.681 * 10^{-13}T^4 + 6.650 * 10^{-10}T^3 - 7.258 * 10^{-7}T^2 + 2.491 * 10^{-4}T + 1.375$$

(Eq. 5)

This equation will yield a value of approximately 1.400 for a temperature of 300°K, for example. This equation was found by entering established chart data for specific heats into graphing software and then computing a 5th order trend line, which was shown to closely fit the chart data within the relevant temperature range.

In the equation for T_2 above, the subscripts denote which state the value is being calculated. For the One-Dimensional (1D) FEA, this typically means that variables with the subscript of "1" are used as input from the "prior crank angle", and variables with the subscript of "2" are calculated at the "current crank angle". As the 1D FEA progresses along from one crank position to the next, the "current" values are repeatedly reassigned as the "prior" values. This methodology will apply to many equations described throughout this text. For the first line of the 1D FEA, there will be no "prior" state to reference. In these cases, values will be assumed or calculated, as starting boundary conditions.

Note that calculating the "current" temperature based on the "prior" ratio of specific heats will tend to accumulate a small error in the results. By keeping the change in crank angle very small, this error can be reduced to the level of inconsequence. The 1D FEA examined here has been set to increments of 0.2 crank angle degrees between steps.

The change in pressure due to an adiabatic change in volume can be found using the following equation:

$$P_2 = P_1 * \frac{V_1}{V_2}^{k_1} \qquad \textit{(Eq. 6)}$$

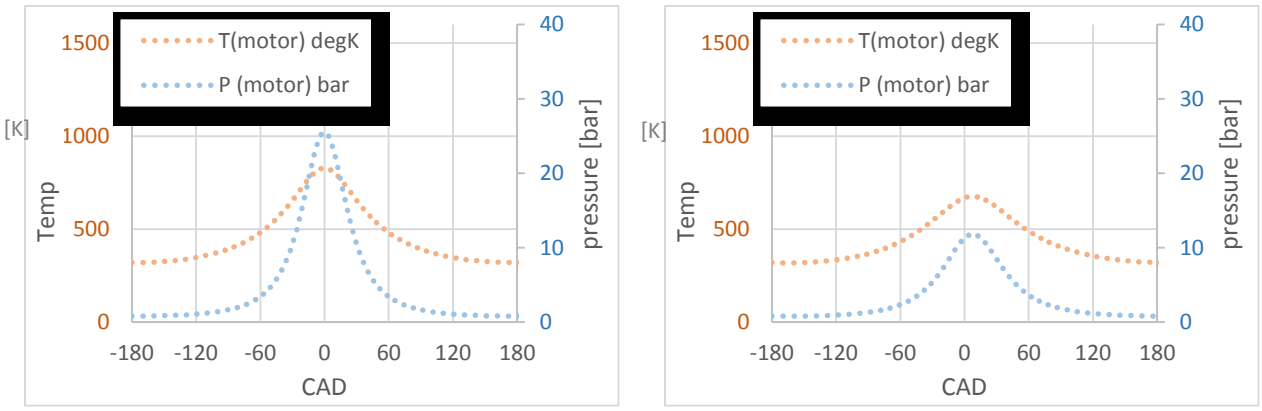

Figure 7: Motoring temperatures and pressures
12:15:1 CR (left) and 6.94:1 CR (right).

In the figure above, two example motoring traces are shown as generated by the FEA. The instance shown on the left is set at a high compression ratio, and on the right, a low compression ratio is shown. Note the maximum values are slightly past zero Crank Angle Degrees (CAD) in the low-compression ratio setting. This is due to the nature of the mechanism; the variator has been angled over from center so the crank angle where volume becomes minimized becomes slightly advanced. It is also clear that the cylinder *pressure* ratio far exceeds the *compression* ratio in both settings. This phenomenon is common to any piston engine operating in a normal atmosphere, and arises due to the ratio of specific heats in the exponent of the above equation being greater than 1.00.

The motoring conditions at any crank angle can now be calculated, given any set of variator angles, starting pressures, and starting temperatures. The next goal is to establish the equations for *fired* cylinder temperatures and pressures. The *fired* conditions as opposed to the *motoring* conditions are calculated with the heat release due to combustion taken into consideration. This will bring the 1D FEA one large step closer to accurately predicting the conditions inside the working volume of the cylinder, but first a few new parameters must be considered.

Chapter 6: Fired Cylinder Pressure and Temperature

The derivation for the fired cylinder pressure begins with the first law of thermodynamics:

$$\Delta U = Q - W \qquad \textit{(Eq. 7)}$$

Meaning that the change in internal energy equals the heat addition minus the work done by the system.

The change in internal energy can be described by the equation

$$\Delta U = mC_v\Delta T \qquad \textit{(Eq. 8)}$$

and the work done by a closed volume can be described by the equation:

$$W = P_{ave}\Delta V \qquad \textit{(Eq. 9)}$$

Furthermore, the average pressure can be described simply in terms of the "prior" and "current" states:

$$P_{ave} = \frac{P_2+P_1}{2} \qquad \textit{(Eq. 10)}$$

At this point, the volume and *motoring* temperature/pressure are known at all points in the FEA, but only the initial *fired* cylinder temperature/pressure is known. Because of this, the *fired* pressure must be redefined in other terms. This is done my incorporating the ideal gas law:

$$P_1 = \frac{mRT_1}{V_1} \; and \; P_2 = \frac{mRT_2}{V_2} \qquad \textit{(Eq. 11)}$$

The above equations can now be combined into the first law of thermodynamics:

$$[U] = [Q] - [(P_{ave}) * \Delta V]$$

Combining with other equations above…

$$[mC_v\Delta T] = [Q] - \left[\left(\frac{mRT_1/V_1 + mRT_2/V_2}{2}\right) * (V_2 - V_1)\right]$$

Which simplifies to

$$[mC_v(T_2 - T_1)] = [Q] - \left[\left(\frac{mRT_1}{2V_1} + \frac{mRT_2}{2V_2}\right) * (V_2 - V_1)\right]$$

This equation must now be solved in terms of T_2 in order to find the *fired* cylinder temperature.

Rearranging the equation yields:

$$T_2C_v - T_1C_v = \frac{Q}{m} - \left[\frac{RT_1(V_2 - V_1)}{2V_1} + \frac{RT_2(V_2 - V_1)}{2V_2}\right]$$

And further rearrangement yields:

$$T_2C_v + \frac{RT_2(V_2 - V_1)}{2V_2} = \frac{Q}{m} - \frac{RT_1(V_2 - V_1)}{2V_1} + C_vT_1$$

The T_2 term on the left-hand side can be factored out to result in the equation:

$$T_2\left(C_v + \frac{R(V_2 - V_1)}{2V_2}\right) = \frac{Q}{m} - \frac{RT_1(V_2 - V_1)}{2V_1} + C_vT_1$$

Which finally yields the following desired form of the equation:

$$T_2 = \left(\frac{Q}{m} - \frac{RT_1(V_2 - V_1)}{2V_1} + C_vT_1\right) / \left(C_v + \frac{R(V_2 - V_1)}{2V_2}\right) \qquad \textit{(Eq. 12)}$$

These equations contain a few new terms: $R, C_v, m \text{ and } Q$.

R is the ideal gas constant. This value is typically looked up from established tables. There are many versions of this constant defined in terms of various units. Care must be taken to match the appropriate units of the *R* constant so that the corresponding units in the other terms of the equation are canceled out. For example, if the energy units are J (Joules) and the mass units are mg (milligrams), then the appropriate form of the *R* constant would be 0.000287 J/mg°K. The order of magnitude of the heat released in a single stroke of a typically sized cylinder is several hundred joules and the air mass contained within a single intake stroke of the same cylinder is on the order of a few hundred milligrams. Because of this, the *R* constant value of 0.000287 J/mg°K will be used in this analysis.

The next new term is $C_v$which is the specific heat, at constant volume. Much like the ratio of specific heats above, this parameter varies primarily with the temperature of the gas, and a polynomial was found by curve fitting tabular data to yield the equation:

$$C_v = -4.663 * 10^{-17}T^5 + 3.497 * 10^{-13}T^4 - 9.785 * 10^{-10}T^3 + 1.196 * 10^{-6}T^2 - 4.284 * 10^{-4}T + 0.761$$

(Eq. 13)

This results in the value of C_v in units of J/g°K. In the 1D FEA program, the value is divided by 1000 to convert to the more convenient units of J/mg°K

The term *m* is the mass of air contained within the cylinder, which will be considered as constant other than during the gas exchange process. The amount of air mass in the cylinder will be determined in a later section based upon intake manifold air density and volumetric efficiency.

The final term is *Q* which is the amount of heat added to the working fluid within the cylinder. It is relatively easy to calculate the total amount of heat that will be added to the working fluid, but in order to accurately model a real-world combustion process, not all of the heat should be added instantaneously. For this parameter, once the total amount of heat added per stroke is determined, another mathematical process is used to break up the total amount into much smaller discrete values of heat, and then each one of those values is added at the appropriate crank angle step. The way in which this is done is examined in the next section.

The fired cylinder pressure is simply the motoring cylinder pressure multiplied by the ratio of fired temperature to motoring temperature as shown in the equation

$$P_{fired} = P_{motoring} * \frac{T_{fired}}{T_{motoring}}$$

(Eq. 14)

Chapter 7: Mass Fraction Burned

To accurately model the heat release during the power stroke of an Otto cycle, the fraction of heat released at any given step in the 1D FEA must be estimated. Complex Computational Fluid Dynamic (CFD) analysis of the combustion process is beyond the scope of this work. A close approximation to this process can be modeled using the Wiebe function:

$$MPB = 1 - exp\left[-b\left(\frac{\theta-\theta_s}{\Delta\theta}\right)^c\right] \quad \textit{(Eq. 15)}$$

MPB is the Mass Percentage Burned. θ is the independent variable, the specific crank angle to be assessed. θ_s is the crank angle when the burn process begins, similar to the spark timing value in an actual engine. The selection of the spark advance angle is a key controlling parameter in actual spark ignition engines. There are typically a few degrees of ignition delay between the spark event and a significant start of combustion. This analysis will focus on the actual start of combustion, so when tuning a real engine based on this data, a few more degrees of advance may be needed. $\Delta\theta$ is the duration in crank angle degrees that the burn occurs. Constants *b* and *c* are values typically assumed to be 5 and 2, respectively (*Heywood, 1988*).

If the number of milliseconds it takes to combust the mixture remained constant over the entire speed range of the engine, then either the mixture would burn over too few a number of crank angle degrees at low rpm, or the mixture would burn over too large a number of crank angle degrees at high rpm. Burning over too low a number of crank angle degrees results in an abnormally rapid rise in cylinder pressures, which may be harmful to structural engine components (pistons, conrods, head studs, etc.). Burning over too high a number of crank angle degrees can result in low thermal efficiency, or in extreme cases, the charge may still be burning when the exhaust valve opens, leading to thermal damage of the downstream components (exhaust valve, turbocharger, etc.). In real world engines, the amount of time (or number of crank angle degrees) over which heat release take place is primarily influenced by combustion chamber geometry and the level of mixture turbulence present in the combustion chamber. The level of turbulence typically being a result of combustion chamber geometry and inlet path geometry. In real-world engines, the level of turbulence should be adjusted to yield the best performance for the given engine, based largely

on its desired effective rpm range. This typically involves shaping the intake path, intake valve-to-seat interface, piston crown, and cylinder head combustion chamber to govern the level of turbulence. Typically, the degree of turbulation will increase proportionally with engine rpm; the higher the rpm, the faster the peak piston speed, the faster the air is drawn in, the higher the Reynolds number, the more turbulence will develop, the faster flame front and thus, the lower the amount of *time* the heat release occurs in. This is often advantageous because at high engine rpm the power stroke lasts for fewer milliseconds, meaning that the mixture also *should* burn over the course of fewer milliseconds. This means that while the burn *time* will change considerably at different rpms, the burn *angle* will naturally change to a much lesser degree. The specific burn angles used in the simulation will be discussed further in the analysis sections blow.

With all input parameters to the Wiebe function either set or calculated, the MPB result can be assessed at any given crank angle. In the 1D FEA the MPB is calculated at each time step in the analysis. Over a four stroke cycle the Mass Percentage Burned will look something like the curve shown below.

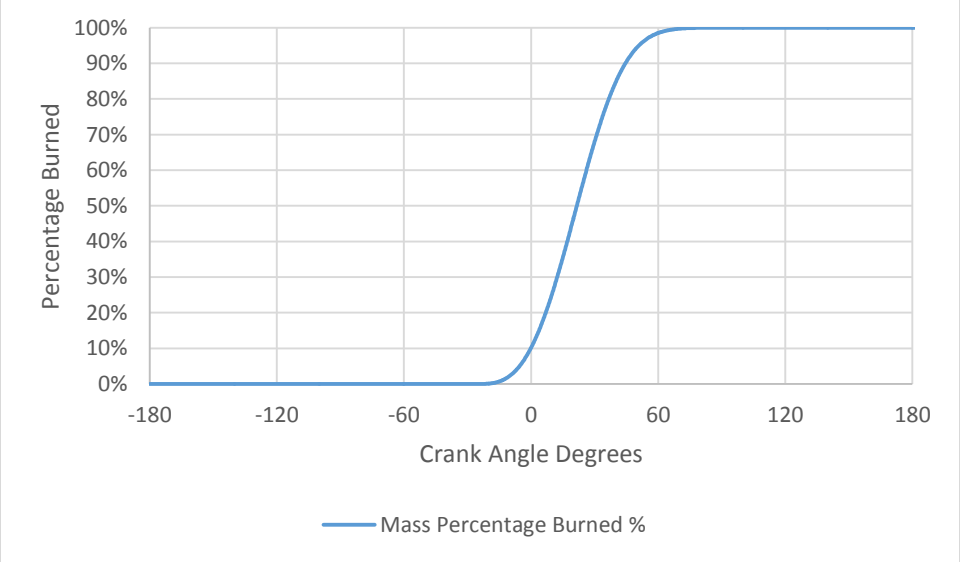

Figure 8: Mass Percentage Burned

Shown with start of combustion at 35°BTDC and a duration of 120°

Another consideration are physical features of an internal combustion engine, which can control the burn duration. The concept of burn duration as a function of turbulence level has been discussed above. Some engines employ features that allow the turbulence level in the cylinder to

be altered, usually by the electronic Engine Control Unit (ECU) based on outside input conditions. The most common approach involves adjusting the velocity of the air entering the cylinder, often by shutting off airflow to one of the two intake valves. This can also be done on engines with a single intake valve if the port is divided into two chambers until just upstream of the valve head. Another potential approach is to include two spark plugs in each cylinder. When it is desirable for the burn duration to be slow, one of the two spark plugs may be deactivated. When it is desirable for the burn duration to be fast, both spark plugs may fire spontaneously, creating two separate flame kernels within the combustion chamber.

When activated, both of these strategies result in the burn duration (in crank angle degrees) being decreased considerably. Because a detailed analysis of the exact burn duration is beyond the scope of this work, a few different possibilities will be explored. In some of the FEA iterations, a relatively rapid combustion process will be modeled, and in other iterations, the burn will be set slower.

Chapter 8: Volumetric Efficiency and Thermal Energy

In the previous section the *shape* of the mass percentage burned was established which will feed into the equation for temperature. In this section, the total amount of thermal energy released over the four-stroke cycle will be determined. In order to determine the amount of heat energy released, the amount of fuel in the cylinder must be determined. To determine the fuel mass in the cylinder, the amount of air mass in the cylinder must be found.

Based on the input variables of intake manifold pressure and temperature, the intake manifold density can be easily calculated using the equation

$$\rho = \frac{P}{RT} \qquad \textit{(Eq. 16)}$$

Where P and T are the pressure and temperature in the intake manifold, respectively. Because it is preferable to report the pressure in units of bar, air mass in units of mg, and volume in units of cm^3, the value of the ideal gas constant, R, that will be used is 0.00287 J/mg°K. For example, at 273°K and 1 bar, STP conditions, this equation yields a density of 1.28 mg/cm^3.

Once the density of air in the intake manifold is known, the amount of air mass that enters the cylinder is found based on the engines Volumetric Efficiency (VE). At 100% VE, the density of air mass trapped in the cylinder (at BDC) will equal the density in the intake manifold. Typically, the VE in an actual engine is a bit lower than 100%. A well-designed cylinder head, intake manifold, and exhaust system should permit the VE to reach peak values as high as 95%. The VE percentage will change significantly with engine rpm. Generally, the VE will be at a maximum value around where the engine torque curve is at a maximum value. Engine designers typically target the torque curve to reach a maximum value somewhere near the middle of the engines full rev range, sometimes higher for race vehicles, or lower for trucks. The target peak rpm for the simulation is around 8000 rpm, so the VE will be set to reach a maximum value of 95% at between 4000 and 5000 rpm. A conservative VE curve will be developed around this point. The VE will drop down to 85% at 1000 rpm, and drop down to 80% by 8000 rpm, and follow a parabolic shape. It should be noted that above and throughout this text the value for VE will be assessed on a *relative*

basis to the intake manifold conditions. Other texts may discuss VE in terms *absolute* to the atmosphere outside of the engine.

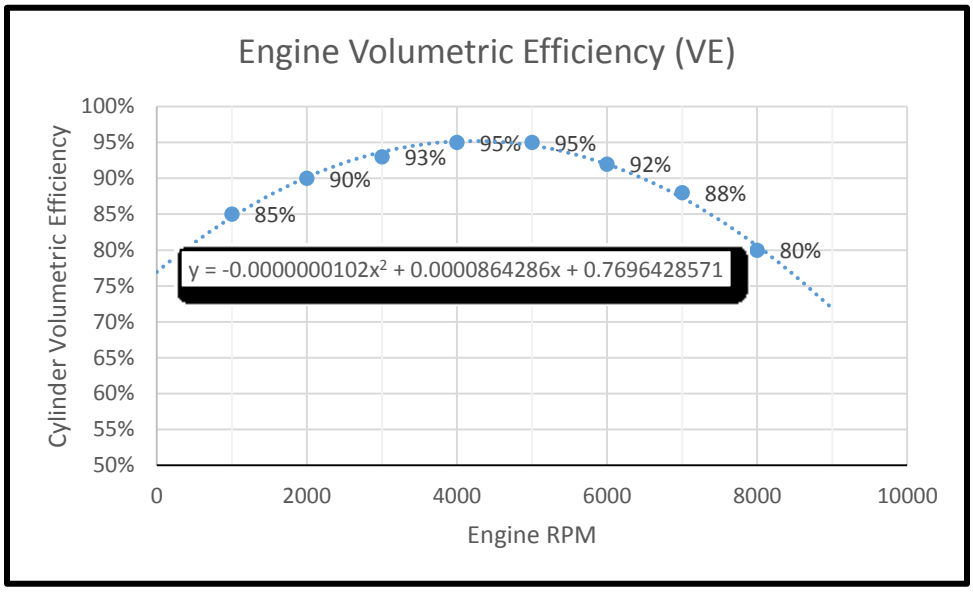

Figure 9: Volumetric Efficiency curve

Microsoft Excel was used to generate a best-fit second order polynomial, which is shown in the figure above. In the 1D FEA, the polynomial will be used to calculate the VE given the rpm value set in the simulation. The VE curve will remain fixed throughout the body of the analysis section below.

With the VE percentage now known given the engine rpm, the air mass trapped in the cylinder can be found using the following equation:

$$m_{air} = \rho_{manifold} * \%VE * V_{max} \qquad \textit{(Eq. 17)}$$

Where V_{max} is the maximum size of the cylinder, which varies somewhat in this variable compression ratio engine, depending on the variator setting. The volume calculated in the previous section is used in the FEA to find the maximum volume for each FEA iteration, and this value is automatically plugged into the equation above for V_{max}.

Now that the amount of air mass trapped in the cylinder is known, the amount of fuel mass trapped in the cylinder can be found. It is assumed that this engine is running on gasoline, which has an air-to-fuel stoichiometric ratio of 14.7:1. In reality, additional fuel may be added to the mixture, especially near peak power. However, this fuel does not react chemically with the air, and

therefore does not release heat. In fact, the purpose of adding this extra fuel is so that it may *absorb* some heat, and keep the exhaust gas temperatures climbing too high, or to avoid detonation within the cylinder. Because of this, the extra fuel that may be added in reality will be ignored in the simulation in regards to the release of heat. The amount of air mass in the cylinder will be divided by 14.7, and this will yield the amount of fuel mass in the cylinder.

$$m_{fuel} = \frac{m_{air}}{14.7} \qquad \textit{(Eq. 18)}$$

With the mass of fuel trapped in the cylinder known, the amount of chemical potential energy can be calculated. Empirical data indicates that the lower heating value of gasoline is 42.4 J/mg on average. A combustion efficiency of 98% will be assumed, meaning that 2% of the air trapped in the cylinder is not able to react chemically with the fuel, typically due to being trapped in crevices within the combustion chamber. The total amount of heat which will be released during the combustion process, can be found with the equation

$$Q_{total} = m_{fuel} * 0.98 * 42.4 \qquad \textit{(Eq. 19)}$$

This *total* amount of heat released will be divided into discrete small releases of heat over the course of the combustion event as determined by the previously established Wiebe function for Mass Percentage Burned (MPB).

Chapter 9: Heat Transfer Out of the Cylinder

Up until this point, the thermodynamic analysis of the conditions within the cylinder have only been examined adiabatically. In this section, the heat lost through the cylinder walls and into the outside environment will be assessed. This will involve calculating a heat transfer coefficient, calculating the exposed surface area, and calculating the difference in temperature between the working fluid and the combustion chamber walls.

First, the Woschni model equations will be used to calculate the heat transfer coefficient. The Woschni model generates results for a spatially-averaged, but not time-averaged heat flux. This means that a new instantaneous flux will be calculated for every time-step in the FEA, but the number generated will be an average value for the entire combined surfaces of the combustion chamber; The piston crown, cylinder walls, and cylinder head will all be assumed to have the same heat transfer coefficient. The Woschni model for a four-stroke, water-cooled, four-valve, spark-ignition *without swirl* predicts an average cylinder gas velocity $v_{fluid(ave)}$ (in meters per second) of:

- $v_{fluid(ave)} = \left[6.18 * v_{piston}\right]$ *(Eq. 20)*
    - *during the gas exchange process (intake and exhaust phases)*
- $v_{fluid(ave)} = \left[2.28 * v_{piston}\right]$ *(Eq. 21)*
    - *during the compression process*
- $v_{fluid(ave)} = \left[2.28 * v_{piston} + 0.00324 \frac{VT_r}{P_r V_r}\left(P - P_{motoring}\right)\right]$ *(Eq. 22)*
    - *during combustion/expansion*

Where

- v_{piston} is the instantaneous speed of the piston.
- V is the instantaneous cylinder volume.
- T_r V_r and P_r are a temperature, volume, and pressure taken at some reference point.
    - Here, the reference point are the states at the *start of compression.*
- P is the instantaneous cylinder pressure.

- $P_{motoring}$ is the instantaneous pressure that *would* be present in the cylinder in the case of motoring conditions.

The units used for volume and pressure are irrelevant since they cancel out. For temperature, units of Kelvin must be used. In the FEA, a series of if/then operations are used to determine which of the three equations above should be used at the given line in the simulation.

Recall from an earlier section, the equation for piston velocity was found by calculating the first derivative of piston position resulting in the equation

$$v_{piston} = -t\sin\theta - \frac{(t\cos\theta)(t\sin\theta + u\sin\gamma)}{\sqrt{l^2 - (t\sin\theta + u\sin\gamma)^2}}$$

Where *t, u,* and *l* are in units of meters. This equation gives the piston speed v_{piston} in units of length *per radian*. To reach a result in meters per second, the v_{piston} result must then be multiplied by the currently selected engine speed in radians per second. Typically, engine speeds are reported in Rotations Per Minute (rpm), so the following complete conversion may be used:

$$\omega_{engine}\left[\frac{radians}{s}\right] = \omega_{engine}\left[\frac{rotations}{minute}\right] * \left[\frac{1\ minute}{60\ s}\right] * \left[\frac{360\ degrees}{1\ rotation}\right] * \frac{\pi}{180}\left[\frac{radians}{degree}\right]$$

For example, an engine speed of 6000 rpm is equal to a speed of about 628 radians/s

Now, given a user-defined input engine rpm, for any line in the simulation the instantaneous piston speed can be found. Furthermore, using the Woschni equations, the average gas velocity can be estimated.

Using the values above, the resulting heat transfer coefficient $H_{Woschni}$ is found using the Woschni correlation:

$$H_{Woschni} = 3.26B^{-0.2}P^{0.8}T^{-0.55}v_{fluid(ave)}^{0.8} \qquad \textit{(Eq. 23)}$$

Where

- $H_{Woschni}$ is a heat transfer coefficient in units of Watts per square meter-Kelvin.
- *B* is the bore of the cylinder in meters.
- *P* is the instantaneous cylinder pressure in kPa.
- *T* is the instantaneous average cylinder temperature in Kelvin.

- $v_{fluid(ave)}$ is the average gas velocity in the cylinder in meters per second found above.

Next, the actual area of the chamber exposed to the working fluid must be found. This area will be divided into three components: The cylinder walls, the top of the piston crown, and the bottom of the cylinder head combustion chamber. The cylinder walls are simply a cylindrical area with diameter equal to the cylinder bore, and the height will be calculated at each step in the FEA based on the position of the piston. The top of the piston crown and bottom of the cylinder head combustion chamber are roughly planar circles with diameter equal to the piston bore. However, since in reality piston crowns and cylinder head combustion chambers have some contours, reliefs, and scallops, the simple circular area will be increased by 15% in an attempt to approximate the additional surface area imposed by these features. This results in the following equation for combustion chamber total approximate area:

$$A_{chamber} = 2 * 1.15\pi \left(\frac{B}{2}\right)^2 + j\pi B \qquad \textit{(Eq. 24)}$$

Where B is the cylinder bore, and j is the instantaneous chamber height, which is easily found at every step in the FEA using the established equations for piston position.

The last step before finding the actual heat flux is to determine the difference in temperature between the working fluid, and the combustion chamber walls. The temperature of the working fluid has been determined in the prior sections, but the temperature of the walls must still be estimated. A detailed analysis of the surface temperatures at many spots within the combustion chamber is beyond the scope of this text. It is clear that a higher surface temperature will tend to reduce the heat flux out of the cylinder, however material consideration imposes practical limits on these temperatures. On the cylinder bore, a thin layer of oil must be present to lubricate the piston rings. It is not practical for this surface to reach temperatures much over 200 °C, or the protective oil will quickly thermally breakdown. The piston crowns are designed to have minimal side clearance to the bore to reduce crevice volume and limit oil carry-over, and thereby reduce unburned hydrocarbon emissions. The piston to bore gap must be kept to a relative minimum, even when the engine has been cold started. Due to these tight design clearances, it is difficult to design an aluminum piston to reach a very high operating temperature, have a tight clearance to the bore when cold, and avoid seizure due to thermal expansion. The cylinder head must be able to retain valve seats, remove heat from the hot exhaust valve heads, and must keep the temperatures

of surfaces in its oil gallery below values that would thermally degrade the oil. For all of these reasons, the surface temperature of the cylinder head at the combustion chamber must also be limited to relatively low values compared to the working fluid temperatures.

For the sake of a simplified analysis, the temperatures of all surfaces exposed to the combustion chamber will be assumed equal. For this analysis, a bulk surface temperature of 200°C (or 473°K) will be assumed.

Based on these equations, the FEA simulation shows that the VCR engine at moderate loads and speeds produces instantaneous surface heat fluxes around 3 megawatts per square meter. Based on the size of the combustion chamber surface areas, a maximum instantaneous heat rejection is approximately 50 kilowatts. Note that these are *peak* instantaneous values at some time step in the simulation; the average values over the entire 4-stroke cycle are much lower. *These values are comparable to example data cited by Heywood in section 12.6.2.*

Chapter 10: Diabatic Gas Temperature

Note that the term "diabatic" is the most commonly accepted antonym of "adiabatic". *Diabatic* suggests that there *is* heat transfer occurring at the system boundary.

With the heat flux out of the cylinder known, a new more realistic gas temperature can be calculated. For each line in the FEA, a new heat transfer coefficient has been established. The FEA also continuously calculates the adiabatic gas temperature within the cylinder. The exposed surface area is continuously recalculated based on the equations for piston position. This yields the heat transfer equation

$$H = h_{Woshni} * A_{chamber} * (T_{adiabatic} - T_{wall}) \quad \textit{(Eq. 25)}$$

Where H is the total heat transfer (per cylinder) in Watts. Recall that a wall temperature of 473°K will be assumed.

To find the number of Joules of thermal energy, $E_{thermal}$, lost to the surroundings in each step of the FEA, the instantaneous value for H is simply multiplied by the step duration of the FEA, multiplied by the engine speed.

$$E_{thermal} = \Delta_{FEA} * \omega_{engine} * H \quad \textit{(Eq. 26)}$$

Where Δ_{FEA} is the number of crank angle degrees spanned by each step in the FEA (set to 0.2 for this particular FEA), and ω_{engine} is the speed of the engine in degrees per second.

With this, a new more accurate calculation for the gas temperature in the cylinder can be found

$$T_{Woschni} = T_{adiabatic} - \left(\frac{E_{thermal} * m_{cylinder}}{C_{v(adiabatic)}}\right) \quad \textit{(Eq. 27)}$$

Where $m_{cylinder}$ is the total calculated air mass within the cylinder, which will vary greatly from one configuration of the FEA to the next. $C_{v(adiabatic)}$ is the specific heat at constant volume of the air within the cylinder, assuming the air is at its previously calculated adiabatic temperature. Any units may be used for the variable within the parenthesis provided they cancel out.

As expected in the FEA, increasing the initial cylinder pressure increases both the heat flux, and drives a greater difference between adiabatic and diabatic temperature traces. It is noteworthy that in the FEA, increasing the engine speed typically increases the heat flux, but slightly *decreases* the difference between adiabatic and diabatic temperature traces. This is because the higher piston velocities are driving higher gas velocities and therefore higher heat transfer rates, but conversely a 4-stroke cycle will take less time to complete, reducing the opportunity for heat to leave the working fluid. Because the Woschni correlation yields a new more accurate gas temperature based on its calculated adiabatic temperature and on its specific heat value *at* that adiabatic temperature, a second iteration of the Woschni process was preformed minimize any compounding error.

New values for h, H, $E_{thermal}$, and $T_{Woschni}$ were found using the previously calculated values as input. This was shown to result in gas temperatures somewhat *higher* than predicted in the first Woschni iteration, though still lower than the adiabatic values. At most speed and load setting, the difference between the first and second Woschni iteration was very small. However, at very high engine loads, particularly at low engine speeds, the difference between the iterations was large, and so a *third* Woschni iteration was conducted. As shown in the charts below, the Woschni iterations tend to converge on a limit value. It is also apparent that the error between the second and third iteration is very small at most FEA settings. The difference between the second and third iteration becomes noticeable at low engine speeds and high loads. This low speed / high load "corner" of the operation map will be somewhat limited because the engine is being modeled as turbocharged (not supercharged), so very high manifold pressures at very low engine rpm are not typically attainable. For these reasons, it is deemed adequate for the FEA to stop at three iterations of the Woschni calculations.

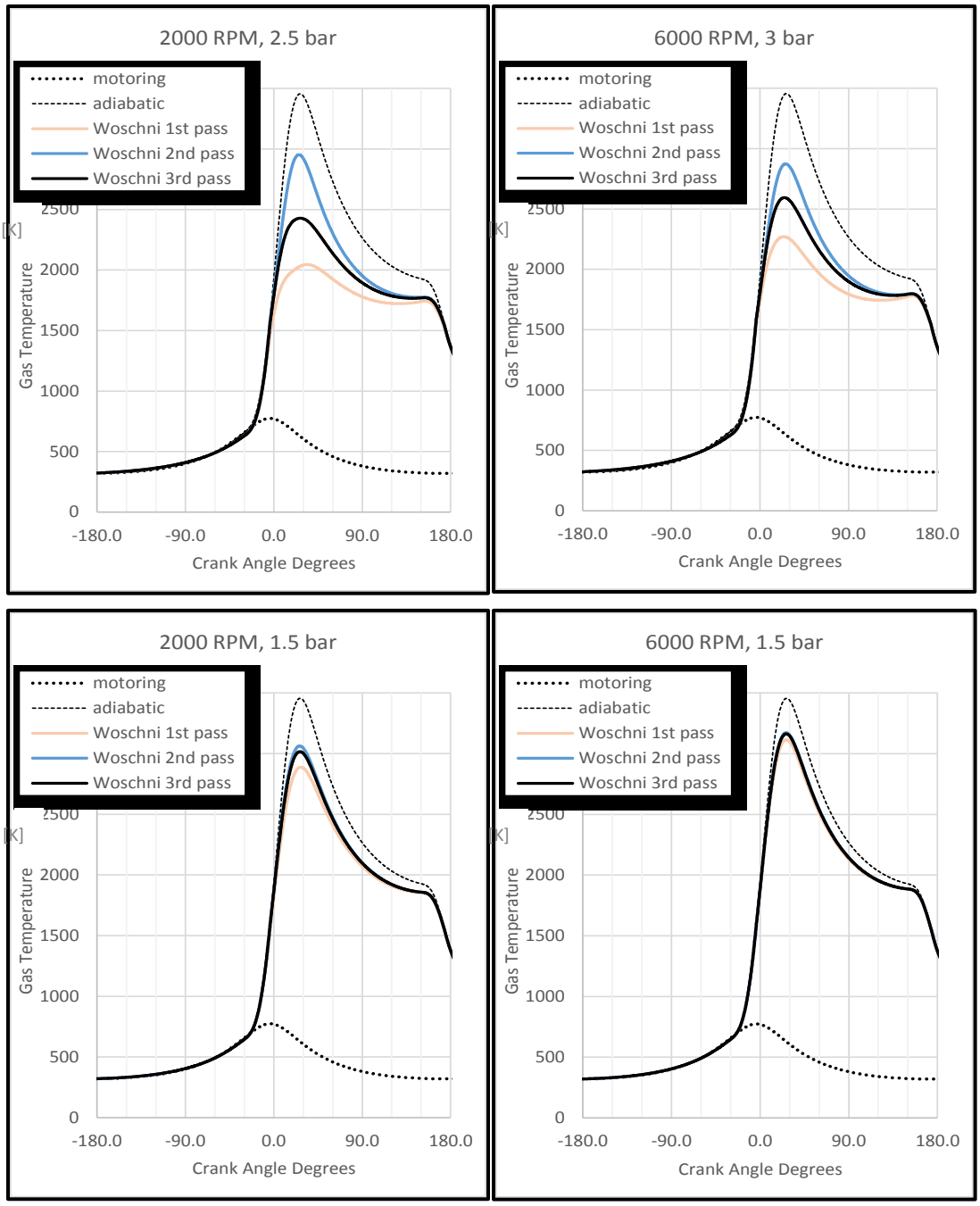

Figure 10: Woschni heat loss iterations

In the figures above, it is clear that there is only a significant difference in the Woschni iterations at high intake manifold pressure conditions. The situation depicted in the upper-left corner of 2.5 bar at 2000 rpm is approaching an unacceptably larger difference between the second and third Woschni iteration. However, this condition is only shown for reference as it will not be practical

to design a turbocharger system capable of producing this much manifold pressure at such a low engine rpm while still being able to meet the other performance goals. The FEA is configured so that three iterations of the Woschni calculations each time the FEA input conditions are changed. Only values found in the *final* iteration are used for subsequent parameter calculations shown below.

Chapter 11: Diabatic Cylinder Pressure

With the diabatic gas temperature $T_{Woschni}$ within the cylinder calculated in the above section, it is possible to calculate the cylinder pressures under the same heat loss conditions using the following equation:

$$P_{Woschni} = P_{motoring} * \left(\frac{T_{Woschni}}{T_{motoring}}\right) \quad \textit{(Eq. 28)}$$

Where $P_{motoring}$ and $T_{motoring}$ are the unfired cylinder pressures and temperatures calculated in an earlier section. In the FEA, this equation results in a trace of the cylinder pressure reflective of the diabatic gas temperatures within the cylinder calculated using the third iteration of the Woschni heat transfer equations. That is, the pressure trace predicted by Woschni is somewhat lower than the adiabatic trace, particularly at high pressures. This pressure curve will be used to assess the brake mean effective pressure in the cylinder, but the curve must first be refined and adjusted as described in the following sections.

Chapter 12: Blow Down

Toward the end of the power stroke, the exhaust valve will open; typically well in advance of bottom dead center. When this occurs, the pressure calculated by $P_{Woschni}$ in the previous section will begin to become inaccurate. After some short amount of time, the pressure in the cylinder will bleed down from the value calculated by $P_{Woschni}$ and approach the Exhaust Manifold Pressure (EMP). A complicated dynamic analysis of the instantaneous pressures within the exhaust manifold due to pulsation are beyond the scope of this work. Instead, a time-averaged exhaust manifold pressure will be assumed. To make this estimate, a simplified equation will be used, which involves some assumptions about exhaust manifold pressures in a relatively free-flowing turbocharged engine. For a well-matched turbine and compressor stage on a gasoline engine, the exhaust manifold pressure should be slightly *lower* than the intake manifold pressure in most situations where the turbocharger is producing positive boost pressure. This phenomenon is owed to the high turbine inlet temperature that is typically present. The turbine must collect enough fluid energy from the exhaust stream to adequately power the compressor to do compression work at high mass flows, plus any inefficiencies in the turbocharger system. The turbine and compressor convert energy per the equations

$$W_{turbine} = \dot{m}_{turbine} * C_p * T_{turbine,inlet} * \left(1 - \left(\frac{P_{turbine,inlet}}{P_{turbine,outlet}}\right)^{k-1/k}\right) * \frac{1}{\eta_{turbine}}$$

(Eq. 29)

$$W_{compressor} = \dot{m}_{compressor} * C_p * T_{compresor,inlet} * \left(1 - \left(\frac{P_{compressor,outlet}}{P_{compressor,inlet}}\right)^{k-1/k-1}\right) * \frac{1}{\eta_{compressor}}$$

(Eq. 30)

It is clear that increasing $T_{turbine,inlet}$ will result in a direct increase to the work $W_{turbine}$. Therefore, the higher the turbine inlet *temperature* available, the lower the turbine inlet *pressure* shall be required to produce the mechanical work used by the compressor. In systems where the exhaust gas temperature is comparatively low, such as on a large diesel engine, then the exhaust

manifold pressure at the turbine inlet may be higher than the intake manifold pressure at the compressor outlet. However, this is typically not the case in a spark ignition gasoline engine under load, provided the turbine and compressor stages of the turbocharger are well matched with respect to each other and to the engine.

It will be assumed that the exhaust manifold pressure will be 80% of the intake manifold pressure whenever the intake manifold pressure is over 1.1 bar (absolute). However, at low to medium load conditions in a spark ignition engine, the intake manifold pressure will be below atmospheric levels. Conversely, the exhaust manifold will always be above atmospheric conditions (ignoring momentary gas dynamics). Therefore, the 80% assumption does not work in these cases. To compensate for settings resulting in intake vacuum conditions (pressure below atmospheric), the exhaust manifold pressure will be assumed to be at 1.1 bar (absolute) at any point the intake manifold pressure is below 1.1 bar (absolute). A simply if-then statement is used in the FEA to determine whether the exhaust manifold pressure will be set to 1.1 bar or alternatively 80% of the intake manifold pressure. In a spark ignition turbocharged engine, the exhaust manifold pressure typically climbs above the intake manifold pressure once the turbine wastegate begins to open as the overall turbine stage efficiency decreases. While not ideal, wastegating is the most common method to limit the work collected by the turbine and thereby limiting the work available to the compressor to act on the incoming air. The result is that the compressor outlet pressure is kept to within a safe limit to avoid excessive cylinder pressures and the resulting detonation and engine damage. However, since the prime purpose of the VCR engine is to allow very high boost pressures without overly stressing the engine, the intake and exhaust manifold pressures will be modeled after a simple turbocharger system that has no wastegate. Therefore, the 80% pressure assumption will remain in effect for all intake manifold pressures over 1.1 bar.

The diabatic cylinder pressures during the power stroke were calculated in the previous section, and now a basic model for the exhaust manifold pressure has been established. It is clear that the pressure in the cylinder will begin to bleed down from $P_{Woschni}$ to $P_{exhaust\ manifold}$ as soon as the exhaust valve opens, but the pressure will not change instantly. To model the quick but non-instantaneous reduction in pressure a Wiebe function will be used. In the 1D FEA, the Wiebe function will be set to begin the pressure transition at the crank angle where the exhaust valves happen to be set to open, and will have completed the bulk of the process over a span of 45 crank

angle degrees. Note that the vast majority of the pressure transition occurs over a span closer to 15 to 20 crank angle degrees, as will be shown in the resulting pressure traces below.

The temperature in the cylinder will also drop during the pressure bleed-down process. To calculate this, a set of values are copied from the body of the FEA, used in a calculation, and the result fed back into the body of the FEA. First, a v-lookup function call is used to copy out the calculated cylinder temperature, pressure, and ratio of specific heats at the instant the exhaust valve has been set to open in the list of input conditions. These values will be known as $T_{@\,EVO}$, $P_{@\,EVO}$, and $k_{@\,EVO}$, respectively. In the subscripts, the "EVO" refers to the instant of "Exhaust Valve Opening". These values obviously vary greatly from one set of FEA input conditions to the next, but the values are unique for each trial of the FEA. Once the v-lookup function brings these values out of the FEA body, they are used in the equation

$$T_{exhaust\ manifold} = T_{@\,EVO}\left(\frac{P_{exhaust\ manifold}}{P_{@\,EVO}}\right)^{k_{@\,EVO}-1/k_{@\,EVO}} \qquad \textit{(Eq. 31)}$$

The $T_{exhaust\ manifold}$ result is then fed back into the body of the FEA. The value is then used as the target cylinder temperature to bleed down to, during the blow down phase. The temperature bleed down follows the same Weibe transition settings as the pressure bleed down described above.

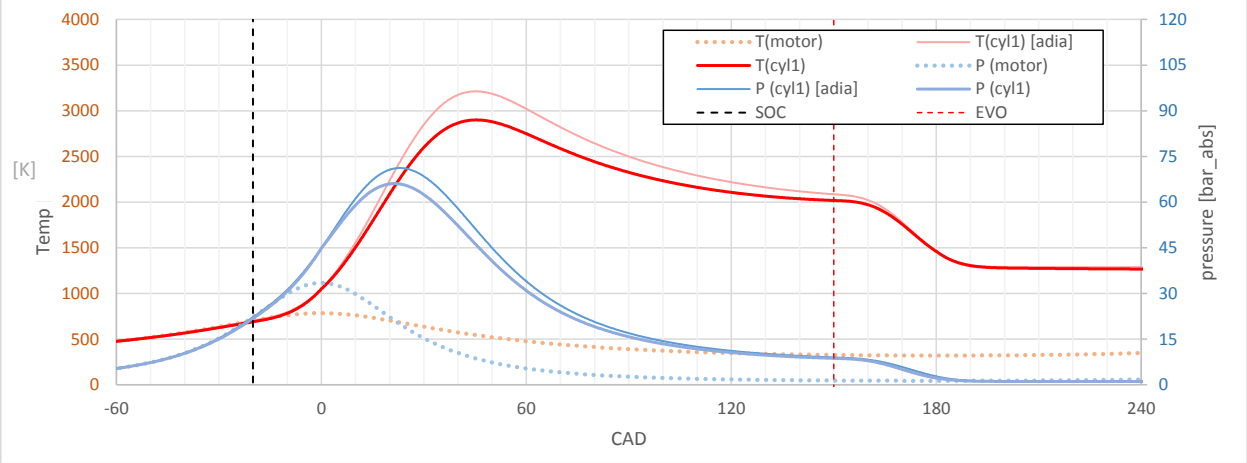

Figure 11: Pressure and Temperature traces

Note that in the figure above, 0° is at top dead center and 180° is bottom dead center. The crank angle at which the exhaust vale opens is shown on the chart as a doted vertical line several degrees before BDC, consistent with typical valve timing in a real engine. Shortly following this event,

the cylinder temperatures and pressures bleed down to exhaust manifold conditions. The curve that describes their bleed down behavior is modeled as a Wiebe function as detailed above. The benefit of opening of the valve in advance of BDC is somewhat evident in examination of the chart. The blow down process does take *some* amount of time, and it is beneficial to release as much pressure as possible from the cylinder by the time the piston begins its upward motion. The more pressure present in the cylinder during the exhaust stroke, the more energy will be taken out of the crankshaft-flywheel system to provide flow work to the exhaust process. This slightly reduces the amount of energy available at the engine output shaft, and is therefore undesirable. However, the positive pressure in the cylinder during the *power stroke* is exactly what is generating the engine work in the first place. Because of this, a balance must be reached to open the exhaust valve early enough to minimize the pressure in the cylinder at the beginning of the exhaust stroke, but not open the exhaust valve so early as to rob the engine of output work unnecessarily.

Another noteworthy result of this process is that the earlier the exhaust valve is opened, the higher the exhaust manifold temperature will be. It can be useful at some speed/load engine settings to open the exhaust valve earlier to provide more thermal energy to the turbocharger turbine. Opening the exhaust valve slightly earlier in the exhaust stroke does rob some energy from the engine crankshaft-flywheel assembly. However, if executed correctly, this should be more than made up for by the extra compression work the turbocharger is now able to provide, thanks to the additional turbine work available. Conversely, opening the exhaust valve too early, particularly at high power engine conditions, can result in excessively high exhaust temperatures, which can destroy the turbocharger or other exhaust system components. This situation leads the engine designer to either find an appropriate balance in exhaust valve timing to adequately satisfy all needs, or employ a variable cam phasing hardware arrangement. To an extent, such a cam phasing system allows the engine calibrator to give the turbine extra thermal energy when it can be used beneficially (throttle tip-in, low to mid-engine speeds), and then reduce the exhaust thermal energy when in abundance (near peak power).

Finding this ideal spot, or series of spots if employing cam phasing, is the result of extensive valve timing simulations and/or real engine testing. However, in the FEA program, the process has been greatly simplified and set to a relatively conventional and static crank angle, and no cam phasing will be simulated. The crank angle for exhaust valve opening can be adjusted in the FEA by simply

changing a cell value, but because valve timing is not the focus of this work, this parameter will not be scrutinized.

Chapter 13: Gas Exchange

Another drastic period of transition occurs during the gas exchange process. Although the blow down phase described above is typically also considered as part of the "gas exchange process", because of the way the 1D FEA is designed, it is better to describe them separately. Furthermore, in an actual engine the gas exchange process can further be broken down into piston-driven exhaust, the valve overlap period, the piston-driven intake, and the final dynamic cylinder-filling portion where air charge continues to enter the cylinder despite the fact that the cylinder volume has begun to decrease. While these discrete phases are often useful to consider separately in a real engine, the gas exchange process has been greatly simplified in the FEA program. In the FEA, the gas exchange process can be summarized as follows:

1. After the blow down process, the cylinder pressure and temperature is assumed to equal exhaust manifold temperature and pressure
2. Once the intake valve opens near TDC, the temperature and pressure in the cylinder quickly, but not instantaneously transition to intake manifold temperature and pressure
3. During the remainder of the intake stroke, the temperature and pressure in the cylinder remain at the intake manifold temperature and pressure

After step 3, the piston has reached BDC and the effective gas exchange process has ended. The amount of air mass in the cylinder at any time during the gas exchange has no effect on any subsequent calculations. However, after BDC the intake passage is considered closed, and the now decreasing cylinder volume begins to produce an appropriate rise in cylinder temperature and pressure as described in the earlier sections. These calculations *do* require an air mass value, which is simply calculated based on the estimated volumetric efficiency curve and intake manifold conditions as described in an earlier section. In this approach, the gas exchange process is modeled as simply a rapid (but non-instantaneous) transition of cylinder pressures and temperatures from exhaust-manifold-like conditions to intake-manifold-like conditions. The assumed volumetric efficiency curve is then employed to determine a reasonable mass of air charge trapped within the cylinder at the moment the intake process ends and the compression process begins. An alternative strategy would be to model a much more complex and dynamic intake, exhaust, and cam timing

system to *generate* a volumetric efficiency curve. However, this level of analysis is typically conducted with purpose-built software such as "GT Power" costing thousands of dollars and is beyond the scope of this work. As an alternative, we have simply estimated a realistic and conservative volumetric efficiency curve, which allows us to set the aforementioned conditions in the cylinder at the start of compression.

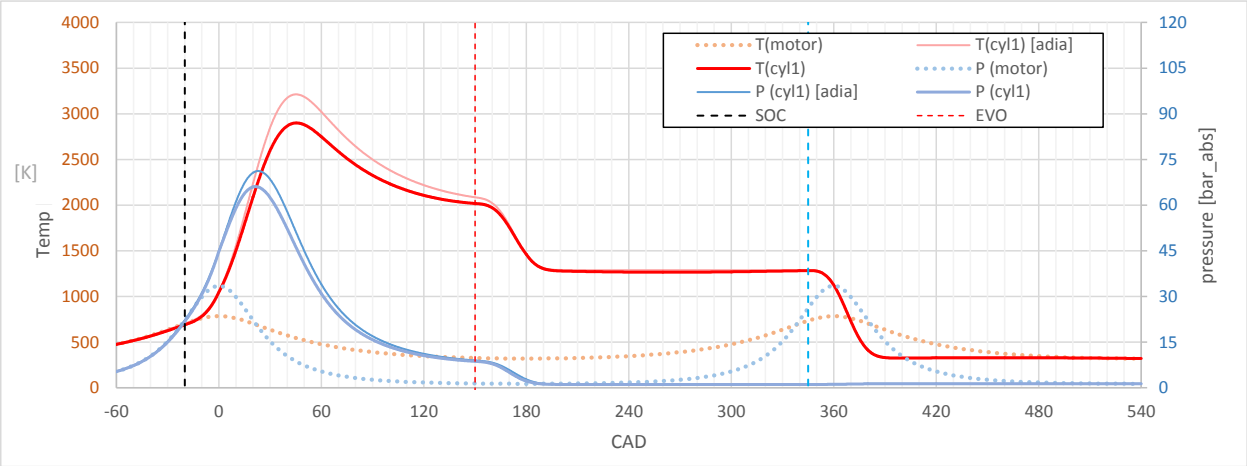

Figure 12: Pressure and Temperature – full cycle

In the figure above, most of the complete 4-stroke cycle is plotted. The exhaust valve opening event is again displayed as a vertical dotted line between 120° and 180° (BDC), and now the intake valve opening event is also shown just before 360° (TDC). Following the intake valve opening event, the temperature of the gas transitions from the exhaust manifold temperature down to the much cooler intake manifold temperature. The curve that shows this transition is a modeled Wiebe function. The cylinder pressure also transitions from exhaust manifold levels to intake manifold levels during this time and following the same Wiebe function. However, the two pressures are very similar to each other in contrast to the peak pressures displayed during the power stroke, so this transition is visible, but not as obvious in the figure.

With the complete four-stroke cycle now modeled for a variety of starting and boundary conditions, it is now possible to calculate important general performance metrics for the engine such as power, and efficiency.

Chapter 14: Engine Performance

In the previous sections, the pressure and temperature in the cylinder was calculated for each discrete section of the 4-stroke cycle. Wiebe functions were used to blend cylinder gas conditions during transition periods such as blow-down and gas exchange. Now that a complete continuous four-stroke simulation has been outlined, important overall engine performance metrics can be calculated.

Thermodynamic net work W_{net} can be calculated for each step in the FEA using the equation

$$W_{net} = P_{ave}\Delta V = \left(\frac{P_2 - P_1}{2}\right) * (V_2 - V_1) \qquad \textit{(Eq. 32)}$$

Because the pressures and cylinder volumes at each step in the FEA are known, it is simple to calculate the work performed at each step. The FEA adheres to the following sign convention for work:

1) When the trapped gas does work on the piston (such as during the power stroke) the values are positive
2) When the piston does work on the gas (such as during the compression stroke) the values are negative.

A summation is then taken of all the work cells to yield a final net work over the 4-stroke cycle, in units of Joules. Typical net values for this engine are about a few hundred Joules, per cylinder, and the sign is positive. If the FEA boundary conditions are set in such a way that would simulate *engine braking*, then the values would sum to a negative total value.

Recall the equation for added thermal energy in the section above

$$Q_{total} = m_{fuel} * 0.98 * 42.4$$

Where m_{fuel} is the fuel mass combusted in the chamber, and the number 42.4 is the energy density for gasoline [in units of MJ/kg]. The result is multiplied by 0.98 as an approximation for the combustion efficiency of the reaction. This equation is used to determine the total thermal energy added to the air mixture during the combustion process at a 98% combustion efficiency, implying

that 2% of the fuel mass added does not release its trapped chemical energy as heat. This is a useful equation for calculating temperatures and pressures in the working gas as was done in the prior sections, however, in order to determine the overall engine efficiency, the 2% of wasted fuel must be accounted for. Therefore, the equation for overall engine thermal efficiency η_{TH} can be expressed as

$$\eta_{TH} = \frac{Work\ Out}{Energy\ In} = \frac{W_{net}}{m_{fuel}*42.4} \quad \textit{(Eq. 33)}$$

In an actual engine there are many sources of inefficiency, such as friction that will result in a measured efficiency considerably lower than the values calculated in the FEA. However, the calculated efficiency values will be useful as a point of comparison from one operational point to the next, and the overall magnitudes should not be assumed reflective of reality.

With W_{net} calculated, a simple equation can be used to calculate output power:

$$PWR = \frac{W_{net}*f}{1000} \quad \textit{(Eq. 34)}$$

Where f is the frequency that the engine executes a four-stroke cycle each second as defined by the equation. The division by 1000 is a conversion factor assuming W_{net} is input in units of Joules, and *PWR* is reported in units of kW.

$$f = \frac{RPM}{(2*60)} \quad \textit{(Eq. 35)}$$

For example, at 3000 rpm, the engine will complete 25 loops of the four-stroke cycle in one second, per cylinder. At a W_{net} of 825 Joules, this will result in a calculated power output of 20.6 kW, per cylinder. For a 5-cylinder engine as discussed above, the total output power would be 103.2 kW.

Chapter 15: Ring and Pinion Gear Tooth Loading

Up to this point, the FEA has primarily focused on thermodynamic calculations. However, some attention will be paid to the level of tooth loading at the variator ring and pinion gear interface. Most of the design characteristics of this engine are not dissimilar from the current art of internal combustion engines. Components such as pistons, wrist pins, main bearings, cylinder liners, and many others would not need to be uniquely designed so as to work in the variable compression ratio engine, therefore in-depth stress and strain calculations for these components is not warranted. However, the variator ring and pinion gear interface has a unique functionality, specific to this variable compression ratio engine design. Therefore, a series of equations will be examined which will lead to the ability to predict the level of loading at these gear teeth. The results will be used to assess the overall practicality of operating the engine at certain settings. That is, if two different settings of the control parameters lead to similar power outputs and thermal efficiencies, but one loads the gear teeth more than the other, the lighter-loading settings will be favored and more thoroughly explored. In a future study, the calculation results may be used to generate specific designs for the gear geometry and material.

The primary force acting on the gear teeth is from the cylinder pressure. The force acting onto the piston from the cylinder pressure must be determined. Because in the previous sections the pressure value in the cylinder for every section of the FEA has been calculated, the force from pressure can be found with the simple equation

$$F_{press.} = (P_{cylinder} - P_{case}) * \pi \left(\frac{B}{2}\right)^2 \qquad \textit{(Eq. 36)}$$

Where B is the cylinder bore $P_{cylinder}$ is the instantaneous cylinder pressure, and P_{case} is the engine Crank Case Pressure (CCP). CCP is typically designed to run just below atmospheric pressure, so for this analysis it will be set at a constant 95,000 Pascals, absolute. If units of Pascals are used for pressure, then Meters should be used for the bore, resulting in Newtons for $F_{press.}$. The pressure in the crank case acts on the underside of the piston, and while typically small compared to cylinder pressure, during the intake stroke when cylinder pressures may also be very low, the crank case pressure may become the dominant source of pressure acting on the piston.

The secondary force acting on the gear teeth is from the piston and connecting rods resistance to liner acceleration, which is a product of the reciprocating motion. The forces acing on the gear teeth due to acceleration are small at low engine speeds, but become exponentially greater at higher speeds.

Recall from an earlier section an equation for piston acceleration was found by taking the second derivative of piston position:

$$a_{piston} = -\frac{t^2 \cos^2\theta}{\sqrt{l^2 - (t\sin\theta + u\sin\gamma)^2}} - \frac{t^2\cos^2\theta(t\sin\theta + u\sin\gamma)^2}{(l^2 - (t\sin\theta + u\sin\gamma)^2)^{3/2}} + \frac{(t\sin\theta)(t\sin\theta + u\sin\gamma)}{\sqrt{l^2 - (t\sin\theta + u\sin\gamma)^2}} - t\cos\theta$$

This equation yields a result in "distance per *radian* squared". In order to produce a value in units of "distance per *second* squared", the result must be multiplied by the square of the engine speed in units of radians per second. This process is conducted at each step in the FEA to produce an instantaneous piston acceleration function. In order to determine the amount of force that results in this acceleration, the mass of the reciprocating assembly must be estimated. A measurement of the piston, wrist pin, circlips, and piston rings from the design-base motorcycle engine shows a total mass of 415 grams. Additionally, the "small end" of the specifically designed aluminum connecting rod was measured as having a mass of 80 grams, yielding a total reciprocating mass of 495 grams. This mass value is then multiplied by the calculated acceleration values at each step in the FEA to produce a continuous acceleration force function.

$$F_{accel.} = m_{recip.} * a_{piston} * \omega^2 \qquad \textit{(Eq. 37)}$$

Where $m_{recip.}$ is the total reciprocating mass as described above, $a_{piston}$is the piston angular acceleration in units of distance per radians squared, and ω is the engine speed in radians per second. Converting the reciprocating mass to kilograms before using the equation will result in an acceleration force in units of Newtons.

A tertiary force acting on the gear teeth will be a result of the sliding friction from the piston, and other nearby joints, such as the wrist pins. These forces will be very small compared to the pressure and acceleration forces, and generating realistic math models to approximate these friction forces would be significantly more involved. For these reasons, the additional forces on the gear teeth from nearby sliding friction will be ignored.

Because the connecting rod is continuously tilting back and forth with respect to the gear teeth, some trigonometric functions must be used to convert the forces acting on the piston to the actual forces passing through the gear mesh.

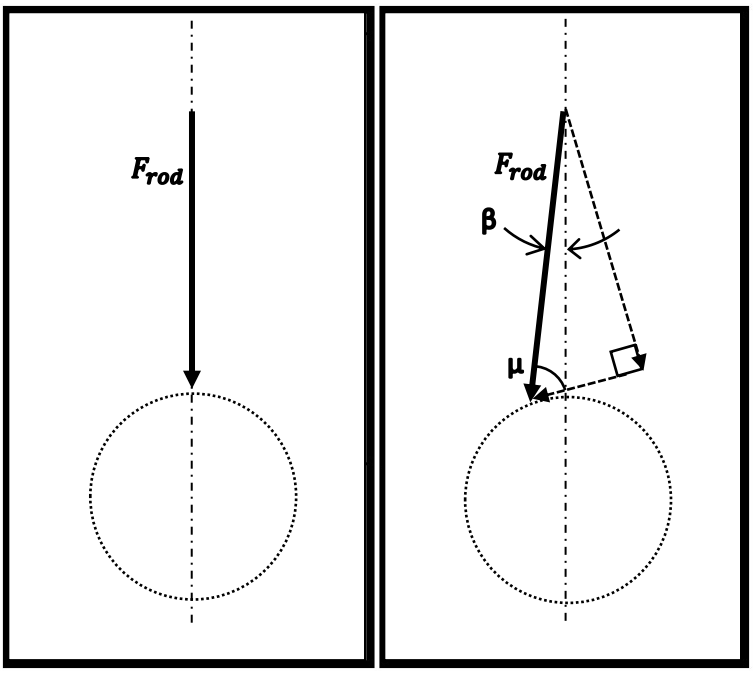

Figure 13: Rod force vector components

Observe that angle β is shown in the image to the right, first defined in the initial engine geometry section above, as the angle between the connecting rod major axis and the centerline of the engine. Because the pressure and acceleration forces act in a direction normal to the piston main axis, they must be divided by the cosine of β to generate the net connecting rod force.

$$F_{rod} = \frac{F_{press.} + F_{accel.}}{cos(\beta)} \qquad \textit{(Eq. 38)}$$

This indicates that F_{rod} will be minimized when the connecting rod is in line with the piston main axis, as β will be 0°, resulting in the denominator equaling unity. At connecting rod angles further from vertical, the denominator will decrease from 1.0, resulting in F_{rod} growing considerably larger than the sum of the pressure and acceleration forces.

In the figure above, the force vector F_{rod} is shown as a solid line. In the image on the right, the component vectors making up F_{rod} are also shown. The first component is tangent to the pitch circle of the gear teeth, and the second component vector is orthogonal to the first. The angle μ is

shown separating F_{rod} and its gear-tangent component vector. It is clear that a larger F_{rod} or an angle μ further from 90° will result in a greater magnitude for the gear-tangent component vector, and thus a greater load on the gear teeth.

In the image on the left, the engine is at a state where the tangent vector magnitude has decreased to zero because F_{rod} is perpendicular to the gear pitch circle. In this state, the angle μ (not pictured) has reached 90°, and angle β (not pictured) has reached 0°. Here, there is zero loading on the gear teeth from F_{rod}, no matter its magnitude.

Clearly, as the engine rotates and the pistons reciprocate, the angle μ will continuously change, resulting in differently scaled component vectors. Using previously established engine geometry, μ can be calculated for every line in the FEA, and its value can be used through trigonometric equations to find the magnitudes of the F_{rod} component vectors, and thus the force loading on the gear teeth.

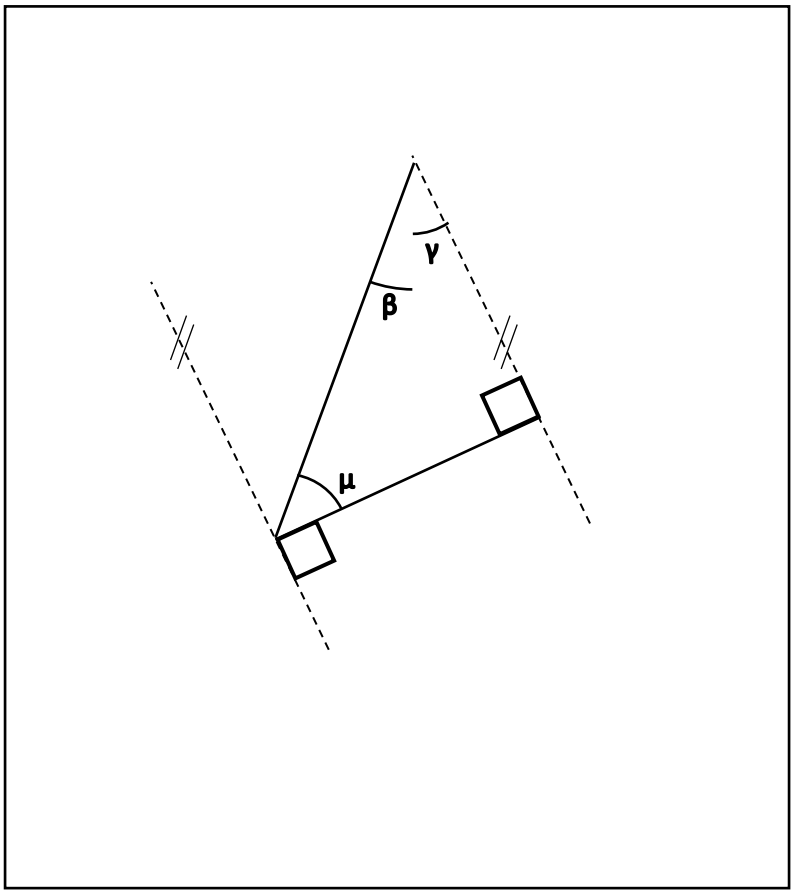

Figure 14: Engine geometry with μ angle

As shown in the diagram above, a parallel line to the variator angle γ can be drawn to the right, and a perpendicular line projected back over to the (Bx, By) coordinate. This line forms angle μ with the connecting rod. Because the summation of the internal angles of a triangle must equal 180°, the angle μ is found using the equation

$$\mu = 180 - 90 - \beta - \gamma \qquad \textit{(Eq. 39)}$$

The value for μ changes for each line in the FEA due to β, and is also directly influenced by the variator angle setting γ, which remains constant during each execution of the FEA. Note that longer connecting rod length to stroke ratios will tend to reduce the maximum values of β, keeping μ closer to 90°, and thereby reducing the peak forces through the gear teeth.

With values for F_{rod} and μ, it is now possible to determine the amount of torque through the synchronizer

$$\tau_{syncho.} = F * r = (F_{rod} \cos \mu) * (u) \qquad \textit{(Eq. 40)}$$

Where *u* is the distance between the center of the synchronizer and the connecting rod attachment pin as shown on the engine geometry diagrams above.

The value for $\tau_{syncho.}$ will change at every step in the FEA, and is only representative of the torque onto the synchronizer from *one* of the pistons. As mentioned in an earlier section, a plurality of pistons may be employed, and the number of pistons should be an odd-number greater than or equal to three. An initial assessment determined that a five-cylinder engine would likely be a good balance between reducing gear tooth unit loading, and keeping the overall engine design relatively economical. For these reasons, a five cylinder design will be assumed, and the function for $\tau_{syncho.}$ will be replicated four times in the FEA to generate the torque profiles from all five cylinders. To do this, a lookup function will be used to copy over instantaneous torque values from the main cylinder (cylinder #1), and shift them by the appropriate number of crank angle degrees to replicate an even firing order typical of a 5-cylinder radial engine. The firing order will be 1, 3, 5, 2, 4 and then back to 1. The number of degrees between cylinder major axis will be 72° (360° / 5 cylinders), however because the engine is a 4-stroke, the number of crank angles between *firing events* will be 144°. Therefore, the $\tau_{syncho.}$ values from cylinder #1 will be copied over to the next cylinder in the firing order, and shifted forward 144° for cylinder #3, 288° for cylinder #5, and so on.

Note that depending on the FEA settings and the engine angular positing being calculated, the values of $\tau_{syncho.}$ may be negative. In this case, the sign convention for $\tau_{syncho.}$ will be that positive values represent clockwise torque onto the synchronizer, and negative values represent counterclockwise torque. With five individual columns in the FEA reporting unique synchronizer torque values originating from each of the respective cylinder, a total net synchronizer torque value will be determined by simply summing the five individual values.

$$\tau_{synchro,net} = \sum_{i=1}^{5} \tau_{synchro,i} \qquad \textit{(Eq. 41)}$$

The function for the five individual torque values in addition to their summation are shown in the graphs below

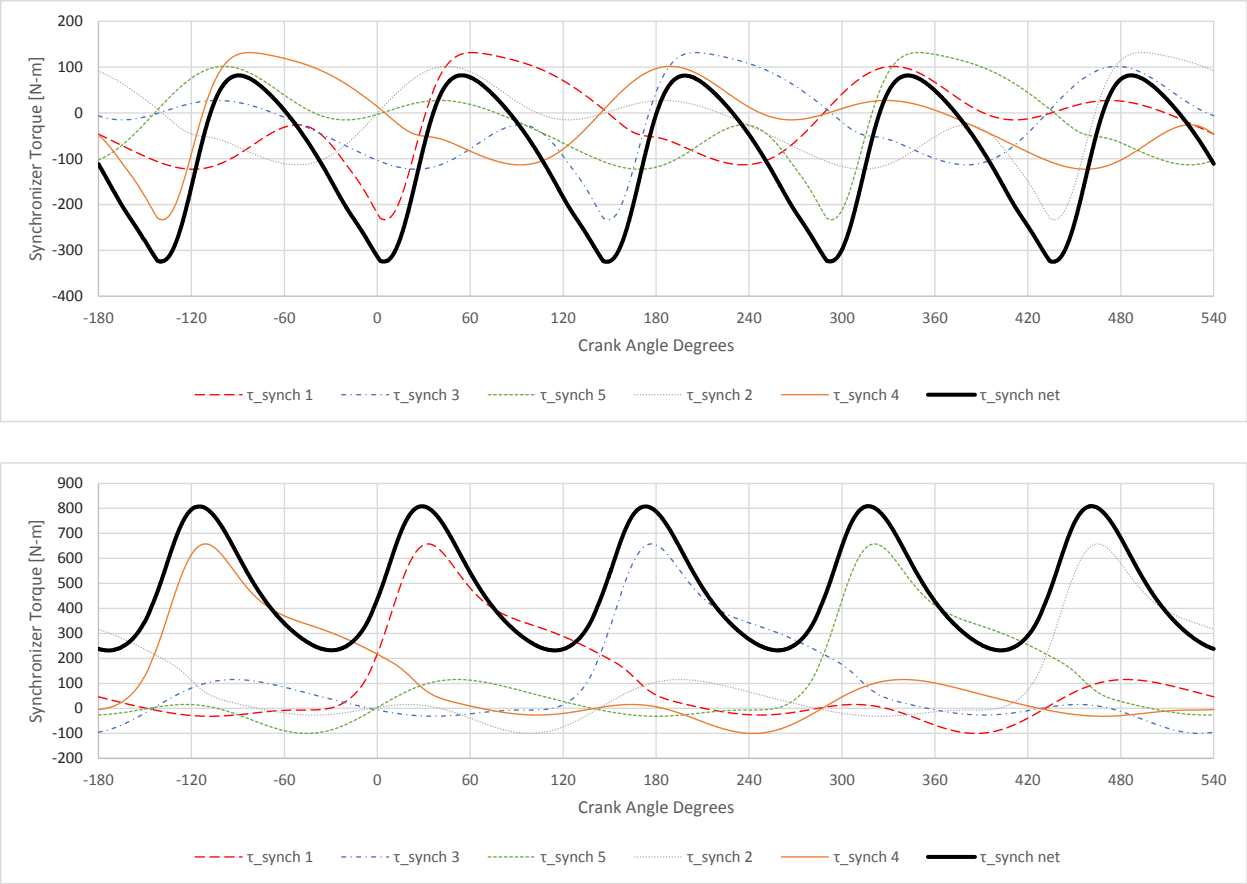

Figure 15: Synchronizer torque function

In the figure above, the variator is set a -5° in the top image, and +5° in the bottom image, with no other parameters adjusted. The compression ratio is the exact same regardless of positive or

negative variator angles. The pressure and temperature profiles also change noticeably due to the different piston motion profiles, but not to such a dramatic effect as the synchronizer torque. Note that at these FEA program settings, when the variator is set to -5°, the net torque value only swings from about +100 N-m to -300 N-m. However, when the variator is set to +5°, the net torque value swings from +800 N-m to +200 N-m. Clearly, the second setting results in a much larger absolute torque value, however it does have the advantage of not presenting a reversal in torque, which can be stressful on gear teeth. A more complex and pointed analysis of the gear teeth would need to be done in order to determine which of the two methodologies would result in better gear durability. For the scope of this work, the setting resulting in the lower absolute values will be assumed as standard, and further variator setting will be in the negative degree range.

The torque in the synchronizer is now known for any combination of FEA program settings, but the actual gear tooth loading must still be determined. The gear geometry in the design model is based on Mazda Wankel engine rotor gears and stationary gears. These gears were selected because in this variable compression ratio engine they will result in a 60 mm stroke, which is very close to the designed stroke of the motorcycle engine used for the pistons, jugs and heads. The gears are designed to operated in a high-load environment with very non-uniform cyclical loading. The gear geometry also lends itself to facilitating positioning of the crankshaft, as the pinion gear has a large through bore. Finally, the tooth contact ratio is maximized because the pinion gear pitch diameter is 2/3 the pitch diameter of the internal ring gear that it meshes with. In short, Mazda designed these gears to tolerate similar conditions as will be found in this variable compression ratio engine.

The gears were measured on a purpose-built gear tooth profile measuring Coordinate Measurement Machine (CMM). The pinion gear, and internal ring gear were measured to have pitch diameters of 61.7 mm and 92.5 mm, respectively. For both gears the diametral pitch is 14, the pressure angle is 25°, and the face width is 15.92 mm. The pinion gear has 34 teeth, and the internal ring gear has 51 teeth. The full list of measured parameters for each gear can be found in the Appendix.

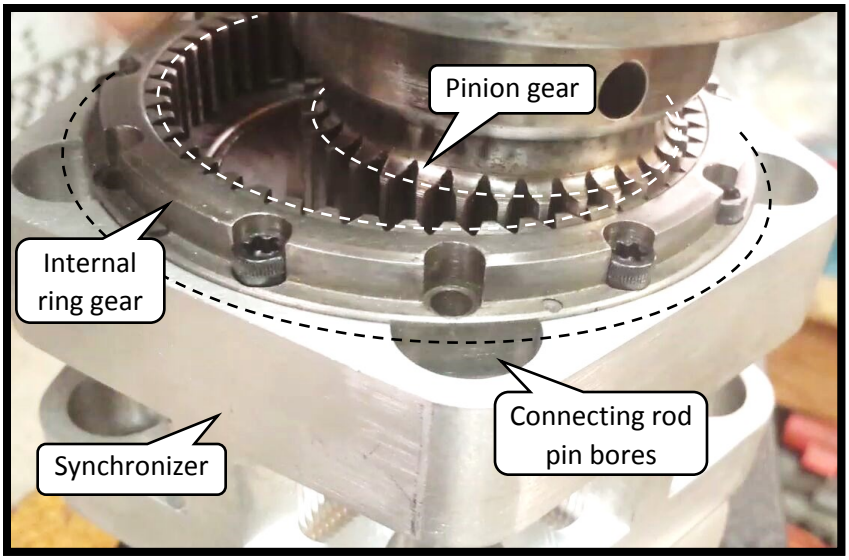

Figure 16: Photograph of pinion and ring gear on synchronizer

In the figure above the pinion gear is shown in-mesh with the internal ring gear. The approximate pitch diameters of the gears are shown in white dotted line. The approximate hole circle for the connecting rod pin bores is shown in a black dotted line. The radius of this black dotted line is the design variable *u,* in this case, 58.5 mm.

Using the Mazda gear geometry as a design guide, it is now possible to determine the amount of loading at the gear tooth mesh. The force at the gear mesh can be found using the synchronizer torque value divided by the moment arm length, which in this case is the radial distance of the ring gear pitch circle.

$$F_{tooth,total} = \frac{\tau_{synchro,net}}{r_{ring}} \qquad \textit{(Eq. 42)}$$

Where r_{ring} is set to 46.25 mm to match the radius of the pitch circle of the Mazda ring gear serving as the design base. Note that the subscript for force above is "tooth, total". This is because the force on an individual tooth will be less than the total value. For any well-designed gear mesh, as the gears rotate and the engaged pair of teeth exit mesh, the subsequent pair of teeth should already have made contact. It is desirable to have as much overlap as possible, and this overlap is measured as *contact ratio.* It is difficult to design a pair of externally meshing gear teeth to have a contact ratio significantly over 2.0 while maintaining a practical tooth geometry. However, since the gears used in this design mesh an external pinion gear with an

internal ring gear, much higher contact ratios are possible. Using equations found in a Kohara Gear Industry Co. LTD. design catalog, the contact ratio between a pinion gear and an internal ring gear is as follows

$$\varepsilon_{contact} = \frac{0.5 * \sqrt{D_{pinion,major}^2 - D_{pinion,minor}^2} + \sqrt{D_{ring,major}^2 - D_{ring,minor}^2} - a_w \sin(\alpha_w)}{m\pi\cos(\alpha)}$$

(Eq. 43)

The description of the above variables and their values as measured on the Mazda gears is summarized in the table below

Term	Description	Units	Ring	Pinion
D_{minor}	minor diameter	mm	88.9	57.4871
D_{major}	major diameter	mm	97.5901	65.3143
m	module	mm	1.81429	1.81428
α	pressure angle	deg	25	25
a_w	operating center distance	mm	15	15
α_w	pressure angle at pitch circle	deg	25	25

Table 1: Gear Geometry

This results in a contact ratio of 5.67:1, meaning that at any given time there are at least five pairs of teeth in mesh, and 67% of the time, a sixth pair of teeth is also in mesh. For the upcoming tooth loading calculations, a worst-case condition of five pairs of teeth in contact will be assumed. This yields the equation for force loading on a single tooth

$$F_{tooth} = \frac{F_{tooth,total}}{FLOOR(\varepsilon_{contact})}$$

(Eq. 44)

Where $FLOOR(\varepsilon_{contact}) = FLOOR(5.67) = 5$ for the Mazda gear geometry.

With the amount of force at an individual gear tooth known, the stress in the tooth can be found using the Lewis equation, which is commonly used in the gear manufacturing industry:

$$\sigma_{tooth} = \frac{F_{tooth} * P_{diametral}}{f * Y}$$

(Eq. 45)

Where *f* is the face width of the tooth, and Y is the Lewis form factor found using the following graph

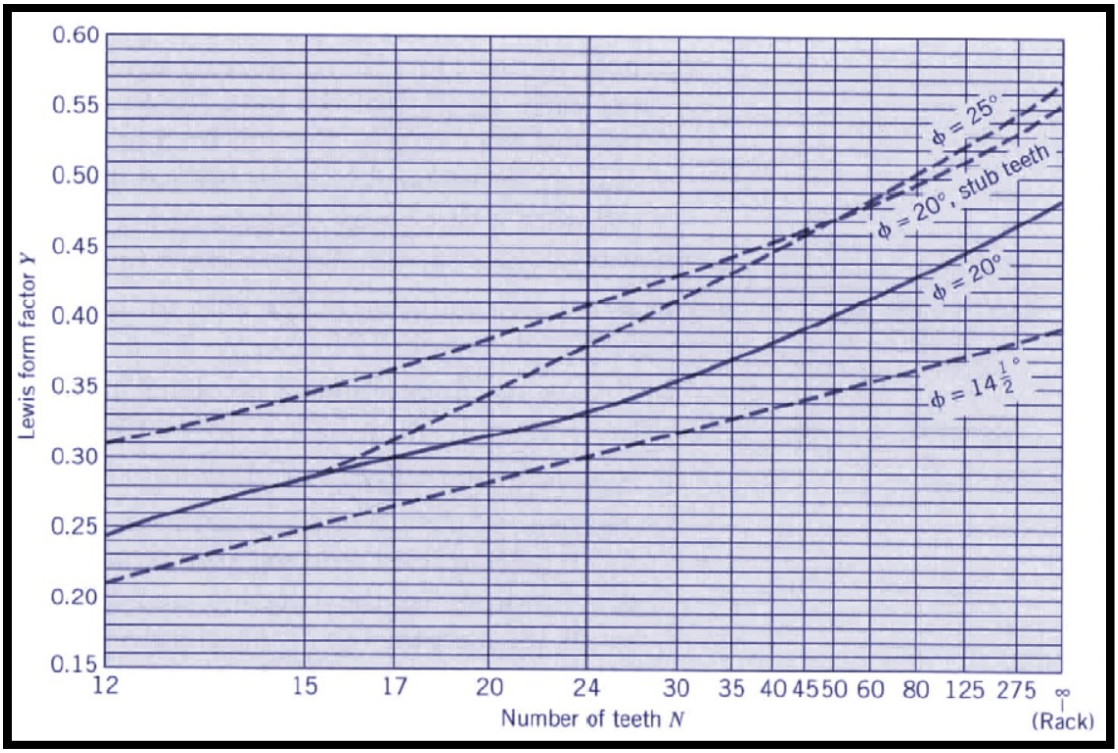

Figure 17: Lewis factor for gear teeth

Recall that the pinion and ring gear have 34 and 51 teeth, respectively. Using the Lewis diagram above, the form factor *Y* would be 0.44 and 0.47 for the pinion and ring gear, respectively. The Lewis equation yields equivalent results using both English *(pounds, inches, teeth per inch, psi)* and Metric units *(Newtons, millimeters, teeth per millimeter, megapascals).*

Using the above equations, along with the measured parameters from the Mazda ring and pinion gears, the tooth stress for each gear is calculated at each step in the FEA. The maximum and minimum values are identified and repeated at the top of the FEA program spreadsheet.

Based on general guidelines for using the Lewis equation, the maximum safe tooth bending stress is typically taken as one-third of the Ultimate Tensile Strength (UTS) of the material used. It is not known what steel alloy of steel the Mazda gears are made from because this information is proprietary. However, a table of steels commonly used in high-stress gears has been compiled below.

Trade Name	Chemistry	Description	Applications	Comments	UTS	⅓UTS
En36C (VAR)	14NiCrMo13	3%NiCrMo case hardening Steel	Gear, shaft and bearings	Low core strength (UTS:1350MPa) Low tempering temperature 140/160 degrees C	1350	450
S156 (VAR)	16NiCrMo17	4¼%NiCrMo case hardening steel	Gear and bearings	Low core strength Low tempering temperature 160/180 degrees C	1380	460
N/A	20NiCrMo13	3%NiCrMo case hardening steel (increased core strength)	Gears and shafts	Higher core strength achieved by increased core carbon content. Low tempering temperature ~150 degrees C	1450	483
N/A	35NiCrMo16	4%NiCrMo alloy steel	Shafts and gears	High core strength Low tempering temperature ~150 degrees C	1950	650
S155 (VAR)	40NiSiCrMoV7	Ultra high strength alloy steel (Si modified	Cross shaft, driveshafts	High core strength (1930MPa) Tempering range 250/300 degrees	1930	643
Hy-Tuf* (VAR)	25NiSiMnMoCr7	High strength alloy steel	Gears and shafts	Tempering temperature 140/180 degrees C	1550	517
N/A	40SiNiCrMoV10	Ultra high strength alloy steel	Driveshafts, highly stressed gears	Tempering temperature 300 degrees C	2050	683
					Megapascals	

Table 2: Common gear Steels

The UTS of the selected alloys range from 1350 to 2050 MPa. The alloy selected by Mazda may have a lower UTS value, but if the gears were to be fabricated with modern state of the art alloys, a UTS of 1500 MPa should be attainable. This equates to 500 MPa for a safe limit to tooth bending stress. The FEA program will be set to flag the calculated bending stress if the maximum value climbs over +500 or falls below -500 MPa.

Chapter 16: Defining Function and Parameters

The ideal function of the internal combustion engine will be defined as follows:

1. To produce a high level of output power
    a. The power delivery should be as linear as possible over the engine speed range to promote good vehicle drivability
    b. The power is considered more important at higher engine speeds, since spirited driving and passing maneuvers occur at high engine speeds
    c. In all of the FEA runs, the output power will be plotted so that its magnitude and shape may be assessed
2. To produce power as efficiently as possible
    a. The efficiency is considered more important at lower engine speeds, since fuel-economy focused driving occurs at low engine speeds
    b. In all of the FEA runs, the thermal efficiency will be plotted so that its magnitude and shape may be assessed

In addition to the two main function outputs above, a few other outputs will be monitored or actively limited:

1. Peak cylinder pressure
    a. This value should be limited in an actual engine to avoid structural damage and the production of excessive regulated emissions.
    b. In all of the FEA runs, a limit of either 80 or 100 bar is set for this parameter
2. Exhaust Gas Temperature (EGT)
    a. This value should be limited in an actual engine to avoid thermal damage to exhaust system components
    b. In some of the FEA runs, the EGT values are plotted and discussed
3. Gear tooth loading
    a. This value should be limited in an actual variable compression ratio engine of this layout in order to prevent gear failure

b. In some of the FEA runs, the tooth loading is plotted and kept within the limits established in the prior section.

Several control parameters will be adjusted in the FEA in order to observe their effects on the outputs. A control parameter is considered a "design variable" when it is controllable by adjusting the fundamental design of the engine, but not adjustable after the engine has been manufactured (such as cylinder bore size). A parameter is considered a "calibration variable" when it is controllable by the Engine Control Unit (ECU) or by some other means, after the engine has been manufactured (such as spark timing). The primary control parameters adjusted in the FEA will be:

- Boost pressure increase over engine speed
    - A design variable that may be adjusted by turbocharger sizing, particularly the Area to Radius ratio ("A/R") of the turbine housing volute.
- Fuel mass burn rate
    - A design variable that may be adjusted by altering the intake path and combustion chamber geometry to influence turbulence levels
    - A calibration variable that may be adjusted by altering the air-fuel ratio, activating a variable turbulence device, or activating a secondary spark plug
- Compression ratio
    - A design variable that may have its upper bound set by sizing of the dead volume above the piston at top dead center
    - A calibration variable that may be adjusted by altering the variator angle
- Start of Combustion
    - A calibration variable that may be adjusted by altering the spark advance angle

Note that adjusting the boost pressure rise over engine speed can also be controlled with calibration parameters that become available when the turbocharger is fitted with a wastegate or variable geometry turbine vanes. However, because this variable compression ratio engine is designed to operate at very high boost pressure, these boost limiting mechanisms will not be considered.

In addition to the iterations of the FEA exploring the performance of the engine under typical conditions, some off-design scenarios will also be considered.

Chapter 17: Baseline Engine Performance

It should be noted that in all of the subsequent analysis, friction is being ignored, and the gas in the cylinder is being modeled as air-standard. Both of these conditions will result in calculated efficiency values much higher than would be possible in reality. The friction is not being considered, so any energy loss due to frictional heating in the piston rings, valve train, fluid motion, etc. is not considered in the results. Because the system is being modeled as air-standard, the actual chemical species that form and react during actual combustion are not considered. This leads to a calculated in-cylinder temperature much higher than reality. This high in-cylinder temperature also contributes to an over-estimate in thermal efficiency. The friction losses present in the variator gear system are examined in a later section, but they are not factored into the initial engine performance and efficiency results.

Because the FEA program is only an approximate representation of a real engine, the output parameters are subject to error. To somewhat normalize this effect, the FEA program will first be used to simulate two conventional engines. They share all of the same design parameters, such as engine geometry. They are both modeled as conventional static compression ratio engines. That is, the variator has been "locked" in the FEA to keep the compression ratio constant. The first engine simulated is a high compression ratio, Naturally Aspirated (NA) engine, and the second is a low compression ratio, highly boosted turbocharged engine. The compression ratio of the NA engine is set to 12.15:1, and the compression ratio of the turbocharged engine has been set to 8.0:1. These engines are meant to represent extremes in NA versus turbocharged engine art, while also remaining realistic. Both virtual engines were tested at engine speeds between 1,000 and 8,000 rpm. The spark timing value was the only control parameter used during these trials of the FEA. The spark timing was adjusted so that the peak cylinder pressure would not exceed 80 bar. Both engines were subject to a linear-progression burn duration from 60 CAD at 1000 rpm to 95 CAD at 8000 rpm. The intake manifold temperature has been fixed at 320°K (47°C).

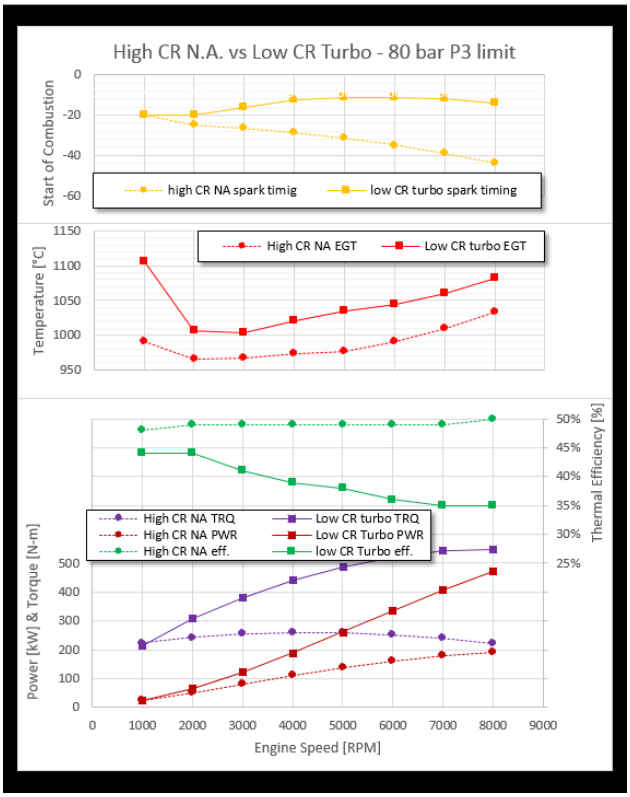

Figure 18: Comparison of two static CR engines

By inspection of the graph, several observations can be made. The most obvious difference between the two engines is that the turbocharged engine produces more than twice the power of the NA engine; however, its thermal efficiency is much lower, particularly at high engine speeds. Closer inspection of the torque curves indicates that the NA engine produces a much more level torque output, typically considered desirable and associated with consistent driving characteristics. Conversely, the torque curve of the turbocharged engine is nearly diagonal, producing significantly more torque at higher engine speeds. This type of torque curve results in a high degree of jerk (the derivative of acceleration) in a vehicle, and can make the vehicle difficult to control or unpleasant during acceleration. This is a particular concern when accelerating out of a corner, as the friction limits of the vehicle tires can quickly (and unexpectedly) become exceeded, resulting in loss of vehicle control.

The Exhaust Gas Temperature (EGT) of the turbocharged engine is also significantly higher than the NA engine. This is due to several reasons, including the higher backpressure, lower compression ratio, and higher overall power output of the turbocharged engine. Typically, EGTs

are limited to 1000 to 1050° Celsius for most turbocharged engine applications. Higher limits are possible if higher-capability nickel-based alloys are used for valves, manifolds, and turbine housings, but this is uncommon due to material costs. More commonly, the engine is calibrated to introduce extra fuel for in-cylinder charge air-cooling, which keeps EGTs under control. The extra fuel beyond the stoichiometric mixture requirement, acts to absorb some of the heat during the compression and power strokes. This has the effect of raw unburned fuel exiting the engine with the rest of the exhaust gas. This is often considered an acceptable strategy, so long as the vehicle aftertreatment system can react the majority of the unburned fuel with its chemically stored oxygen reserves, producing water and carbon dioxide in the process. This strategy also comes with a large thermal efficiency penalty because a significant amount of fuel entering the engine is not chemically reacting inside the combustion chamber, and releases no heat until entering the downstream aftertreatment. This penalty is usually considered acceptable because it is only required when the engine is near peak power output, which happens a very small percent of the time for a normal vehicle. In the case of an endurance race vehicle, excessive implementation of this strategy could result in more frequency pit stops for refueling. The FEA has not been configured to use an excessive fueling strategy for exhaust gas cooling. Therefore, the EGT result values will continue to be monitored, and noted if increasing to extraordinary values.

Finally, in comparing the two baseline engines above, the difference in the spark advance setting has also been plotted. This was the control parameter used to ensure the peak cylinder pressures did not exceed 80 bar. It is typical for an engine to require *more* spark advance (greater negative value in the plot above) as engine speed increases, but require *less* spark advance as intake manifold pressure increases. This generalization is also evident in the plots above, as the NA engine (with a consistent manifold pressure of 1.0 bar) required progressively more and more spark advance as the engine speed increases. However, the shape of the spark timing function of the turbocharged engine is more complex, as the need for *more* advance with higher speeds was at odds with the need for *less* advance with higher boost pressures.

Chapter 18: VCR versus Turbocharged Engine Performance

With a set of baseline data established, the highly boosted turbocharged engine will be compared to the Variable Compression Ratio (VCR) engine. Both engines were subject to the same intake manifold pressure function of 0.33 bar increase in manifold pressure for every 1,000 rpm increase in engine speed, starting at 1.0 bar absolute at 1,000 rpm

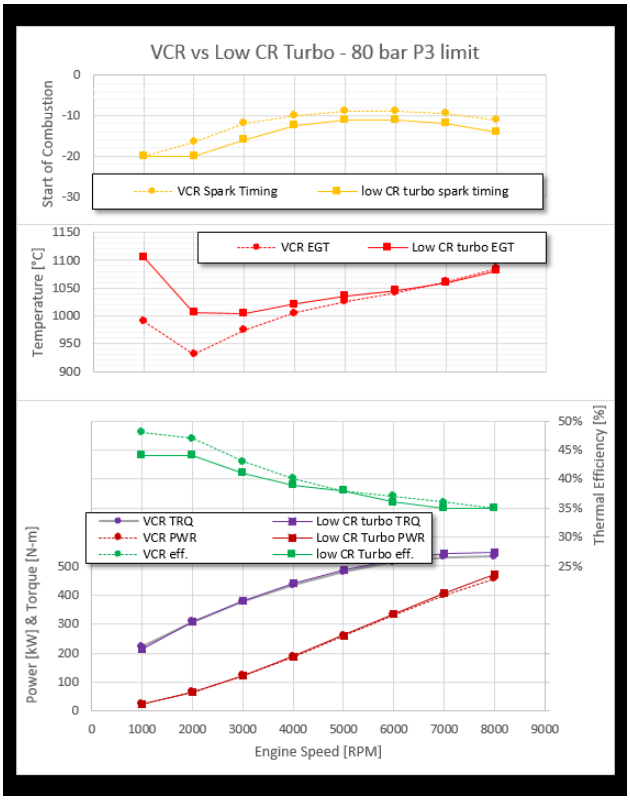

Figure 19: Baseline turbo engine compared to VCR

Compared to the baseline turbocharged engine, the VCR engine produces nearly identical power and torque output. At lower engine speeds, the efficiency of the VCR engine is significantly higher than the turbocharged engine, and the EGT is lower. Both of these advantages are due to the VCR engine being set with a high compression ratio at low speeds before the boost pressure has risen significantly. In this way, the VCR engine behaves more like the high compression ratio NA engine at lower engine speeds.

Chapter 19: Limiting Pressure - Spark Timing vs Compression Ratio

As shown in the prior section, it is possible to keep the peak cylinder pressure under acceptable limits by adjusting the spark timing, changing the compression ratio, or some combination of both. The balance between the settings of these control parameters will be examined here.

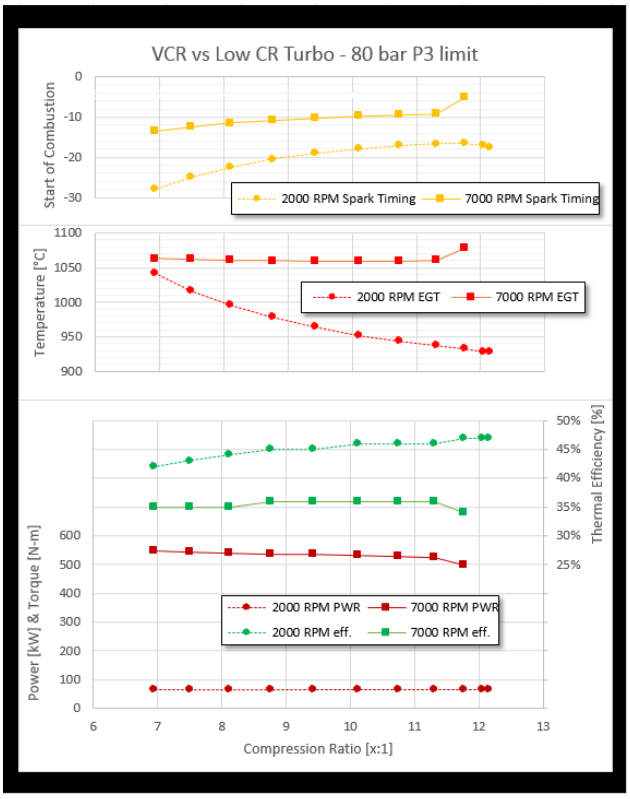

Figure 20: Spark-timing pressure limiting versus CR pressure limiting

The effects of spark-timing-based pressure limiting versus compression ratio-based pressure limiting is shown in the figure above at both 2,000 and 7,000 rpm. Note that the x-axis is compression ratio value, ranging from the low ratio of 6:1, up to the high ratio of 13:1.

The difference in pressure-limiting methods is pronounced at lower engine speeds. There is a 10% increase in thermal efficiency from one end of the chart to the other. There is a large advantage if a high compression ratio, and relatively late spark timing is used. Based on this, it would be best

to operate the engine with a high compression ratio, late spark setting to maximize fuel economy. There would be almost no penalty in output power to operate the engine in this way.

It is also clear that the EGT changes greatly at the 2,000 rpm point depending on the compression ratio and spark settings. At high compression ratios, the EGTs are low, and at low compression ratios, the EGTs climb to very large values. Typically it would be beneficial to minimize EGT values to reduce thermal fatigue on exhaust system components, and fortunately (but not coincidentally) the engine settings that yield the highest efficiencies also result in the lowest EGTs. However, in some situations it may be desirable to increase the EGTs. After a cold start up, the aftertreatment system is at ambient temperature. The catalytic converters found in modern aftertreatment systems must be warmed up to a certain value in order to function. In order to get the aftertreatment system warmed up as quickly as possible, engine calibration engineers will often make adjustment to increases the EGT levels just after a cold start-up has occurred. This is often accomplished by advancing the exhaust cam, opening the turbocharger wastegate, or retarding the spark advance, depending on which options are mechanically available. Having this compression ratio adjustment method to control EGTs after start-up could be useful to the engine calibration process.

A second benefit to being able to increase EGTs is more performance-oriented. During spirited driving, when rapidly going from a light engine load to a high engine load, it is desirable to provide the turbocharger with additional thermal energy. By increasing the exhaust temperature momentarily, the turbo can be given a short burst of additional energy to help reach boost target values quicker. Again, this strategy is sometimes implemented using exhaust cam phasing, but having a different way to increase the exhaust temperature could be valuable to the engine calibration engineer.

The graph above shows that at high engine speeds, there is little effect on performance weather the pressure is limited by spark timing or by compression ratio. At 7,000 rpm, there is only a slight penalty in power output at high compression ratios and late spark timing. There is virtually no effect on overall thermal efficiency or exhaust gas temperatures. Above 11.8:1 compression ratio, the ignition timing could not be retarded enough to produce a peak pressure under 80 bar. To further investigate this apparent similarity, the pressure and temperature values over the 4-stroke cycle were plotted for several FEA configurations as shown below.

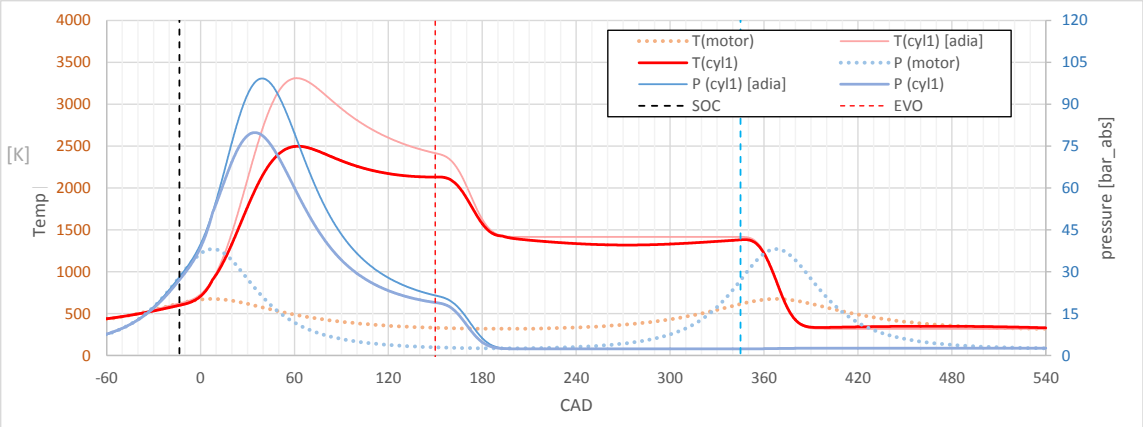

Figure 21: Pressure temperature trace – lowest CR

7,000 rpm, CR 6.94:1, SOC 13.5° BTDC. 80 bar peak pressure limit.

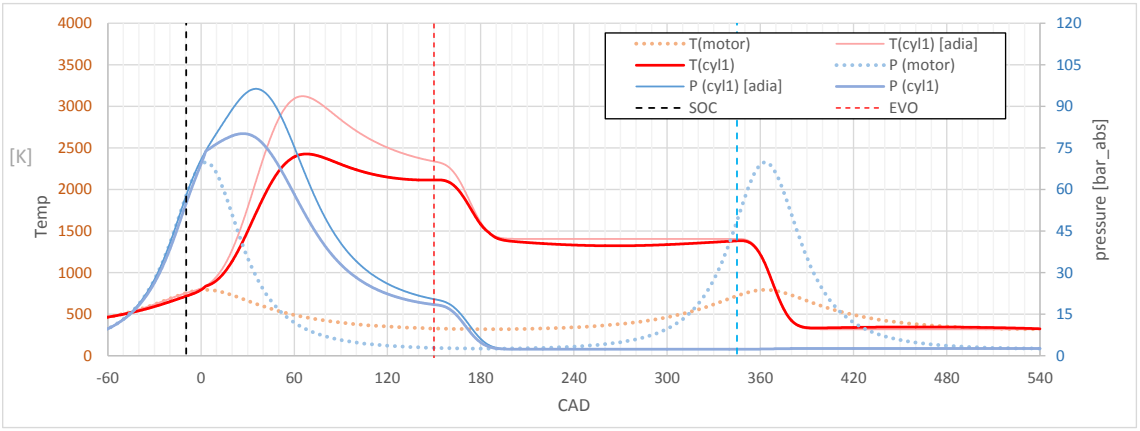

Figure 22: Pressure temperature trace – peak efficiency

7,000 rpm, CR 10.74:1, SOC 9.5° BTDC. 80 bar peak pressure limit.

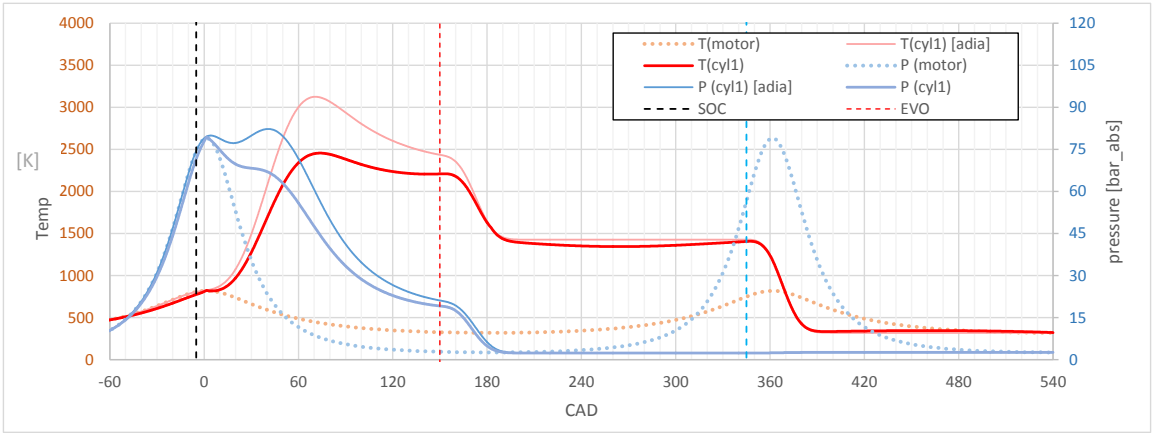

Figure 23: Pressure temperature trace – highest CR

7,000 rpm, CR 11.76:1, SOC 5° BTDC. 80 bar peak pressure limit.

While the shape of the pressure functions at the lowest compression ratio setting looks very typical of a trace recorded on an actual engine, the other two settings look very atypical, particularly the highest compression ratio setting with the very late spark timing. While numerically there appears to be very little difference in performance at any of the settings above, the higher compression ratio setting with late timing may result in some unusual engine torque pulsations due to the "double-peak" in the pressure function. Because of this, at high engine speeds and high loads, a lower engine compression ratio will be favored and coupled with a relatively early spark timing.

The pressure and temperature traces at the lower engine speed FEA settings were also examined to ensure there were no abnormalities.

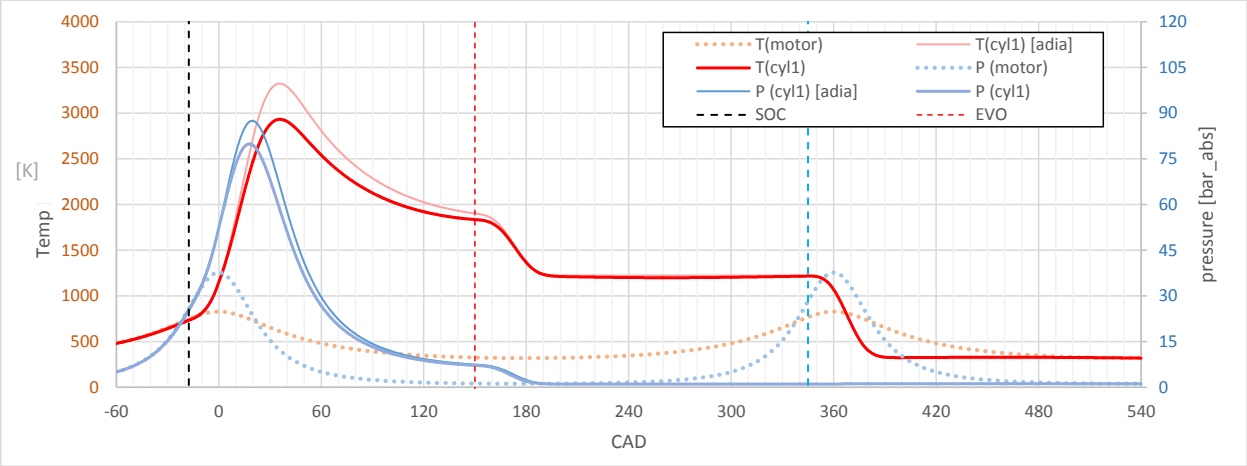

Figure 24: Pressure temperature trace – highest CR 2,000 rpm
CR 12.15:1, SOC 17.5° BTDC

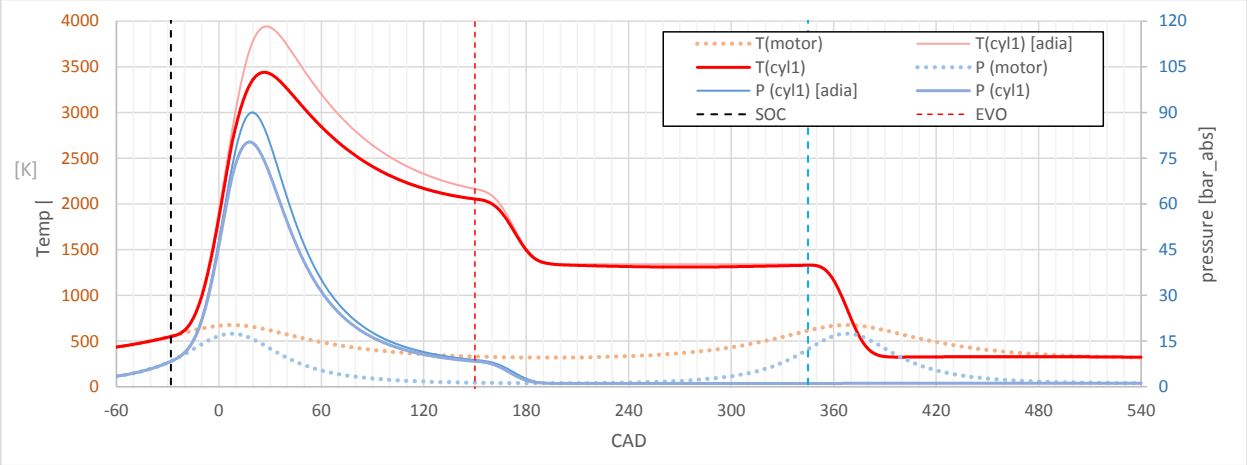

Figure 25: Pressure temperature trace – lowest CR 2,000 rpm
CR 6.94:1, SOC 28° BTDC

At lower engine speeds and boost pressure values, there is much less contrast in pressure function shape. Both of the above graphs seem viable, although the lower compression ratio setting with very high spark advance does result in high peak cylinder *temperatures,* which may lead to excessive NOx formation.

The observations regarding each of the pressure-limiting methods are summarized in the table below.

Pressure-Limiting Method	High Speed, High Boost	Low Speed, Low Boost
High CR, Late Spark	Good Power, Abnormal Pressure Profile	Best Efficiency
Low CR, Early Spark	Best Power	High Combustion Temp

Table 3: Spark versus CR pressure control

Based on the collective analysis of both pressure-limiting methods, the subsequent FEA runs will be conducted with high CR - late spark for low speed/boost, and low CR – early spark for high speed/boost operation.

Chapter 20: Cruising Conditions

At full load, the VCR engine has been shown to present high efficiencies at low speeds, and high power output at high speed. However, a typical passenger car engine is only at full load a small percentage of time. A more practical configuration to consider is a highway cruising scenario. To maintain highway speeds, a vehicle must only generate around 20 kW depending on drag forces, rolling resistance, and accessory power requirements. The engine transmission is typically configured so that the engine speed is around 2,000 rpm during highway cruise. In this analysis, the FEA program will be set at an engine speed of 2,000 rpm, and the power will be limited to 20 kW. There are multiple methods by which the output power can be set at this limit. The intake manifold pressure can be lowered to below ambient pressure levels, the spark timing can be adjusted and the compression ratio may be lowered. If the compression ratio is kept as high as possible, then in order to produce only 20 kW of power, the intake manifold pressure must be lowered to 0.41 bar. This configuration results in a thermal efficiency of 45.5%.

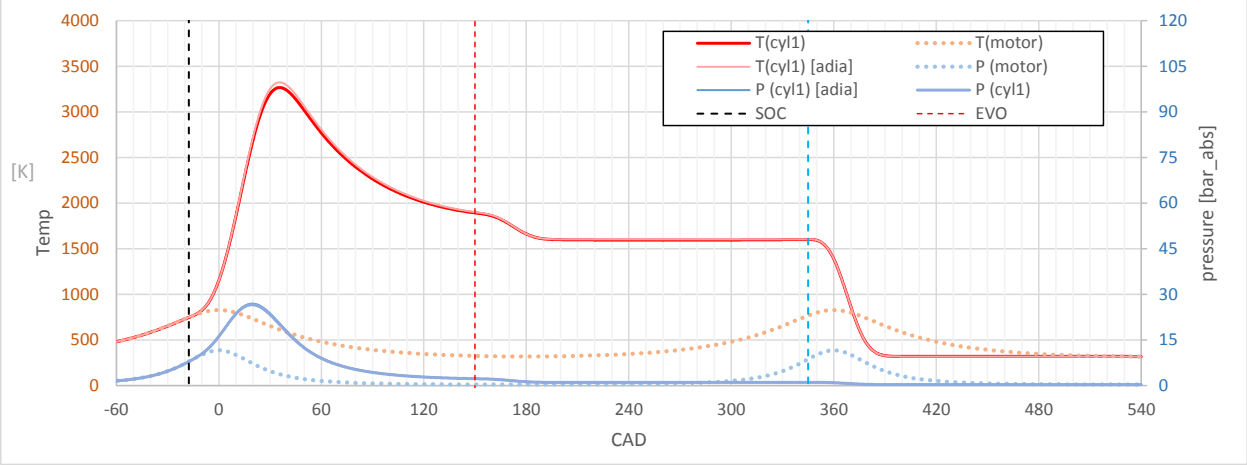

Figure 26: 20 kW output power

0.41 bar intake manifold pressure, 17.5° spark advance, 12:15:1 CR, 45.5% η_{TH}

The significant vacuum conditions in the intake manifold increase pumping losses, though the pressure being far below ambient does present an advantage to drivability. The intake throttle can be opened and the manifold conditions can be quickly increased to near-ambient pressure values. Transitioning from 0.41 bar at 2,000 rpm to 1.0 bar at the same rpm is representative of a

"tip in" in which the driver goes from a cruise condition into a passing maneuver. Typically this process would be accompanied by a gear change in the transmission so that the engine speed is significantly increased, resulting in more available power. However, having a good amount of power available at the low engine speed is beneficial and avoids the need for excessive gear shifting.

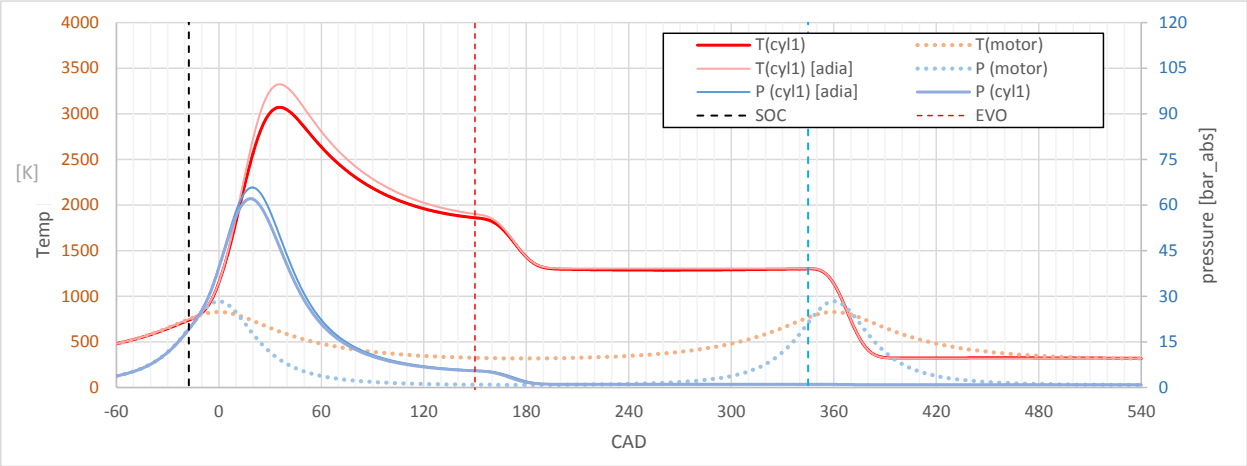

Figure 27: Tip-in from cruise

51 kW output power at 2,000 rpm. 1.0 bar intake manifold pressure

Chapter 21: Performance at Various Burn Rates

The FEA Program was executed with different types of fuel mass burn rates to test the effects. The first burn scenario was set to last for 60 crank angle degrees at 1,000 rpm, and linearly increase to 95 crank angle degrees at 8,000 rpm. The second scenario has a range of 60 to 74 crank angle degrees from 1,000 to 8,000 rpm. This contrast is meant to approximate a low versus a high level of combustion chamber turbulence. These FEA iterations are peak-pressure limited first to 100 bar, then repeated using an 80 bar limit.

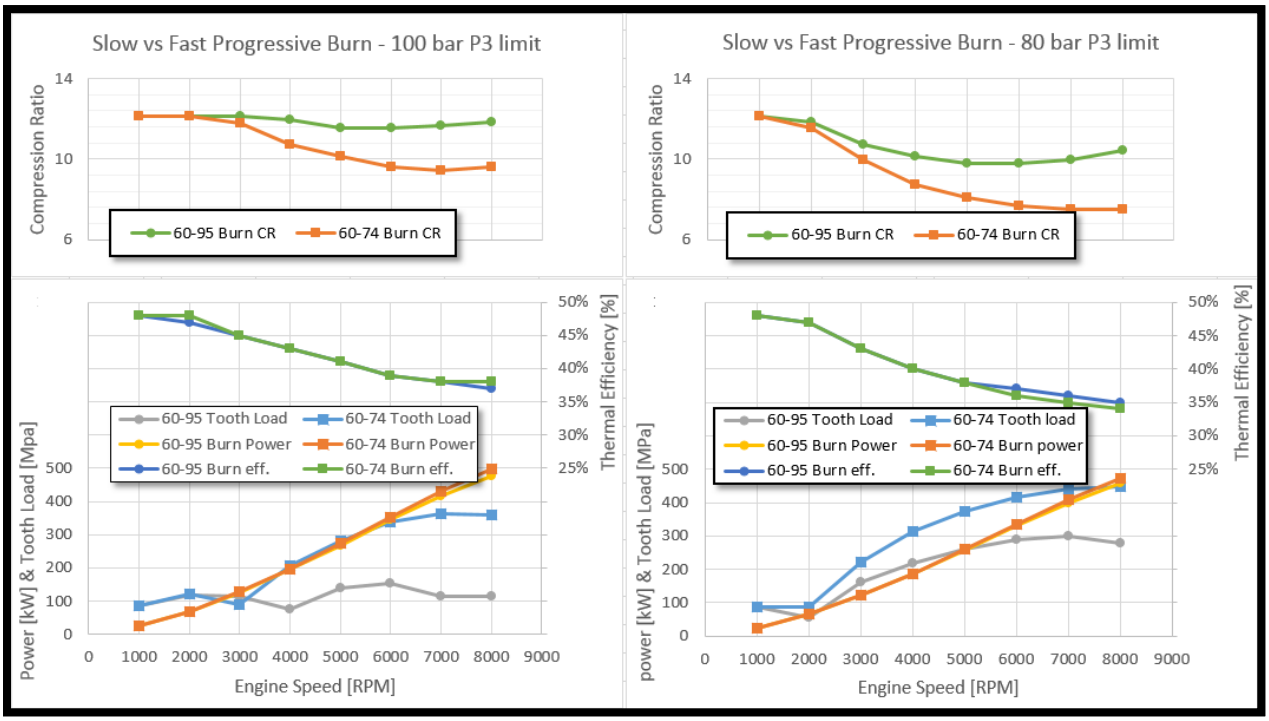

Figure 28: Various burn rates at limited pressure

The loading on the gear teeth is plotted in the graphs above. Note that for the different burn rates, the output power does not change much, but there is a large difference in gear tooth loading. A faster burn rate results in much lower tooth loads, especially at high engine speeds. This is because for the slower burning scenario, the cylinder pressure has a later peak, and this coincides with when the connecting rod is tilted and the resultant force vector into the gear teeth

is large. For the sake of reducing gear tooth loading, the pressure in the cylinder should be minimized during periods of large rod tilt angles.

Chapter 22: Downsized Engine Model

Up until this point, none of the FEA iterations have been done at different engine displacements. In the prior FEA runs, the total swept volume of all five cylinders was just over 2.0 L. This displacement would be considered medium-sized by modern trends, but the heavy degree of turbocharger in the VCR results in a very high power density. For this reason, it would be reasonably to explore significantly reduced displacement to inspect the effects on engine performance. The FEA program will be set to a reduced piston bore while leaving the stoke at 60 mm. This is because the prior geometry had an uncharacteristically high bore to stroke ratio, so reducing the bore from this point will trend to a more passenger-car typical "square" bore to stroke ratio. To make the bore to stroke ratio perfectly square, a 60 mm stroke will be used which will result in a total engine displacement of only about 850 cubic cm (0.85 L). An engine this size would be considered large for a motorcycle, but very small for a passenger car. However, owing to the nature of the VCR engine, an engine this small will produce adequate levels of output power for a passenger car.

The best practices investigated in the prior sections will be used. The faster progressive burn duration ranging from 60 to 74 crank angle degrees from 1,000 to 8,000 rpm will be modeled. Peak cylinder pressure will be limited to 100 bar, higher than most of the prior FEA trials limited to 80 bar. The smaller cylinder bore will result in a 40% reduction in piston area. Considering this, a 25% increase in cylinder pressure will still result in much lower forces in the engine.

The same boost rise profile will be used. *In practice, a much smaller turbocharger would need to be fitted to the engine to maintain the same boost rise profile as set to the larger 2.0 L engine.* The peak pressure will be limited by reducing spark timing at engine speeds below 3,000 rpm, and will transition to a compression ratio pressure-limiting strategy by 5,000 rpm and over.

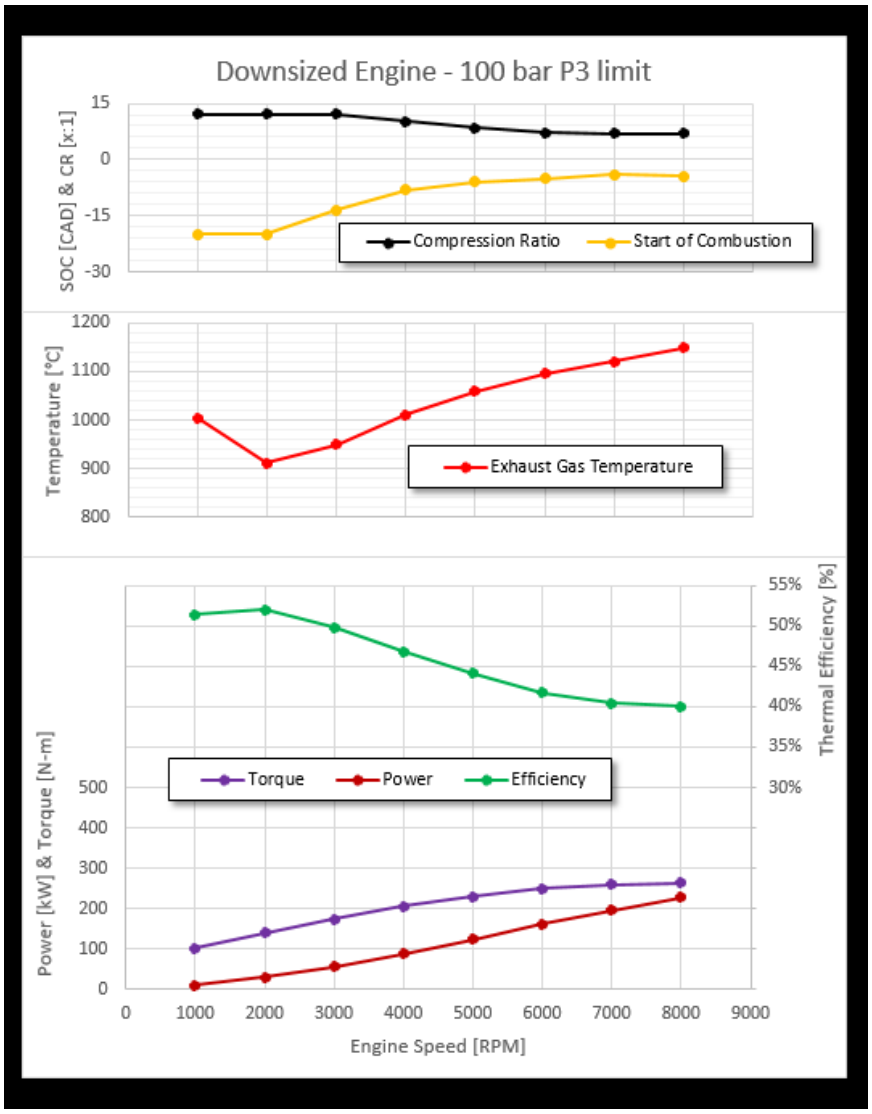

Figure 29: Downsized 850 cc VCR engine

As shown in the top-most section of the graph, the compression ratio was kept at maximum until an engine speed of 3,000 rpm was reached. This promoted keeping the thermal efficiency high. As the engine speed increased further, the compression ratio was decreased to maintain a 100 bar peak cylinder pressure. Under these conditions, the downsized engine produces a maximum power of 227 kW at 8,000 rpm. This the same level of power found in a typical large sedan or crossover vehicle, which are typically powered by at least 2.0 L turbocharged engines, or even larger displacement NA engines.

The engine when in this downsized consideration was also checked for highway cruise performance. Using the same stipulations in the prior section, the engine was adjusted to produce

only 20 kW of power at 2000 rpm. The compression ratio was set at maximum, and the start of combustion set to 17.5° BTDC. The intake manifold pressure only needs to be at a slight vacuum of 0.90 bar in order to limit power to 20 kW. The reduced pumping loss and higher cylinder pressures result in an indicated thermal efficiency of 50.8%. Compare this to the highway cruise conditions in the larger 2.0 L engine which required a significant intake vacuum of 0.41 bar to limit power to 20 kW, yielding an indicated thermal efficiency of only 45.5%.

However, because under these conditions, the downsized engine intake manifold is not much below ambient pressure, going to wide open throttle and achieving an intake manifold pressure of 1.0 bar would not produce much increase in output power immediately. After one to two seconds, the turbocharger would begin providing positive boost, and even if the engine speed remains constant, the intake manifold pressure would reach a steady state value of 1.33 bar, and the output power would increase to 30 kW. This would still likely be an insufficient power output given the probably expectations of the driver. Because of this situation, the engine and transmission would likely be calibrated to change down one or more gears if the driver were to suddenly request full torque from a highway cruise condition. This is a typical shifting strategy for production vehicles, but would be less likely to be needed in the larger 2.0 L VCR engine investigated above. In the event of a manual transmission, the driver would be expected to carry out the required gear changes.

Chapter 23: Gear Mesh Frictional Losses

The addition of the gear mesh required for the functionality of the variator mechanism will introduce a new source of frictional loss within the engine. The expected losses due to the gear mesh will be examined.

An equation for the efficiency of an internal spur gear mesh is introduced:

$$\eta_{mesh} = 1 - \frac{50\mu_{friction}}{\alpha} * \frac{G_s^2+G_t^2}{G_s+G_t} \quad \textit{(Eq. 46)}$$

Where

$$G_s = \left(\frac{R_N}{P_N} - 1\right) * \left[\sqrt{\left(\frac{R_{major}}{R_p}\right)^2 - (cos\,\alpha)^2} - sin\,\alpha\right] \quad \textit{(Eq. 47)}$$

$$G_t = \left(\frac{\frac{R_N}{P_N}-1}{1}\right) * \left[\sqrt{\left(\frac{P_o}{P_p}\right)^2 - (cos\,\alpha)^2} - sin\,\alpha\right] \quad \textit{(Eq. 48)}$$

Note that these equations are specific to *internally* meshed spur gears, to match the geometric mechanism in the variator assembly. Externally meshed spur gears and helical gear are analyzed with similar but different equations.

The description of the above variables and their values as measured on the Mazda gears is summarized in the table below

Term	Description	Units	Value
α	Pressure angle	degrees	25
μfriction	Coefficient of friction	[none]	0.16
RN	Ring Gear – Number of teeth	teeth	51
PN	Pinion Gear – Number of teeth	Teeth	34
Rmajor	Ring Gear – Major diameter	mm	97.5901
Rp	Ring Gear – Pitch diameter	mm	92.5286
Po	Pinion Gear – Outer diameter	mm	65.3143
Pp	Pinion Gear – Pitch diameter	mm	61.6857

Table 4: Gear geometry values

For the friction coefficient, a value of 0.16 is used. This is a typical value for steel sliding against steel in a well-lubricated environment, which is an accurate description of these steel gear teeth in mesh within the engine crankcase. With the geometric values from the Mazda gears and a friction coefficient of 0.16 used in the equation, a mesh efficiency of 98.35% results. Reference tables confirm that this is a reasonable value for a well-designed spur gear mesh. Because the variator mechanism relies on two gear meshes in series, this efficiency must be squared to yield the overall efficiency of the complete variator mechanism. The squaring of this percentage results in an overall variator efficiency of 96.74%.

Due to the nature of the variator kinematics, the level of power transmitted through the mesh varies considerably as the engine executes a full 720° of rotation. The VCR engine simulation program is again used to calculate the instantaneous power being transmitted by the gear teeth. The instantaneous torque in N*m transmitted through the mesh was previously calculated in order to assess the level of stress at the gear teeth. This column of values is now multiplied by the set engine rpm, and then divided by 9,549 to yield the instantaneous power being transmitted by the mesh in kW. This is taken as an absolute value as occasionally, and depending on the variator setting, the direction of power flow reverses into the mesh. This absolute value is then multiplied by the 96.74% estimated efficiency of two Mazda gear meshes in series. The Power in, Power out, and Power loss due to friction are then plotted for an engine setting at the highest levels of power output and again at a highway cruise condition.

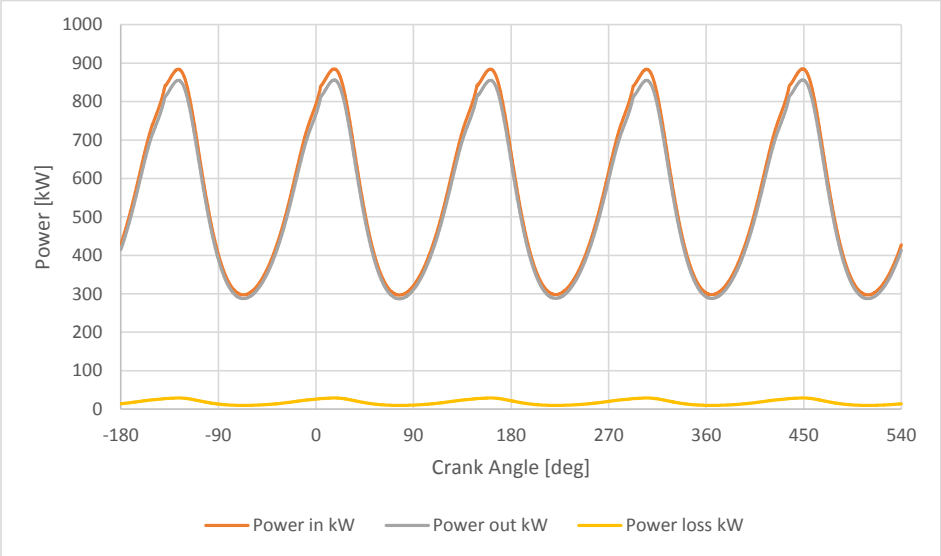

Figure 30: Gear efficiency – high power

8000 rpm, 3.33 bar intake pressure 497 kW output power – Max Power setting

At a VCR simulation setting that yields a maximum power of 497 kW, the average power loss due to friction is around 18 kW, which equates to an overall efficiency of 96.38%.

Next, the VCR simulator is populated with values that approximate a highway cruise condition so that the overall gear mesh efficiency can be examined at a more typical level of power output.

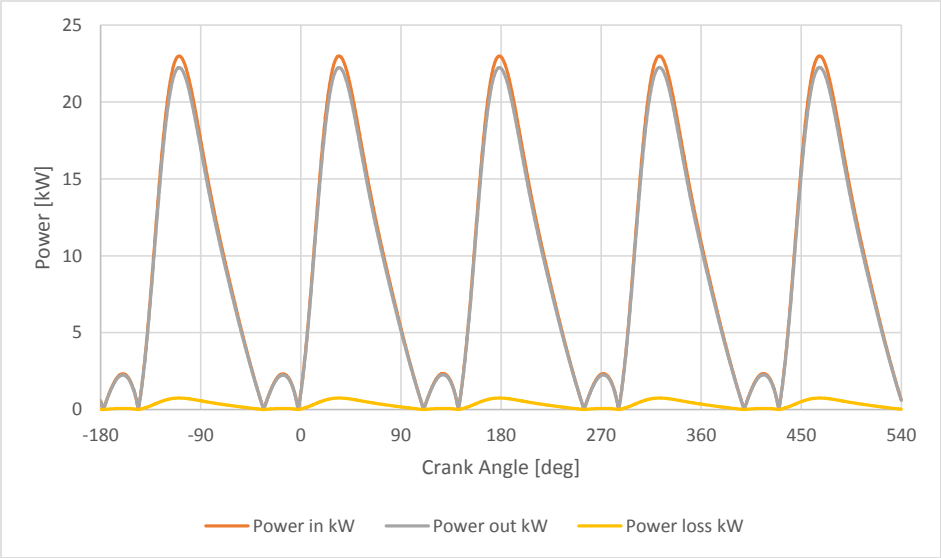

Figure 31: Gear efficiency – low power
2000 rpm, 0.42 bar intake pressure 20 kW output power – Highway cruise setting

At a VCR simulation setting approximating a highway cruise condition, the power loss due to gear friction is considerably lower. This is primarily due to the variator being set at a low angle to target a high compression ratio. At low variator angles, the flow of power from the cylinders is more *directly* transmitted to the crankshaft without heavily relying on the variator gear mesh. At these settings, the averaged power loss to friction over a full 720° of engine angle is only 0.31 kW. A 0.31 kW loss given a 20 kW input power equates to an overall mesh efficiency of 98.44%.

The addition of the variator mechanism introduces a new source of friction loss not found in a typical internal combustion engine. However, the radial cylinder layout presents an opportunity to counteract this new friction source by reducing the friction losses associated with the main and rod journal bearings. A detailed CFD analysis of the friction losses within a plain journal are beyond the scope of this work, but a few observations can be made.

In the single-row radial configuration, there are only two main journals and a single rod journal. The VCR mechanism requires the addition of an intermediate journal to locate the variator pinion

gear. This yields a total of four high-surface-speed journals. Furthermore, designing the engine with seven, nine or eleven cylinders would not increase the journal count. Conversely, an inline engine with a count of five cylinders would have five rod journals and six main journals, for a high-surface-speed journal count of eleven. Even the more common inline four-cylinder engine will typically employ nine journals. While the main and rod journal count in the VCR engine is inherently lower than the count in a typical inline of V-configuration engine, the journals are heavily loaded more times per revolution of the crank than a single journal in an inline or V-configuration. Because the frictional losses in a hydrodynamic bearing are dependent upon bearing load, a four-journal VCR engine will not necessarily have four ninths (4/9) the amount of journal friction losses as in inline four-cylinder, but the total friction loses will likely be lesser to some significant amount.

Additionally, there is a greater opportunity for a single-row radial engine to have both of its main plain bearings replaced with rolling contact low friction bearings. On-inline and V-engines it is only possible to replace the two outside main bearings with rolling element bearings without resorting to special high-tolerance split race roller bearings, or built-up crankshafts. On an inline or V-configuration engine even if some or all of the main plain bearings are replaced with rolling element bearings, the heavy cyclical forces from the adjacent cylinders will load the bearing in the same one or two angular positions. Roller bearings used on both main journal locations in a radial configuration will take heavy loading at as many evenly spaced angular locations, as there are cylinders. Therefore, a viable solution is to use a pair of large, heavy-duty rolling element bearings on the radial engine, where five *nearly equally heavy-duty bearings* would need to be used on an inline-four. These effects make roller bearing conversion on the radial VCR engine much more attractive than on an inline or V-configuration. No matter the type of engine, roller conversion on some or all of the main bearings directly results in reduced friction losses at the journals, and indirectly can lead to a decrease in parasitic losses from the oil system, as a rolling element bearing requires significantly less oil flow and pressure than a plain journal interface.

The frictional losses due to the added gear meshes has been examined and shown to be a low percentage of transmitted power, particularly at highway cruise conditions. The count and type of main bearing used on a radial engine configuration also creates some opportunity to partially, or completely counteract this added source of friction. Due to this, the losses introduced by the gear mesh does not appear to be detrimental to the viability of the VCR engine configuration.

Chapter 24: Conclusion

The inclusion of some mechanism to adjust the compression ratio of an engine is not a new concept. Many engine manufacturers continue to develop VCR engine technology. Most of the VCR mechanical concepts examined in a recent patent search involve the addition of multiple highly stressed components with the engine. While the VCR mechanism examined herein also introduces a unique highly stressed member in the form of the synchronizer gearing, the load levels at this mesh have been examined throughout the above analysis, and should prove to stand up to typical forces within the engine. The internal ring and pinion mesh having a very high tooth contact ratio plays a large part in keeping the stress within an individual tooth to a low value. The internal ring gear arrangement is also integral to the overall crankshaft and main bearing packaging. The pistons, connecting rods, cylinders and cylinder heads would not be subject to any extraordinary forces in comparison to a typical production static-compression ratio engine. Quite to the contrary, the nature of the VCR engine allows the engine calibration engineer keep the forces within the engine to consistent and relatively low values, despite the opportunity for heavily boosted operation yielding very high power densities.

The thermodynamic benefits of the VCR engine are clear. During periods of low-power operation, such as highway cruise, the engine can be set to operate at a very high compression ratio to keep efficiency high. When maximum power is requested, the compression ratio can be lowered significantly so that the on setting turbo boost pressure does not cause structural damage to the engine. Furthermore, the engine is conceptually able to produce such a high power density, a very small engine displacement well under 1.0 L may be employed, which additionally enhances the low-power efficiency by reducing pumping losses due to significant intake manifold vacuum.

The prospect of designing a variable compression ratio engine leads to many performance and efficiency advantages. The thermodynamic analysis conducted herein quantifies many of these advantages. The structural and friction analysis have also shown that such a design should carry no inherent weaknesses, and is worthy of further study.

Chapter 25: Future Investigation

While the engine is potentially able to produce a large amount of power and torque, the *shape* of the torque curve is generally unfavorable. Much like the highly boosted static compression ratio engine simulated as a baseline, the shape of the torque curve is essentially diagonal. A much flatter torque curve would increase vehicle drivability. In order to achieve a flatter torque curve while not significantly reducing its peak value, more boost pressure would need to be available at lower engine speeds. There are several methods in which this can be achieved:

1. Sequential turbochargers
    a. Two or more turbos of different size both connected to the engine
    b. The smaller turbo produces very fast boost rise rates up to a moderate rpm, then valving in the exhaust and intake system transfer functionality to the larger turbocharger with a higher peak flow capability
2. Dual-boosting (Supercharger and turbocharger)
    a. Engine-driven supercharger provides near instantaneous boost rise rates at low engine speeds
    b. At higher engine speeds, the large turbocharger out-flows the supercharger, which is then bypassed or mechanically disengaged from the engine.
3. Pneumatic boost assist.
    a. Reserve tanks of compressed air can provide boost to the intake manifold for short burst while the turbocharger comes up to pressure
    b. This method is typically only viable on vehicles already fitted with a high pressure air system, such as freight trucks or busses
4. Electronic boost assist.
    a. One or more electronically driven compressors can provide quick boost rise rates while the larger turbocharger comes up to boost

In addition to the methods of increasing manifold boost pressure at low speeds mentioned above, the vehicle could simply be fitted with a hybrid system whereby the electric motor could provide additional torque when the internal combustion engine is at low speed, low boost, and thus low torque output. The electric motor could then act as a generator to level off the top-end of the torque curve while collecting reserve energy for the next torque-assist event. Electric motors typically have very high output toque at very low speeds, so a properly configured hybrid electric system could work very harmoniously with a downsized, highly boosted VCR engine.

All the methods listed above typically add a significant amount of expense to the powertrain. Building upon the Excel FEA program to explore some of these possibilities could serve as a basis for a more focused analysis.

Bibliography

Heywood, John B. Internal Combustion Engine Fundamentals. McGraw-Hill 1988

Budynas, Richard G. and Nisbett, J. Keith. Mechanical Engineering Design. McGraw-Hill 2011

NASA Propulsion Index <https://www.grc.nasa.gov/WWW/K-12/airplane/shortp.html> Last *Viewed 6/30/2017*

Garrett Turbocharger Product Guide
<https://www.turbobygarrett.com/turbobygarrett/turbochargers> *Last Viewed 6/30/2017*

Fandrich, Helmut Edward. Stratified Charge Scavenging of a Two-Stroke Engine at Part Throttle. University of British Columbia 1960

Pearce, William. Nordberg Radial Stationary Engine.
<https://oldmachinepress.com/2014/01/12/nordberg-stationary-radial-engine/ > *Last Viewed 6/30/2017*

Kohara Gear Industry Co., LTD. Practical Information on Gears.
<http://www.khkgears.co.jp/de/gear_technology/pdf/gear_guide2.pdf> > *Last Viewed 6/30/2017*

Roymechx Mechanical Engineering Information
<http://www.roymech.co.uk/Useful_Tables/Drive/Gear_Efficiency.html> *Last Viewed 11/6/2017*

Engineering Toolbox
< https://www.engineeringtoolbox.com/friction-coefficients-d_778.html> *Last Viewed 11/6/2017*

Wolfram Alpha
< https://www.wolframalpha.com/> *Last Viewed 11/6/2017*

Appendix A: Crankshaft Balance

The balance of the VCR engine crankshaft requires some special considerations due to the unique geometry of the engine. The first major consideration is the axial location of the balance weights. In a conventional 1-row radial engine, one large balance weight is present on each side of the single large rod journal. The two balance weights are roughly equal in mass, and evenly spaced axially on either side of the rod journal. This arrangement minimizes the dynamic imbalance of the rotating assembly.

In the radial VCR engine, there are two possible mechanisms used synchronize the conrod base disk with the external compression ratio variator. One of these mechanisms employs a pinion gear assembly which passes through a bearing system within one of the two crank counterweight. While this mechanism is advantageous in that a counterweight mass may be placed on both sides of the rod journal, helping to minimize or altogether eliminate dynamic imbalance, it necessarily relies on a gear mesh which must transmit high levels of torque at a relatively low contact ratio. An example of this arrangement is the postwar Nordberg radial engine shown below.

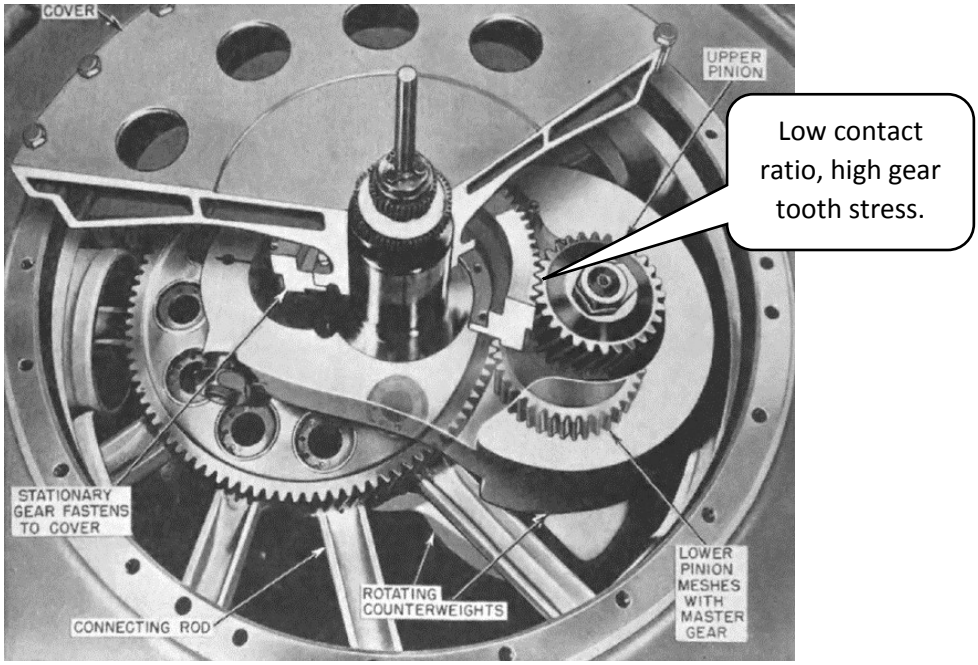

Figure 32: 11-cylinder Nordberg radial engine circa 1950

The benefits of this system may outweigh the disadvantages in engine arrangements with higher numbers of cylinders where the expansion work of one cylinder may more directly be applied to compression work of the next cylinder in firing order. In the case of the 11-cylinder Nordberg engine, there are only ~65.45° of crankshaft rotation between firing events. Conversely, in the case of lower cylinder count radial engines using 3, 5, or 7 cylinders there are 240°, 144°, and ~103° of crank rotation between combustion events, respectively. Because of this higher degree of torque ripple, the gear teeth are tasked with transmitting a great deal of force into and out of the crankshaft flywheel assembly. Because of this effect, the alternative synchronization mechanism, which results in a much greater tooth contact ratio, will be studied in detail. This mechanism uses a pair of internal ring gears mounted to an orbiting assembly to create gear meshes between the conrod base disk and the external compression ratio variator. An example of this geometry is shown below.

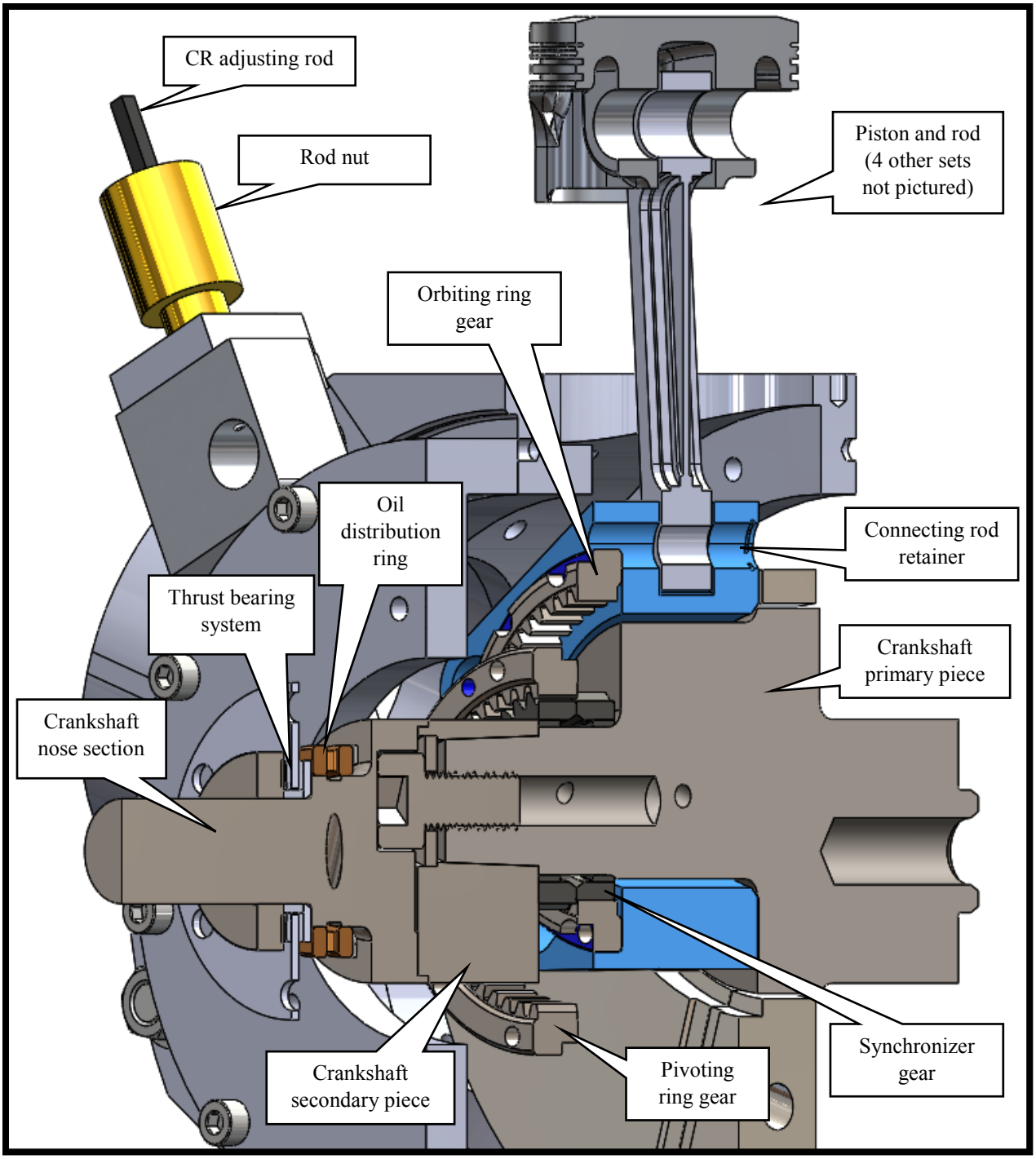

Figure 33: Double ring gear style synchronizing mechanism

The major disadvantage to the double ring gear synchronizer is that it must be positioned on the crank assembly in a way that completely negates the use of a conventional counterweight in this area. So instead of an evenly distributed counterweight mass on either side of the rod journal, a

more novel counterbalance positioning strategy must be employed. For example, all of the primary balance mass may be placed on only one side of the rod journal, opposite of the synchronizer. It would be possible to achieve a good static balance with this basic arrangement, but in order to achieve an acceptable dynamic balance, additional measures must be taken. There are at least two possible counterweight schemes that can work to achieve this, each with advantages and disadvantages.

In the first configuration shown below, a lower amount of total balance mass is needed, but a large bending force must pass through the crankshaft. This may be problematic for any design employing a built-up crankshaft, which is a common design practice in radial engines.

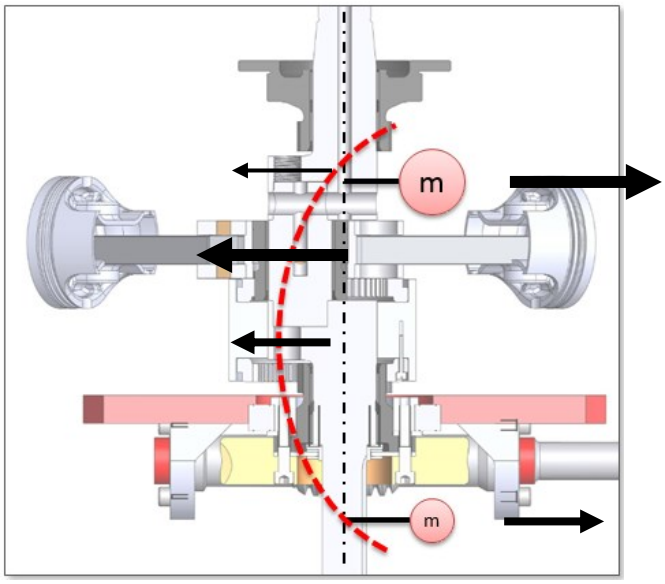

Figure 34: Counterweight arrangement with minimal balance mass

The second configuration requires the main counterweight to over-balance the crank, and then this additional mass must be compensated for by adding another mass at a different axial position, 180° away from the main balance mass. This design requires a much larger total amount of crankshaft mass, but drastically reduces the bending forces passing through the bulk of the crankshaft. It should also be noted that a lower mass flywheel may be employed to partially or completely offset the additional mass required.

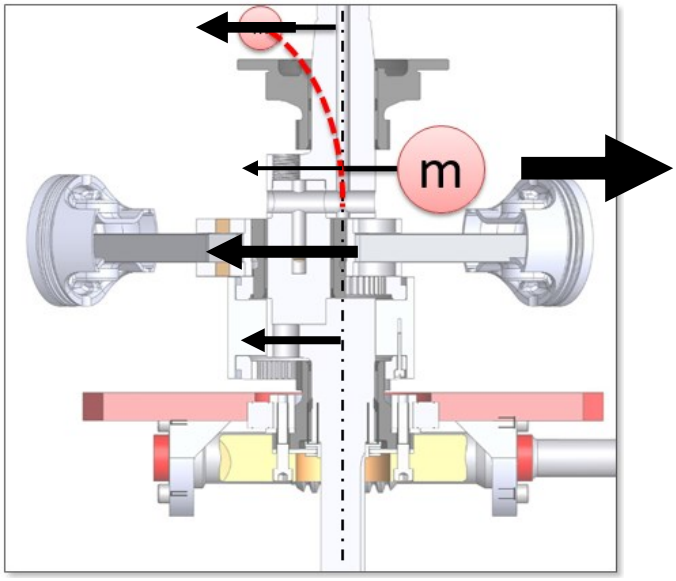

Figure 35: Counterweight arrangement with minimal bending load through crank

For concern of the built-up crankshaft joint capacity, and the minimal need to keep rotating mass low for performance reasons, the prototype engine will be constructed using the minimal bending load approach, at the expense of higher rotating mass. If deemed necessary, the flywheel mass may be altered to adjust the performance characteristics of the engine. Furthermore, the entire accessory drive of the prototype engine will be at the front, so space for additional balance masses at this end of the crankshaft is very limited, however there is ample room for an external balance mass at the rear of the crankshaft.

Appendix B: Balance Factor

The term "balance factor" pertains to the percentage of reciprocating mass that is counterbalanced in the rotating crank counterweights. It is clear that any mass orbiting around the crankshaft in a circular path, such as the rod journal, can and should be completely counterbalanced by an opposing mass on the crankshaft. However, the reciprocating components move in a near-sinusoidal linear motion path, and therefore cannot be directly counterbalanced. In many types of inline and V-engines it is common to use a balance factor of around 50% for the reciprocating mass. That is, a mass equivalent of about half of the mass of the reciprocating parts is added to the crankshaft counterweights. A value of around 50% is often selected because it results in a relatively even distribution of force around the perimeter of the main bearings.

Consider the alternative extreme balance factors in a single cylinder engine with the cylinder main axis oriented vertically. A 100% balance factor would result in very low amount of force into the top and bottom of the main bearings, as the reciprocating near-sinusoidal motion of the up/down piston would be nearly completely counteracted by an exactly-sinusoidal down/up motion of the rotating counterweight. However, the counterweight will also generate an exactly-sinusoidal left/right force that will be transferred into the sides of the main bearing. A 0% balance factor will similarly create little to no side forces on the main bearing, but the unbalanced motion of the piston will result in high up/down forces into the bearing. Typically, a balance factor at or near 50% creates a good compromise in force distribution.

Once the balance factor is decided upon, a *bobweight* is prepared to match the reciprocating mass multiplied by the balance factor. This means that the bobweight will often be about half the mass of the reciprocating group it is representing. The bobweight is then secured to the rod journals of the crankshaft before the final crankshaft balancing operations. Note that there are special considerations that must be given to the connecting rod mass balance since the rods do not truly move in a purely rotational or reciprocating path. These considerations are outside of the scope of this work, as the rods in this radial engine design are balanced by a different approach, which will be described below. The above methodology applies well for many inline and V-engines,

however, determining the balance factor and bobweight mass for a radial engine requires a different approach due to the location and orientation of the cylinders.

In order to first approximate the balance factor in a radial engine that does not use a master rod, a simple sketch may be used. In the figure below a 3-cylinder radial engine with a 30mm throw, a 53.5mm radius conrod big-end pin circle, and a 120mm rod length is shown. The engine is represented at TDC for the top cylinder. It is apparent that the top cylinder piston wrist pin is centered at a Y-coordinate of +203.5mm. By inspection, the other two wrist pins are centered at a Y-coordinate of -77.8mm. This results in an average position of:

(203.5-77.8-77.8)/3 = 15.96

Alternatively when the sketch is situated so that the top cylinder is at BDC, the average center of the wrist pins shifts to -14.03mm. Based on this analysis we can conclude that, assuming each of the three reciprocating groups are even in mass, that the collective center of gravity of the three groups orbits in a near-circular path with radius between 15.96 and 14.03mm.

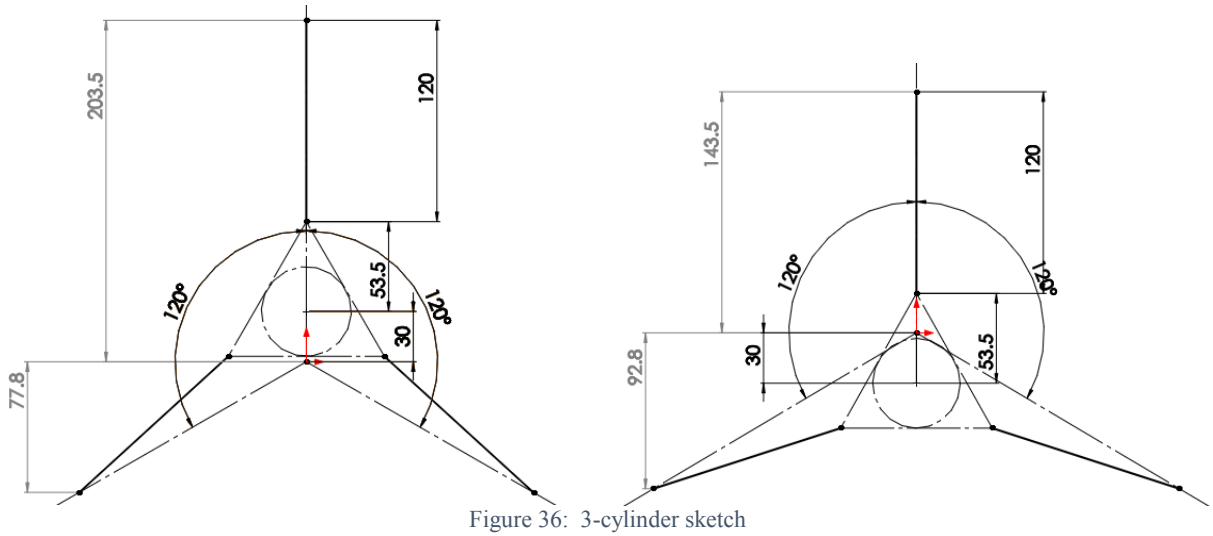

Figure 36: 3-cylinder sketch
top cylinder at TDC (right) and BDC (left)

This sketch-driven analysis was repeated for engines with higher number of cylinders, but with the same throw, conrod pin radius, and rod length. The results are shown in the table below with all units in mm.

Cylinder 1 at TDC									
		cyl #1	cyl #2	cyl #3	cyl #4	cyl #5	cyl #6	cyl #7	average
3-cylinder	X	0	134.8	-134.8					0
	Y	203.5	-77.83	-77.83					15.94667
5-cylinder	X	0	170.55	86.95	-86.95	-170.55			0
	Y	203.5	55.42	-119.68	-119.68	55.42			14.996
7-cylinder	X	0	148.46	159.11	63.24	-63.24	-159.11	-148.46	0
	Y	203.5	118.39	-36.32	-131.33	-131.33	-36.32	118.39	14.99714

Cylinder 1 at BDC									
		cyl #1	cyl #2	cyl #3	cyl #4	cyl #5	cyl #6	cyl #7	average
3-cylinder	X	0	160.78	-160.78					0
	Y	143.5	-92.83	-92.83					-14.0533
5-cylinder	X	0	152.92	115.48	-152.92	-115.48			0
	Y	143.5	49.69	-158.95	-158.95	49.69			-15.004
7-cylinder	X	0	119.21	172.13	205.91	-205.91	-172.13	-119.21	0
	Y	143.5	95.07	-39.29	-180.03	-180.03	-39.29	95.07	-15

Table 5: reciprocating group CG path radii
The radius followed by the system center of gravity approaches 15mm as the cylinder count increases.

A simulation was created to map out the exact path of the collective reciprocating mass CG. In addition, the path of the collective connecting rod CG is also calculated and plotted. Finally, the average magnitude of the reciprocating CG radius is found and plotted as a reference circle on the plot.

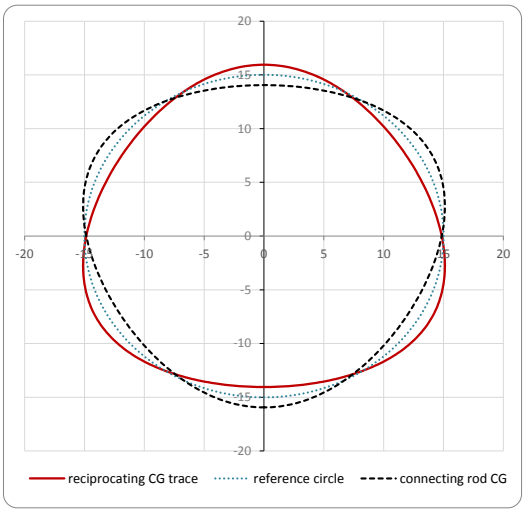

Figure 37: CG paths for engine components
3-cylinder configuration. The reference circle is at a radius of 15.01mm. The connecting rod length has been set to 120mm.

By examination of the plot above, the CG traces of the reciprocating group and the rods can be seen to deviate from that of their average circular equivalent. This arises due to the motion of the pistons being not completely sinusoidal in nature, as is the case in any conventional piston engine. If the rod length is increased, this deviation shrinks, and if the rod length is shortened, this deviation

grows. If the connecting rods could be designed to be infinitely long, the deviation would become nonexistent. To illustrate this effect, the simulation was repeated at 80mm and 200mm connecting rods, without changing any other design parameters.

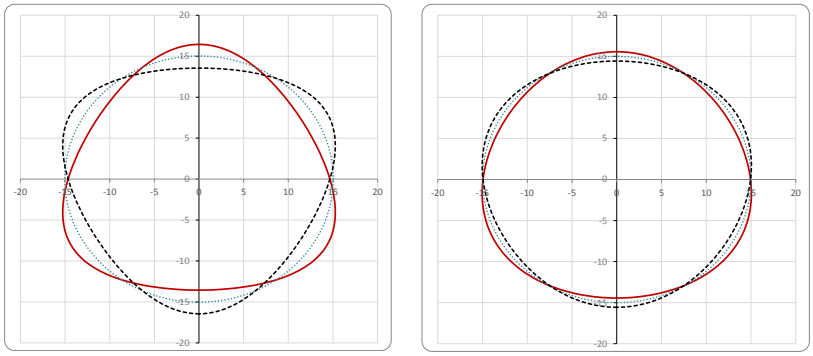

Figure 38: CG trace
80mm rods (left) and 200mm rods (right)

Based on the results of the sketch approximation and the simulation, it is clear that the collective CG of the reciprocating parts moves in a near-circle with radius approaching 15mm. Additionally, the collective CG of the connecting rods also moves in a near-circle with radius 15mm. However, the bobweights that will be used to represent these parts during the crank balancing process will be attached to the conrod base disk. This means that the collective CG of the bobweights will be forced to move in an exactly circular path with radius 30mm, since the throw of the engine is 30mm by design. Because of this, the bobweights must be designed so that their mass is much lower than the parts they are representing, because they are being forced around a larger circle than the CG of the actual parts. Specifically, the bobweight mass can be found with the following equation.

$$m_{bobweight} = \left[m_{recip\ ASM} * \frac{r_{recip\ CG\ path,\ average}}{r_{bobweight\ CG\ path}}\right] + \left[m_{conrod} * \frac{r_{conrod\ CG\ path,\ average}}{r_{bobweight\ CG\ path}}\right]$$

The components for the prototype engine were measured on a digital scale. A piston assembly with rings, wrist pin, and snap rings mass to 415 grams, and a connecting rod masses to 159 grams. Because the CG path radius was found to be 15mm and the bobweight CG path radius is locked at 30mm, the equation above reduces to:

$$m_{bobweight} = \left[415 * \frac{15}{30}\right] + \left[159 * \frac{15}{30}\right]$$

$= 287$g (single bobweight - three required to balance a 3-cylinder engine crankshaft)

Appendix C: Gear CMM Data

English Internal Spur Gears Screen Shaper 2.25

		Given	Standard	Diff.Produced Using Std.
1	Circular Pitch	0.2244	0.2244	
2	Diametral Pitch	14	14	
3	Module Pitch	1.81429	1.81429	
4	Pressure Angle	25	25	
5	Number of teeth	51	51	
6	Pitch Diameter	3.64286	3.64286	
7	Base Pitch	0.20337	0.20337	
8	Base Diameter	3.30155	3.30155	
9	Minor Diameter	3.5	3.5	
10	Major Diameter	3.82143	3.82143	
11	Whole Depth	0.16071	0.16071	
12	Addendum	0.07143	0.07143	
13	Dedendum	0.08929	0.08929	
14	Land at Minor	0.05025	0.05025	
15	Circular Tooth Width	0.1122	0.1122	
16	Circ.Space Width	0.1122	0.1122	
17	Measure under Wire	3.46452	3.46452	
18	Wire Size	0.1234	0.1234	

Pin Contact	Apex Diam.	Base Space
3.6381	3.85788	0.20065

Involute PA	Inv.Gen.PA	T.I.F.Diam.	Roll AngTIF	PA at TIF	Roll Ang Min
0.02998	N/A	N/A	N/A	N/A	20.16204

English External Spur Gears Screen Hob 2.1571

		Given	Standard	Diff.Produced Using Std.
1	Circular Pitch	0.2244	0.2244	
2	Diametral Pitch	14	14	
3	Module Pitch	1.81429	1.81429	
4	Pressure Angle	25	25	
5	Number of teeth	34	34	
6	Pitch Diameter	2.42857	2.42857	
7	Base Pitch	0.20337	0.20337	
8	Base Diameter	2.20103	2.20103	
9	Minor Diameter	2.26327	2.26327	
10	Major Diameter	2.57143	2.57143	
11	Whole Depth	0.15408	0.15408	
12	Addendum	0.07143	0.07143	
13	Dedendum	0.08265	0.08265	
14	Land at Major	0.0399	0.0399	
15	Chordal Tooth Thick	0.11216	0.11216	
16	Circ.Tooth Thick	0.1122	0.1122	
17	Measure over Wire	2.60126	2.60126	
18	Wire Size	0.12343	0.12343	

Span of 6 teeth measures 1.18454 Contact Diam. 2.49954

Pin Contact	Apex Diam.	Base Tooth
2.42362	2.63539	0.16766

Involute PA	Inv.Gen.PA	T.I.F.Diam.	Roll AngTIF	PA at TIF	RollAngMaj
0.02998	N/A	2.29086	16.53575	16.09832	34.60988

Appendix D: Boost Rise Profile

The image below shows a typical turbocharger compressor map in the background, and a blue "lug line" in the foreground.

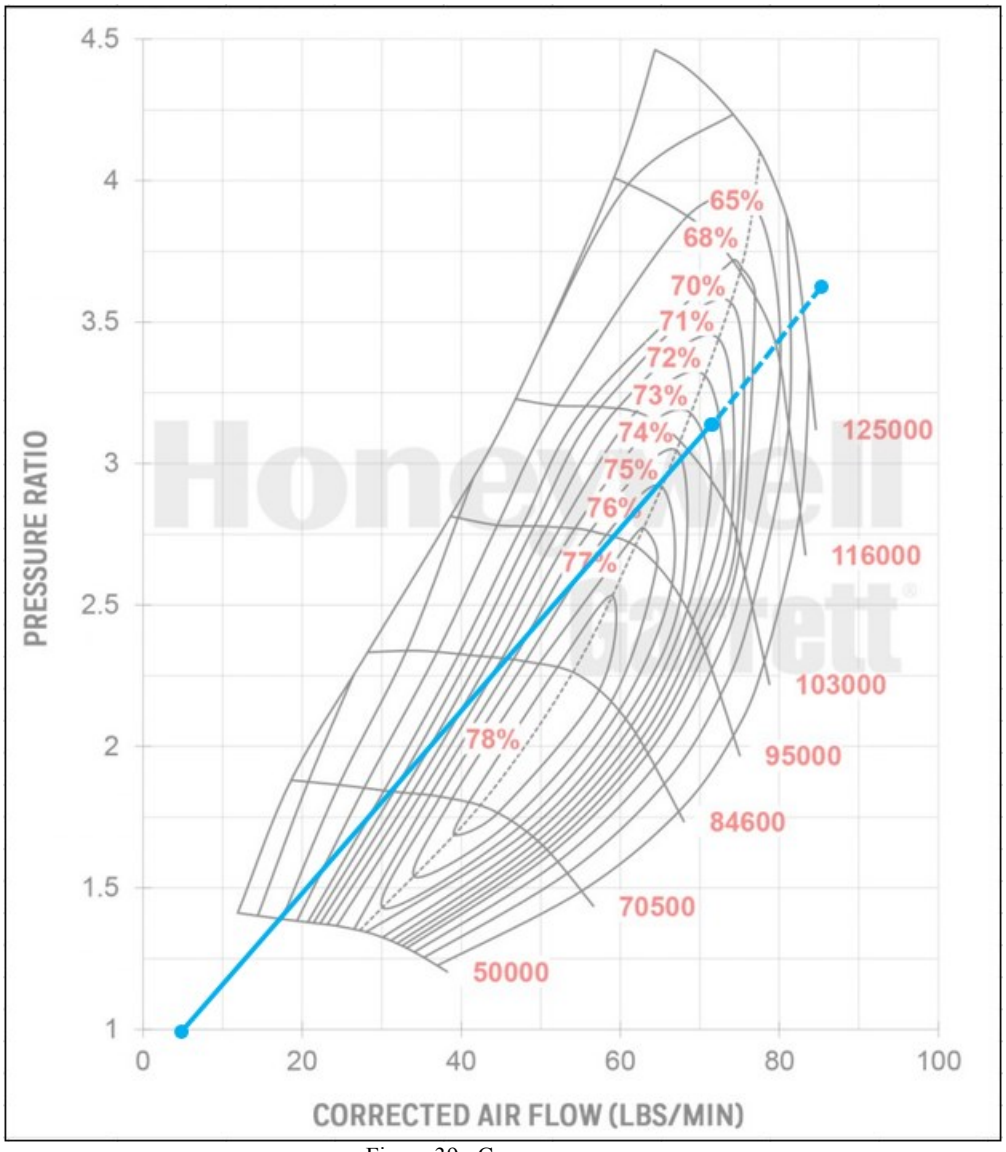

Figure 39: Compressor map
Garrett GTX4088R Turbocharger with typical VCR lug line

The compressor map demonstrates the effective useable range of the compressor given a mass flow and pressure ratio. The lug line overlay is a representation of the desired point of operation.

It is the function of the design of the turbine stage and the calibration of the engine (such as exhaust valve timing) to ensure that the desired operating point is the actual point reached in reality. A full analysis of compressor/turbine matching with exhaust gas properties is beyond the scope of this work. Therefore, an approximate linear lug line will be used, and it will be assumed that a turbine stage and engine calibration could be implemented to reach the lug line. In reality, lug lines are downward curving due to the engine breathing characteristics, not a perfectly straight line as shown above. In the case of a turbocharger fitted with a wastegate, the lug line will increase diagonally up to a certain point (typically about 1/3 to ½ of the way across the useable width of the map), and then abruptly level-off and remain horizontally flat to the right of the inflection point. This behavior is driven by the opening of the wastegate, which intentionally lowers the turbine stage efficiency, providing the compressor will reduced mechanical power. This method is usually needed on spark ignition engines to limit the intake manifold pressure to prevent engine knock. Large diesel engines only *sometimes* employ a wastegate on the turbocharger as they are typically build to tolerate higher cylinder pressures, and are not subject to engine knock due to the stratification of fuel injection.

The solid part of the blue line represents the typical operating range of the VCR simulation between 1,000 and 8,000 rpm. The additional dotted section represents the additional range needed for the trials involving engine speeds up to 11,000 rpm. These trials were not explicitly covered in the body of this work, but compared to the 8,000 rpm points investigated, they resulted in significantly greater output power levels at further decreased thermal efficiency. Note that on this map, engine speeds around 11,000 rpm would extend past the mapped portion of the compressor, which typically equates to exceeding the rotational speed limit of the turbocharger. If the 2.0 L VCR engine were designed to operate at 11,000 rpm, the resulting mass flow rate may prompt the selection of a slightly larger turbocharger, so as not to exceed its speed limits. However, it is common for race engines to push the turbocharger slightly past its manufacturer recommended speed limit. This strategy comes with the cost of reduced durability, typically manifested in premature compressor-side Low Cycle Fatigue (LCF) failure. In that regard, the compressor map above would be debatably appropriate for the application.

Appendix E: Piston Acceleration Equation

In the body of the text above the derivation for piston velocity was shown in full, but the derivation for the piston acceleration was too lengthy to show there. Alternatively, the full derivation for piston acceleration is covered here. Note that the symbol used for angular position θ has been replaced with 'x', and the symbol for variator angle γ has been replaced with 'y'.

Step 1

Possible derivation:

$$\frac{d}{dx}\left(\frac{d}{dx}\left(t\cos(x)+u\cos(y)+\sqrt{l^2-(t\sin(x)+u\sin(y))^2}\right)\right)$$

Step 2

Differentiate the sum term by term and factor out constants:

$$=\frac{d}{dx}\left(t\,\frac{d}{dx}(\cos(x))+\frac{d}{dx}(u\cos(y))+\frac{d}{dx}\left(\sqrt{l^2-(t\sin(x)+u\sin(y))^2}\right)\right)$$

Step 3

The derivative of $\cos(x)$ is $-\sin(x)$:

$$=\frac{d}{dx}\left(-\sin(x)\,t+\frac{d}{dx}(u\cos(y))+\frac{d}{dx}\left(\sqrt{l^2-(t\sin(x)+u\sin(y))^2}\right)\right)$$

Step 4

The derivative of $u\cos(y)$ is zero:

$$=\frac{d}{dx}\left(t\,(-\sin(x))+0+\frac{d}{dx}\left(\sqrt{l^2-(t\sin(x)+u\sin(y))^2}\right)\right)$$

Step 5

Using the chain rule, $\frac{d}{dx}\left(\sqrt{l^2-(t\sin(x)+u\sin(y))^2}\right)=\frac{d\sqrt{u}}{du}\,\frac{du}{dx}$, where $u=l^2-(t\sin(x)+u\sin(y))^2$ and $\frac{d}{du}\left(\sqrt{u}\right)=\frac{1}{2\sqrt{u}}$:

$$=\frac{d}{dx}\left(t\,(-\sin(x))+0+\frac{\frac{d}{dx}\left(l^2-(t\sin(x)+u\sin(y))^2\right)}{2\sqrt{l^2-(t\sin(x)+u\sin(y))^2}}\right)$$

Step 6

Differentiate the sum term by term and factor out constants:

$$=\frac{d}{dx}\left(t\,(-\sin(x))+0+\frac{\frac{d}{dx}(l^2)-\frac{d}{dx}\left((t\sin(x)+u\sin(y))^2\right)}{2\sqrt{l^2-(t\sin(x)+u\sin(y))^2}}\right)$$

Step 7

The derivative of l^2 is zero:

$$=\frac{d}{dx}\left(t\,(-\sin(x))+0+\frac{0-\frac{d}{dx}\left((t\sin(x)+u\sin(y))^2\right)}{2\sqrt{l^2-(t\sin(x)+u\sin(y))^2}}\right)$$

Step 8

Using the chain rule, $\frac{d}{dx}\left((t\sin(x)+u\sin(y))^2\right)=\frac{du^2}{du}\frac{du}{dx}$, where $u=t\sin(x)+u\sin(y)$ and $\frac{d}{du}(u^2)=2u$:

$$=\frac{d}{dx}\left(t(-\sin(x))+0+\frac{0-2\frac{d}{dx}(t\sin(x)+u\sin(y))(t\sin(x)+u\sin(y))}{2\sqrt{l^2-(t\sin(x)+u\sin(y))^2}}\right)$$

Step 9

Differentiate the sum term by term and factor out constants:

$$=\frac{d}{dx}\left(t(-\sin(x))+0+\frac{0-t\frac{d}{dx}(\sin(x))+\frac{d}{dx}(u\sin(y))\,2(t\sin(x)+u\sin(y))}{2\sqrt{l^2-(t\sin(x)+u\sin(y))^2}}\right)$$

Step 10

The derivative of $\sin(x)$ is $\cos(x)$:

$$=\frac{d}{dx}\left(t(-\sin(x))+0+\frac{0-2\left(\cos(x)\,t+\frac{d}{dx}(u\sin(y))\right)(t\sin(x)+u\sin(y))}{2\sqrt{l^2-(t\sin(x)+u\sin(y))^2}}\right)$$

Step 11

The derivative of $u\sin(y)$ is zero:

$$=\frac{d}{dx}\left(t(-\sin(x))+0+\frac{0-2\left(t\cos(x)+0\right)(t\sin(x)+u\sin(y))}{2\sqrt{l^2-(t\sin(x)+u\sin(y))^2}}\right)$$

Step 12

Differentiate the sum term by term and factor out constants:

$$=-t\left(\frac{d}{dx}(\sin(x))\right)-t\left(\frac{d}{dx}\left(\frac{\cos(x)(t\sin(x)+u\sin(y))}{\sqrt{l^2-(t\sin(x)+u\sin(y))^2}}\right)\right)$$

Step 13

The derivative of $\sin(x)$ is $\cos(x)$:

$$=-\left(t\left(\frac{d}{dx}\left(\frac{\cos(x)(t\sin(x)+u\sin(y))}{\sqrt{l^2-(t\sin(x)+u\sin(y))^2}}\right)\right)\right)-\cos(x)\,t$$

Step 14

Use the product rule, $\frac{d}{dx}(uv)=v\frac{du}{dx}+u\frac{dv}{dx}$, where $u=\cos(x)$ and $v=\frac{t\sin(x)+u\sin(y)}{\sqrt{l^2-(t\sin(x)+u\sin(y))^2}}$:

$$=-(t\cos(x))-\cos(x)\frac{d}{dx}\left(\frac{t\sin(x)+u\sin(y)}{\sqrt{l^2-(t\sin(x)+u\sin(y))^2}}\right)+\frac{\frac{d}{dx}(\cos(x))(t\sin(x)+u\sin(y))}{\sqrt{l^2-(t\sin(x)+u\sin(y))^2}}\,t$$

Step 15

Use the product rule, $\frac{d}{dx}(uv)=v\frac{du}{dx}+u\frac{dv}{dx}$, where $u=t\sin(x)+u\sin(y)$ and $v=\frac{1}{\sqrt{l^2-(t\sin(x)+u\sin(y))^2}}$:

$$=-(t\cos(x))-t\left(\frac{\left(\frac{d}{dx}(\cos(x))\right)(t\sin(x)+u\sin(y))}{\sqrt{l^2-(t\sin(x)+u\sin(y))^2}}+\frac{d}{dx}\left(\frac{1}{\sqrt{l^2-(t\sin(x)+u\sin(y))^2}}\right)(t\sin(x)+u\sin(y))+\frac{\frac{d}{dx}(t\sin(x)+u\sin(y))}{\sqrt{l^2-(t\sin(x)+u\sin(y))^2}}\cos(x)\right)$$

Step 16

Using the chain rule, $\frac{d}{dx}\left(\frac{1}{\sqrt{l^2-(t\sin(x)+u\sin(y))^2}}\right)=\frac{d}{du}\frac{1}{\sqrt{u}}\frac{du}{dx}$, where $u=l^2-(t\sin(x)+u\sin(y))^2$ and $\frac{d}{du}\left(\frac{1}{\sqrt{u}}\right)=-\frac{1}{2u^{3/2}}$:

$$=-(t\cos(x))-t\left(\frac{\left(\frac{d}{dx}(\cos(x))\right)(t\sin(x)+u\sin(y))}{\sqrt{l^2-(t\sin(x)+u\sin(y))^2}}+\cos(x)\left(\frac{\frac{d}{dx}(t\sin(x)+u\sin(y))}{\sqrt{l^2-(t\sin(x)+u\sin(y))^2}}+(t\sin(x)+u\sin(y))\frac{-\frac{d}{dx}(l^2-(t\sin(x)+u\sin(y))^2)}{2\left(l^2-(t\sin(x)+u\sin(y))^2\right)^{3/2}}\right)\right)$$

Step 17

The derivative of $\cos(x)$ is $-\sin(x)$:

$$=-(t\cos(x))-t\left(\cos(x)\left(-\frac{\left(\frac{d}{dx}(l^2-(t\sin(x)+u\sin(y))^2)\right)(t\sin(x)+u\sin(y))}{2\left(l^2-(t\sin(x)+u\sin(y))^2\right)^{3/2}}+\frac{\frac{d}{dx}(t\sin(x)+u\sin(y))}{\sqrt{l^2-(t\sin(x)+u\sin(y))^2}}\right)+\frac{(t\sin(x)+u\sin(y))\,-\sin(x)}{\sqrt{l^2-(t\sin(x)+u\sin(y))^2}}\right)$$

Step 18

Differentiate the sum term by term and factor out constants:

$$=-(t\cos(x))-t\left(-\frac{\sin(x)(t\sin(x)+u\sin(y))}{\sqrt{l^2-(t\sin(x)+u\sin(y))^2}}+\cos(x)\left(\frac{\frac{d}{dx}(t\sin(x)+u\sin(y))}{\sqrt{l^2-(t\sin(x)+u\sin(y))^2}}-\frac{(t\sin(x)+u\sin(y))\left(\frac{d}{dx}(l^2)-\frac{d}{dx}((t\sin(x)+u\sin(y))^2)\right)}{2\left(l^2-(t\sin(x)+u\sin(y))^2\right)^{3/2}}\right)\right)$$

Step 19

The derivative of l^2 is zero:

$$=-(t\cos(x))-t\left(-\frac{\sin(x)(t\sin(x)+u\sin(y))}{\sqrt{l^2-(t\sin(x)+u\sin(y))^2}}+\cos(x)\left(\frac{\frac{d}{dx}(t\sin(x)+u\sin(y))}{\sqrt{l^2-(t\sin(x)+u\sin(y))^2}}-\frac{(t\sin(x)+u\sin(y))\left(-\left(\frac{d}{dx}((t\sin(x)+u\sin(y))^2)\right)+0\right)}{2\left(l^2-(t\sin(x)+u\sin(y))^2\right)^{3/2}}\right)\right)$$

Step 20

Simplify the expression:

$$=-(t\cos(x))-t\left(-\frac{\sin(x)(t\sin(x)+u\sin(y))}{\sqrt{l^2-(t\sin(x)+u\sin(y))^2}}+\cos(x)\left(\frac{\left(\frac{d}{dx}((t\sin(x)+u\sin(y))^2)\right)(t\sin(x)+u\sin(y))}{2\left(l^2-(t\sin(x)+u\sin(y))^2\right)^{3/2}}+\frac{\frac{d}{dx}(t\sin(x)+u\sin(y))}{\sqrt{l^2-(t\sin(x)+u\sin(y))^2}}\right)\right)$$

Step 21

Using the chain rule, $\frac{d}{dx}\left((t\sin(x)+u\sin(y))^2\right)=\frac{du^2}{du}\frac{du}{dx}$, where $u=t\sin(x)+u\sin(y)$ and $\frac{d}{du}\left(u^2\right)=2u$:

$$=-(t\cos(x))-t\left(-\frac{\sin(x)(t\sin(x)+u\sin(y))}{\sqrt{l^2-(t\sin(x)+u\sin(y))^2}}+\cos(x)\left(\frac{\frac{d}{dx}(t\sin(x)+u\sin(y))}{\sqrt{l^2-(t\sin(x)+u\sin(y))^2}}+\frac{(t\sin(x)+u\sin(y))\,2\,\frac{d}{dx}(t\sin(x)+u\sin(y))\,(t\sin(x)+u\sin(y))}{2\left(l^2-(t\sin(x)+u\sin(y))^2\right)^{3/2}}\right)\right)$$

Step 22

Simplify the expression:

$$=-(t\cos(x))-t\left(-\frac{\sin(x)(t\sin(x)+u\sin(y))}{\sqrt{l^2-(t\sin(x)+u\sin(y))^2}}+\cos(x)\left(\frac{\left(\frac{d}{dx}(t\sin(x)+u\sin(y))\right)(t\sin(x)+u\sin(y))^2}{\left(l^2-(t\sin(x)+u\sin(y))^2\right)^{3/2}}+\frac{\frac{d}{dx}(t\sin(x)+u\sin(y))}{\sqrt{l^2-(t\sin(x)+u\sin(y))^2}}\right)\right)$$

Step 23

Differentiate the sum term by term and factor out constants:

$$=-(t\cos(x))-t\left(-\frac{\sin(x)(t\sin(x)+u\sin(y))}{\sqrt{l^2-(t\sin(x)+u\sin(y))^2}}+\cos(x)\left(\frac{\frac{d}{dx}(t\sin(x)+u\sin(y))}{\sqrt{l^2-(t\sin(x)+u\sin(y))^2}}+\frac{t\,\frac{d}{dx}(\sin(x))+\frac{d}{dx}(u\sin(y))\,(t\sin(x)+u\sin(y))^2}{\left(l^2-(t\sin(x)+u\sin(y))^2\right)^{3/2}}\right)\right)$$

Step 24

The derivative of $\sin(x)$ is $\cos(x)$:

$$=-(t\cos(x))-t\left(-\frac{\sin(x)(t\sin(x)+u\sin(y))}{\sqrt{l^2-(t\sin(x)+u\sin(y))^2}}+\cos(x)\left(\frac{\frac{d}{dx}(t\sin(x)+u\sin(y))}{\sqrt{l^2-(t\sin(x)+u\sin(y))^2}}+\frac{(t\sin(x)+u\sin(y))^2\left(\frac{d}{dx}(u\sin(y))+\cos(x)\,t\right)}{\left(l^2-(t\sin(x)+u\sin(y))^2\right)^{3/2}}\right)\right)$$

Step 25

The derivative of $u\sin(y)$ is zero:

$$=-(t\cos(x))-t\left(-\frac{\sin(x)(t\sin(x)+u\sin(y))}{\sqrt{l^2-(t\sin(x)+u\sin(y))^2}}+\cos(x)\left(\frac{\frac{d}{dx}(t\sin(x)+u\sin(y))}{\sqrt{l^2-(t\sin(x)+u\sin(y))^2}}+\frac{(t\sin(x)+u\sin(y))^2\left(t\cos(x)+0\right)}{\left(l^2-(t\sin(x)+u\sin(y))^2\right)^{3/2}}\right)\right)$$

Step 26

Simplify the expression:

$$=-(t\cos(x))-t\left(-\frac{\sin(x)(t\sin(x)+u\sin(y))}{\sqrt{l^2-(t\sin(x)+u\sin(y))^2}}+\cos(x)\left(\frac{t\cos(x)(t\sin(x)+u\sin(y))^2}{\left(l^2-(t\sin(x)+u\sin(y))^2\right)^{3/2}}+\frac{\frac{d}{dx}(t\sin(x)+u\sin(y))}{\sqrt{l^2-(t\sin(x)+u\sin(y))^2}}\right)\right)$$

Step 27

Differentiate the sum term by term and factor out constants:

$$= -(t\cos(x)) - t\left(-\frac{\sin(x)\,(t\sin(x)+u\sin(y))}{\sqrt{l^2-(t\sin(x)+u\sin(y))^2}}+\cos(x)\left(\frac{t\cos(x)\,(t\sin(x)+u\sin(y))^2}{\left(l^2-(t\sin(x)+u\sin(y))^2\right)^{3/2}}+\frac{t\,\frac{d}{dx}(\sin(x))+\frac{d}{dx}(u\sin(y))}{\sqrt{l^2-(t\sin(x)+u\sin(y))^2}}\right)\right)$$

Step 28

The derivative of $\sin(x)$ is $\cos(x)$:

$$= -(t\cos(x)) - t\left(-\frac{\sin(x)\,(t\sin(x)+u\sin(y))}{\sqrt{l^2-(t\sin(x)+u\sin(y))^2}}+\cos(x)\left(\frac{t\cos(x)\,(t\sin(x)+u\sin(y))^2}{\left(l^2-(t\sin(x)+u\sin(y))^2\right)^{3/2}}+\frac{\frac{d}{dx}(u\sin(y))+\cos(x)\,t}{\sqrt{l^2-(t\sin(x)+u\sin(y))^2}}\right)\right)$$

Step 30

Simplify the expression:

Answer:

$$= -(t\cos(x)) - t\left(-\frac{\sin(x)\,(t\sin(x)+u\sin(y))}{\sqrt{l^2-(t\sin(x)+u\sin(y))^2}}+\cos(x)\left(\frac{t\cos(x)\,(t\sin(x)+u\sin(y))^2}{\left(l^2-(t\sin(x)+u\sin(y))^2\right)^{3/2}}+\frac{t\cos(x)}{\sqrt{l^2-(t\sin(x)+u\sin(y))^2}}\right)\right)$$